

SYNTHESIS OF EGGSHELL-DERIVED  
HYDROXYAPATITE AND ITS DEPOSITION ON TITANIUM  
BY ELECTROPHORETIC METHOD

MALIAH AMIRI ROUDAN

FACULTY OF ENGINEERING  
UNIVERSITY OF MALAYA  
KUALA LUMPUR

2018

**SYNTHESIS OF EGGSHELL-DERIVED  
HYDROXYAPATITE AND ITS DEPOSITION ON  
TITANIUM BY ELECTROPHORETIC METHOD**

**MALIHAN AMIRI ROUDAN**

**THESIS SUBMITTED IN FULFILMENT OF THE  
REQUIREMENTS FOR THE DEGREE OF DOCTOR OF  
PHILOSOPHY**

**FACULTY OF ENGINEERING  
UNIVERSITY OF MALAYA  
KUALA LUMPUR**

**2018**

**UNIVERSITY OF MALAYA**  
**ORIGINAL LITERARY WORK DECLARATION**

Name of Candidate: **MALIHAN AMIRI ROUDAN**

Matric No: **KHA130119**

Name of Degree: **DOCTOR OF PHILOSOPHY**

Title of Project Paper/Research Report/Dissertation/Thesis (“this Work”):

**SYNTHESIS OF EGGSHELL-DERIVED HYDROXYAPATITE AND ITS DEPOSITION ON TITANIUM BY ELECTROPHORETIC METHOD**

Field of Study: **MECHANICAL-MATERIAL ENGINEERING**

I do solemnly and sincerely declare that:

- (1) I am the sole author/writer of this Work;
- (2) This Work is original;
- (3) Any use of any work in which copyright exists was done by way of fair dealing and for permitted purposes and any excerpt or extract from, or reference to or reproduction of any copyright work has been disclosed expressly and sufficiently and the title of the Work and its authorship have been acknowledged in this Work;
- (4) I do not have any actual knowledge nor do I ought reasonably to know that the making of this work constitutes an infringement of any copyright work;
- (5) I hereby assign all and every rights in the copyright to this Work to the University of Malaya (“UM”), who henceforth shall be owner of the copyright in this Work and that any reproduction or use in any form or by any means whatsoever is prohibited without the written consent of UM having been first had and obtained;
- (6) I am fully aware that if in the course of making this Work I have infringed any copyright whether intentionally or otherwise, I may be subject to legal action or any other action as may be determined by UM.

Candidate’s Signature

Date:

Subscribed and solemnly declared before,

Witness’s Signature

Date:

Name:

Designation:

# **SYNTHESIS OF EGGSHELL-DERIVED HYDROXYAPATITE AND ITS DEPOSITION ON TITANIUM BY ELECTROPHORETIC METHOD**

## **ABSTRACT**

Hydroxyapatite (HA) is a well-known bioactive material, which has wide range of applications. One of the important purposes of using this material is the replacement of bone in human body, because of its similarity to bone structure and its excellent biocompatible nature. Calcium oxide is one of the main constituents of HA and can be obtained from various sources to synthesize hydroxyapatite. Some of these methods include sol-gel, hydrothermal and wet chemical method. Calcium can be found within the natural sources such as eggshell, seashell and animal bone and can be converted into calcium oxide thorough heat treatment process. In this study, synthesis and sintering behaviour of HA using eggshell as the source of Calcium has been conducted in a systematic manner. We synthesized HA using eggshell powder as a calcium oxide source via wet chemical precipitation method. Stoichiometric amount of Calcium oxide produced from calcining eggshell at 900 °C, added to orthophosphoric acid, measured by stoichiometric ratio, then precipitated followed by aging overnight. Final solution was filtered and dried, then used as green powder to make the disc samples using 20 mm mold. The green samples were sintered in air at various temperatures ranging from 900 °C to 1400 °C at a ramp rate of 10 °C per minute and one hour holding time. The sintered samples were evaluated for HA phase stability, relative density, grain size, Vickers hardness and fracture toughness. X-Ray diffractometer (XRD) was used to analyze the phase composition. Field emission scanning electron microscope (FESEM) and energy dispersive spectroscopy (EDS) were carried out for microstructure characterization and elemental analysis, respectively. The XRD results indicated that the HA phase remained untill 1300 °C. However a secondary phase of tricalcium phosphate (TCP) was observed

at 1350 °C which was also confirmed by SEM examination. The relative density, Vickers hardness and fracture toughness were found to increase between 900 to 1100 °C and reached a plateau thereafter. A relatively density of 98.5%, high Vickers hardness of 5.9 GPa and fracture toughness of 1.09 MPam<sup>1/2</sup> were achieved at 1250 °C. The average grain size at this temperature was 2.5 µm. In the subsequent study, synthesized eggshell-hydroxyapatite was coated onto titanium substrate using electrophoretic deposition technique. Different voltage, current, time and weight were tested to determine optimum parameter for obtaining a crack free coated film. Coated samples were then sintered in a tube furnace at various temperatures under argon atmosphere. Analysis of the samples showed a homogenous and uniform HA coating. XRD analysis revealed that the HA phase was stable after sintering up to 1050°C. Cross section view of the coated samples confirmed good adhesion between coated layer and substrate. Overall, this research has demonstrated the viability of producing highly crystalline, phase pure hydroxyapatite from bio-waste eggshells and applying it as a coating material onto titanium. The synthesized hydroxyapatite had a stoichiometric Ca/P ratio of 1.67 without compromising on the thermal stability of the HA phase and the sintered eggshell-derived HA body exhibited excellent mechanical properties suitable for biomedical application.

Keywords: Hydroxyapatite, Biowaste, Synthesis, Electrophoretic deposition, Sintering.

# **SYNTHESIS OF HYDROXYAPATITE EGGSHELL-DERIVED DAN DEPOSISI ITU PADA TITANIUM OLEH METODE ELECTROPHORETIC**

## **ABSTRAK**

Hydroxyapatite (HA) dikenali sebagai bahan bioaktif, yang mempunyai pelbagai aplikasi, salah satu tujuan penting dalam menggunakan bahan ini adalah penggantian tulang dalam tubuh manusia, kerana persamaan dengan struktur tulang dan sifat biokompatibel itu. Kalsium oksida adalah bahan utama dalam kebanyakan kaedah dilaporkan seperti sol-gel, hidroterma dan kaedah kimia basah, yang dapat berasal dari sumber yang berlainan. Sejumlah besar kalsium boleh didapati dalam sumber-sumber semula jadi seperti kulit telur, kerang dan tulang haiwan yang boleh dengan mudah ditukar kepada kalsium oksida proses rawatan haba menyeluruh. Dalam kajian ini, tingkah laku prosedur penyediaan dan pensinteran HA diekstrak daripada kulit telur dilaporkan. Kulit telur HA disediakan dengan menggunakan serbuk kulit telur kalsinan sebagai sumber kalsium oksida melalui kaedah pemendakan kimia basah. Kalsium oksida dihasilkan daripada kalsinasi yang kulit telur di 900 °C, ditambah kepada asid ortofosforik, yang diukur oleh nisbah stoikiometri, kemudian dicetuskan diikuti oleh penuaan semalaman. Penyelesaian akhir telah ditapis dan kering, kemudian digunakan sebagai serbuk hijau untuk membuat sampel pallet menggunakan 20 mm acuan. sampel mentah telah disediakan dan disinter di udara pada pelbagai suhu antara 900 °C untuk 1400 °C pada kadar tanjakan daripada 10 °C seminit dan memegang masa satu jam. Sampel tersinter telah dinilai dari segi HA kestabilan fasa, ketumpatan relatif, saiz butiran, kekerasan Vickers dan keliatan patah. X-ray pembelauan (XRD) telah digunakan untuk mengesahkan pembentukan fasa, mikroskop imbasan elektron (FESEM) dan tenaga spektroskopi serakan (EDS) telah dijalankan bagi mencirikan analisis mikrostruktur. Keputusan XRD menunjukkan bahawa fasa HA kekal stabil walaupun selepas pensinteran di 1300 °C. Walau bagaimanapun fasa yang kedua fosfat trikalsium

(TCP) diperhatikan pada 1350 °C dan ini boleh dikaitkan dengan mikrostruktur seramik. Di samping itu, ketumpatan relatif, kekerasan Vickers dan keliatan patah didapati meningkat dengan cepat antara 900 ke 1100 °C dan sampai dataran tinggi selepas itu. A agak ketumpatan 98.5%, kekerasan Vickers tinggi 5.9 GPa dan patah keliatan 01:09 MPam<sup>1/2</sup> telah dicapai pada 1250 °C walaupun mempunyai saiz butiran besar 2.5 µm pada suhu ini. Dalam bahagian kedua kajian, disintesis hydroxyapatite seperti yang digunakan pada substrat titanium menggunakan teknik lapisan elektroforesis. Salutan adalah sebahagian termasuk dua bahagian, pertama untuk meningkatkan kualiti lapisan sampel hijau dan kedua untuk meningkatkan sampel tersinter. Voltan yang berbeza, arus elektrik, masa dan berat telah diuji untuk mencari parameter optimum untuk mendapatkan perlindungan bebas retak dan filem bersalut yang tinggi. Sampel kemudian disinter pada relau tiub pada pelbagai suhu tembakan di bawah suasana gas argon. Analisis mikrograf menunjukkan analisis struktur. XRD homogen dan seragam mendedahkan kestabilan fasa HA selepas pensinteran. keratan rentas paparan sampel yang disahkan lekatan yang baik antara lapisan bersalut dan substrat. Secara keseluruhan, kajian ini telah menunjukkan kemungkinan mengeluarkan sangat kristal, fasa tulen hydroxyapatite bio-bahan buangan daripada kulit telur. Bio seramik yang diperolehi memenuhi nisbah Ca/P stoikiometri 1.67 tanpa menjejaskan kestabilan haba fasa HA dan badan tersinter HA yang diperolehi daripada kulit telur mempamerkan sifat mekanik yang baik sesuai untuk kegunaan bioperubatan.

Keywords: Hydroxyapatite, Biowaste, Sintesis, Pemendapan electrophoretic, Sintering.

## ACKNOWLEDGEMENTS

Foremost, I would like to express my sincere gratitude to my supervisor, Prof. Ir. Dr. Ramesh Singh for continues support, for his patient, motivation, immense knowledge, and for his detailed and constructive comments throughout this work. He helped me in all time of research and writing of this thesis. I could not have imagined having a better advisor and mentor. The special thank goes to my helpful supervisor, the supervision and support that he gave truly help the progression of this work.

I would like to thank my family members. Great thanks for supporting me throughout my life and for encouraging me to pursue this degree. Without them, I would not have finished the degree.



## TABLE OF CONTENTS

Abstract .....	iii
Abstrak .....	v
Acknowledgements .....	vii
Table of Contents .....	viii
List of Figures .....	xiii
List of Tables.....	xvi
List of Symbols and Abbreviations.....	xvii
List of Appendices .....	xix
<b>CHAPTER 1: INTRODUCTION.....</b>	<b>1</b>
1.1 Background.....	1
1.2 Problem Statement and Aim of Study .....	3
1.3 Objectives .....	4
1.4 Thesis Outline.....	5
<b>CHAPTER 2: LITERATURE REVIEW.....</b>	<b>6</b>
2.1 Introduction.....	6
2.2 Bioceramics .....	7
2.2.1 Calcium Phosphate .....	8
2.2.2 Hydroxyapatite .....	9
2.3 Synthesis of Hydroxyapatite.....	14
2.3.1 Wet Chemical Synthesis.....	16
2.3.2 Dry Chemical Synthesis .....	19
2.4 Sintering of Hydroxyapatite .....	20
2.5 Coating Technique.....	23

2.5.1	Dip Coating .....	24
2.5.2	Electrophoretic Deposition.....	25
2.5.3	Ion Beam Deposition.....	30
2.5.4	Plasma Electrolytic Oxidation.....	30
2.5.5	Plasma Spraying.....	31
2.5.6	Sputter Coating.....	32
2.5.7	Pulse Laser Deposition.....	34
2.5.8	Sol-gel Coating.....	36
2.5.9	Thermal Spray .....	36
2.6	Comparison of Coating Techniques .....	38
2.7	Summary.....	41
 <b>CHAPTER 3: MATERIALS AND METHODS .....</b>		<b>42</b>
3.1	Introduction.....	42
3.2	Materials .....	43
3.3	Powder Preparation Method .....	45
3.3.1	Conversion of Eggshell to Calcium Oxide via Calcinations Method.....	45
3.3.2	Synthesize HA via Wet Chemical Precipitation Method .....	46
3.4	Samples Fabrication.....	47
3.4.1	Compacting of Green Powder .....	47
3.4.2	Convectional Sintering .....	47
3.4.3	Grinding and Polishing.....	48
3.5	Electrophoretic Coating Process.....	48
3.5.1	Powder Preparation .....	48
3.5.2	Suspension Preparation .....	49
3.5.3	Substrate and Electrode .....	49
3.5.4	Deposition Procedure .....	49

3.5.5	Sintering .....	51
3.6	Characterization.....	52
3.6.1	Fourier Transforms Infrared Spectroscopy (FTIR).....	52
3.6.2	Thermogravimetric Analysis.....	52
3.6.3	Particle Shape and Size Analysis .....	52
3.6.4	Optical Microscopic Inspection.....	52
3.6.5	X-Ray Diffraction (XRD).....	53
3.6.6	Field Emission Scanning Electron Microscope (FESEM).....	54
3.6.7	Energy Dispersive X-Ray Spectroscopy (EDX) .....	54
3.6.8	Atomic Force Microscopy.....	54
3.6.9	Cross Sectional Analysis .....	54
3.6.10	Density.....	55
3.6.11	Micro Hardness and Fracture Toughness .....	56
3.6.12	Nanoindentation .....	57
3.6.13	Bioactivity Test (Wettability).....	57
 <b>CHAPTER 4: RESULTS AND DISCUSSIONS .....</b>		<b>58</b>
4.1	Characterization of Crushed Eggshell as Raw Material.....	58
4.1.1	XRD Analysis of Chicken Eggshell.....	58
4.1.2	FTIR Analysis of Chicken Eggshell.....	59
4.1.3	Thermogravimetric Analysis of Crushed Eggshell .....	61
4.2	Characterization of Calcined Eggshell as Calcium Source .....	62
4.2.1	XRD Analysis of Calcium Oxide Powder.....	62
4.2.2	FTIR Analysis of Calcium Oxide Powder .....	64
4.3	Characterization of As-Synthesized Hydroxyapatite.....	65
4.3.1	XRD Analysis of As-Synthesized Hydroxyapatite .....	66
4.3.2	FTIR Analysis of As-Synthesized Hydroxyapatite .....	68

4.3.3	Microstructural Analysis of As-Synthesized Hydroxyapatite.....	69
4.3.4	Thermogravimetric Analysis of As-Synthesized Hydroxyapatite Powder .....	70
4.3.5	Morphological Analysis of As-Synthesized Hydroxyapatite Powder.....	71
4.4	Characterization of Sintered Eggshell Based Hydroxyapatite .....	72
4.4.1	XRD Analysis of As-Sintered Hydroxyapatite .....	73
4.4.2	FTIR Analysis of As-Sintered Hydroxyapatite Powder.....	75
4.4.3	Microstructural Analysis of As-Sintered Hydroxyapatite.....	76
4.4.4	EDS Analysis of As-Sintered Hydroxyapatite .....	79
4.4.5	Grain Size Analysis .....	80
4.4.6	Bulk Density Analysis.....	81
4.4.7	Linear Shrinkage Analysis .....	83
4.4.8	Vickers Hardness Analysis.....	84
4.4.9	Fracture Toughness Analysis .....	85
4.5	Characterization of Deposited Film of Hydroxyapatite on Titanium Substrate ....	87
4.5.1	Microscopic Evaluation of Coated Surface.....	92
4.5.2	XRD Analysis of Sintered HA Coating .....	94
4.5.3	Microstructural Analysis of Sintered HA Coating.....	97
4.5.4	EDS Analysis of Sintered HA Coating .....	99
4.5.5	Topography Analysis of Sintered HA Coating .....	100
4.5.6	Cross Sectional Analysis of Sintered HA Coating.....	103
4.5.7	Indentation Analysis of Sintered HA Coating.....	105
4.5.8	Wettability Analysis of Sintered HA Coating.....	106
<b>CHAPTER 5: CONCLUSIONS AND FUTURE WORKS .....</b>		<b>108</b>
5.1	Conclusion .....	108
5.2	Suggestions for Future Work.....	110

References .....	111
List of Publications and Papers Presented .....	134
Appendix A .....	137
Appendix B .....	153

Universiti Malaya

## LIST OF FIGURES

Figure 2.1: Schematic of a human bone structure (Rho et al., 1998).....	6
Figure 2.2: Synthesis of hydroxyapatite via natural sources: (a) animal bone; (b) eggshells bio-waste; (c) exoskeleton of marine organisms; (d) naturally derived biomolecules; and (e) biomemberane (Sadat-Shojai et al., 2013). ....	13
Figure 2.3: TEM images of synthesized HA powders derived from (a) wet chemical precipitation and (b) sol–gel synthesis (Ramesh et al., 2015). ....	16
Figure 2.4: Influence of reaction pH, process temperature, and duration of hydrothermal treatment on morphology, phase, and particle size of the calcium phosphate powder (Sadat-shojai et al., 2012).....	18
Figure 2.5: SEM images of hydroxyapatite sintered by (a) conventional sintering and (b) microwave sintering at 1050 °C (Tan et al., 2015). ....	22
Figure 2.6: Schematic diagram of dip coating process (Kunst et al., 2015). ....	24
Figure 2.7: Schematic diagram of electrophoretic deposition method (Khanaki et al., 2015). ....	26
Figure 2.8: Thickness of coating thin films achieved by various deposition techniques (Boccaccini et al., 2015).....	29
Figure 2.9: Schematic diagram of plasma electrolytic oxidation technique (Adeleke et al., 2018). ....	31
Figure 2.10: Schematic of sputter coating method (Tarafdar et al., 2015). ....	33
Figure 2.11: Schematic diagram of pulse laser deposition technique (Azadmanjiri et al., 2016). ....	34
Figure 2.12: Schematic of thermal spray deposition technique (Ahmad et al., 2016)....	38
Figure 3.1: Summary of all process. ....	42
Figure 3.2: Temperature curve of calcinations process. Tr= room temperature and Tc= calcination temperature. ....	45

Figure 3.3: Temperature curve of conventional sintering, employed for coated sample sintered at 1000 °C. $T_r$ =room temperature and $T_s$ =sintering temperature. ....	51
Figure 4.1: XRD pattern of chicken eggshells revealing phase pure $\text{CaCO}_3$ .....	59
Figure 4.2: FTIR spectrum of crushed eggshell.....	60
Figure 4.3: TGA analysis of eggshell powder. ....	62
Figure 4.4: XRD pattern of calcium oxide powder.....	63
Figure 4.5: FTIR spectrum of calcium oxide powder.....	65
Figure 4.6: Figure 4.6: XRD pattern of as-synthesized hydroxyapatite powder. ....	67
Figure 4.7: FTIR spectrum of as-synthesized hydroxyapatite powder. ....	68
Figure 4.8: Micrograph of as-synthesized hydroxyapatite powder.....	69
Figure 4.9: TGA/DTA analysis of eggshell-derived hydroxyapatite powder.....	70
Figure 4.10: TEM micrograph of eggshell-derived hydroxyapatite powder. ....	72
Figure 4.11: XRD signatures of HA samples sintered at various temperatures, (900 °C-1300 °C) revealing fully HA phase. ....	74
Figure 4.12: XRD signatures of HA samples sintered at 1350 °C-1400 °C. The unmarked peaks represents HA phase.....	75
Figure 4.13: FTIR spectrum of as-sintered hydroxyapatite. ....	76
Figure 4.14: FESEM micrographs of eggshell-derived HA sintered at (a) 900 °C, (b) 1000 °C, (c)1100 °C, (d) 1200 °C, (e) 1250 °C, (f) 1300 °C, (g)1350 °C and (h) 1400 °C. ....	78
Figure 4.15: Typical EDX analysis of eggshell-derived HA sintered at 1300°C.....	80
Figure 4.16: The variation of grain size as a function of sintering temperature. ....	81
Figure 4.17: Variation in relative density of eggshell-derived HA samples sintered at various temperatures. ....	82
Figure 4.18: Variation in linear shrinkage of eggshell-derived HA samples sintered at various temperatures. ....	84

Figure 4.19: The effect on sintering temperatures on the Vickers hardness of eggshell-derived HA.....	85
Figure 4.20: Fracture toughness variation with sintering temperature for eggshell-derived HA.....	86
Figure 4.21: Microscopic images of deposited film of hydroxyapatite on titanium substrate via EPD before heat treatment. ....	93
Figure 4.22: Microscopic images of sintered specimen before (a) and after (b) modification. ....	94
Figure 4.23: XRD signatures of coated substrates sintered at various temperatures: (a) 900 °C, (b) 950 °C, (c) 1000 °C and (d) 1050 °C. All peaks corresponded to the HA phase. ....	96
Figure 4.24: FESEM images of HA coating sintered at (a) 900 °C, (b) 950 °C, (c) 1000 °C and (d & e) 1050 °C.....	98
Figure 4.25: Typical EDX analysis of sintered HA coating at 1050 °C. ....	99
Figure 4.26: 3D images of sintered coating surface at a scale of 5 nm <sup>2</sup> .....	100
Figure 4.27: 3D images of sintered coating surface sample according to scale of 10 μm <sup>2</sup> . ....	102
Figure 4.28: The schematic view of surface roughness profile. ....	102
Figure 4.29: FESEM images of the cross-sectional area of HA coated substrate sintered at 1050 °C.....	103
Figure 4.30: FESEM micrograph of HA coated substrate sintered at 1050 °C showing the nature of the bonding at the interface between the HA coating/Ti substrate and compositional analysis across the interface. ....	104
Figure 4.31: Micrograph image of nano-indentation on HA grains (as shown by the arrows) in the field view of 5 μm×5 μm. ....	106
Figure 4.32: Water drops on non-coated surface (a) and coated surface (b). ....	107



## LIST OF TABLES

Table 2.1: Bioceramics classification (Ishikawa et al., 2015). .....	7
Table 2.2: Different forms of calcium phosphates compounds (Eanes, 1988). .....	8
Table 2.3: General information of hydroxyapatite (Zhang, 2013). .....	9
Table 2.4: Comparison of hydroxyapatite ceramic composition vs human bone, dentine and enamel (Ishikawa et al., 2015). .....	10
Table 2.5: Comparison of physical and mechanical properties of hydroxyapatite, enamel and bone (LeGeros, 1993). .....	11
Table 2.6: Different hydroxyapatite structure with modulated shapes (Sadat-Shojai et al., 2013) .....	15
Table 2.7: Influence of pH on mechanical properties of hydroxyapatite (Inthong et al., 2013). .....	19
Table 2.8: Thermal effects on hydroxyapatite (Levingstone, 2008; Berndt et al., 2014). .....	21
Table 2.9: Effective parameters on powder flowability (Freeman, 2007). .....	28
Table 2.10: Advantages and disadvantages of different coating techniques to deposit hydroxyapatite on titanium implants (Mohseni et al., 2015; Choudhury & Agrawal, 2012). .....	39
Table 3.1: List of employed materials and their characteristics.....	44
Table 3.2: Examined coating parameters. ....	50
Table 3.3: JCPDS data reference codes. ....	53
Table 3.4: Descriptions of symbols utilized in density formula. ....	55
Table 4.1: Physical and chemical properties of as-synthesized hydroxyapatite. ....	66
Table 4.2: Examined parameter during deposition process. ....	88

## LIST OF SYMBOLS AND ABBREVIATIONS

$\alpha$ – TCP	:	$\alpha$ – Tricalcium phosphate
$\beta$ – TCP	:	$\beta$ – Tricalcium phosphate
AFM	:	Atomic Force Microscopy
CaO	:	Calcium Oxide
CaP	:	Calcium phosphate
Ca/P	:	Calcium to phosphorus molar ratio
CIP	:	Cold Isostatic Pressing
cp	:	Chemical precipitation
CS	:	Conventional sintering
DCPA	:	Dicalcium phosphate anhydrous
DCPD	:	Dicalcium phosphate dihydrate
EDS/EDX	:	Energy-dispersive X-ray spectroscopy
em	:	Emulsion
EPD	:	Electrophoretic Deposition
FESEM	:	Field emission Scanning Electron Microscope
FTIR	:	Fourier-transform infrared spectroscopy
h	:	Hour
H <sub>3</sub> PO <sub>4</sub>	:	Orthophosphoric Acid
HA/HAp	:	Hydroxyapatite
HIP	:	Hot isostatic pressing
hl	:	Hydrolysis
hth	:	Hydrothermal
IBD	:	Ion Beam Deposition
JCPDS	:	Joint Committee on Powder Diffraction Standards

mch	:	Mechanochemical synthesis
MPa	:	Mega Pascal
MW	:	Microwave sintering
NH <sub>4</sub> OH	:	Ammonium hydroxide
OCP	:	Octacalcium phosphate
PEO	:	Plasma Electrolytic Oxidation
PLD	:	Plasma Laser Deposition
sch	:	Sonochemical
sg	:	Sol-gel technique
SiC	:	Silicon carbide
ss	:	Solid state reaction
TCP	:	Tricalcium phosphate
TEM	:	Transmission Electron Microscopy
TGA/DTA	:	Thermogravimetric Analyzer / Differential Thermal Analyzer
TTCP	:	Tetracalcium phosphate
T.D	:	Theoretical density
Wt. %	:	Weight percent
XRD	:	X-ray powder diffraction

## LIST OF APPENDICES

<b>Appendix A: JCPDS Files</b>	137
JCPDS No. 009-0432 for HA	137
JCPDS No. 37-1497 for CaO	140
JCPDS No. 44-1481 for Ca(OH) <sub>2</sub>	142
JCPDS No. 09-7500 for TCP	144
JCPDS No. 04-1503 for Titanium	148
JCPDS No. 01-5328 for Titanium Oxide	150
<b>Appendix B: Laboratory Apparatus and Equipment</b>	153
Synthesis Process	153
Figure B-1: Synthesis Process including, Titration (a), Filtration (b) and drying(c).	153
Sample Preparation Process	154
Figure B-2: Sample preparation process: weighting machine (a), pressing mould (b) and pressed sample (c).	154
Sintering Equipment	155
Figure B-3: Sintering equipment: Box furnace (a), Tube furnace (b).	155
Characterization Equipment	156
Figure B-4: Characterization equipment: X-Ray diffractometer (a) and Atomic force microscopy (b).	156

## CHAPTER 1: INTRODUCTION

### 1.1 Background

Hydroxyapatite (HA) with chemical formula  $[\text{Ca}_5(\text{PO}_4)_3(\text{OH})]$  is one of the widely researched materials because of its diverse applications especially in biomedical engineering. The biocompatibility nature and the chemical structure of this material being similar to that of hard tissues enables HA to integrate well with natural bone.

One of the major limitation of HA is the low mechanical properties such as hardness and fracture toughness ( $\leq 1 \text{ MPam}^{1/2}$ ) which restrict its usage to low-load bearing applications (Prokopiev & Sevostianov, 2006; Clifford et al., 2017; Pon et al., 2016). Hence, much work is still required to improve the mechanical properties of HA. Such initiatives have focused on improving the synthesis method and the sintering of hydroxyapatite using conventional as well as nonconventional techniques.

The preparation of HA mostly focused on using the hydrothermal, mechanochemical, sol-gel and wet chemical methods. Different starting precursors were used and subjected to a variety of process steps. Nevertheless, in all cases, calcium and phosphate are normally the main composition found in the precursors. For example, the source of phosphate could be from phosphoric acid and the calcium source would be calcium oxide or calcium carbonate.

Calcium oxide can be derived from natural sources such as eggshell, seashell, bovine and chicken bones. Depending on the starting precursors and the method of synthesis, different quality of final product could be produced, particularly resulting in a stoichiometric or nonstoichiometric HA characterized by having different powder morphology and particle size.

One of the way to expand the usage of HA for load-bearing applications would be to coat HA on metallic implant such as titanium and stainless steel. This is another way to achieve the combination of substrate strength and biocompatibility of coated surface which makes the implant viable for load bearing devices (Sadat-Shojai et al., 2013; Hassan et al., 2016; Ferraz et al., 2004; Kazemi et al., 2017). For instance Blind et al. (2005), reported that HA coating allows for quick osteo-integration to take place between the metallic implant surface and bony tissues. According to the literatures, the hydroxyapatite coating could also serve to improve the corrosion resistance of the metallic implant (Stoch et al., 2001; Kwok et al., 2009).

Many coating techniques have been investigated such as plasma spraying, thermal spraying, sputter coating, electrophoretic deposition and dip coating. Surface quality and thickness of deposited film would depend on the coating process. All of these techniques have their advantages and disadvantages. In particular, electrophoretic deposition is one of the favourable method used for hydroxyapatite coating. Simple setup and the ability to apply the coating on complex shape at a desired thickness of coating layer are the main advantages of this process (Zhitomirsky & Gal, 1997; Boccaccini et al., 2010).

In terms of sintering, there are many consolidation methods that can be employed to densify hydroxyapatite which include the pressureless sintering method, hot isostatic pressing and microwave sintering. The pressureless sintering is the most widely used technique although this method requires very slow heating rate and can be time consuming if compared to microwave sintering which takes minutes to sinter the ceramic (Ramesh et al., 2008; Nath et al., 2006; Panyata et al., 2012; Pramanik et al., 2007).

## 1.2 Problem Statement and Aim of Study

Hydroxyapatite is amongst the few biomaterial which is categorized as bioactive, because of its similarity to the structure of human bone, ability to support bone growth and enhancement of osseointegration. However, the major drawback of this biomaterial include low fracture toughness and tensile strength makes it unsuitable for load bearing applications. Particle size, phase purity, stability in high temperature and Ca/P stoichiometry, are some of the important processing parameters that affected the mechanical properties of hydroxyapatite. Using different starting materials and employing various synthesis procedures, could improve the quality of produced powder (Jayakumar et al., 2010; White et al., 2014).

Calcium oxide can be derived from many natural sources such as bovine bone, fish bone, eggshell, coral and sea shells. This natural source can improve the quality of the synthesized powder due to their similarity in their chemical composition when compare to natural bone composition and comprised of some elements such as magnesium, sodium and potassium, which are commonly found in bone structure (Mondal et al., 2012; Sadat-Shojai et al., 2013; Pandharipande & Sondawale, 2016).

Chicken eggshell which is a waste material, consists of about 95% calcium carbonate. Based on the reports, yearly amount of about 8 million tons chicken eggshells produced in the world, which could be recycled to produce calcium for various applications instead of extracting calcium mineral which can be costly and energy intensive process (Abdulrahman et al., 2014; De Angelis et al., 2017).

Hydroxyapatite have been used in orthopaedic, dental and maxillofacial applications, but fabricating complex shapes from hydroxyapatite is another limitation of this material. As such, coating of HA on metallic complex geometry provides an alternative solution for orthopaedic applications (Soballe et al., 1992).

Therefore, the ultimate aim of this research was to incorporate eggshell as the calcium precursor to synthesize hydroxyapatite (HA) powder using a modified wet-chemical method. The eggshell-derived HA was then coated onto titanium substrate and evaluated for potential use in clinical applications.

### **1.3 Objectives**

In the present work, the aim of this study is to produce crystalline and pure hydroxyapatite powder having high thermal stability by using bio-waste chicken eggshells as the calcium source through a modified wet chemical technique. This research investigates the HA phase stability, mechanical properties and microstructural evolution of the synthesized HA when sintered at various temperatures. The second part of the research evaluates the possibility of using electrophoretic deposition (EPD) method to coat hydroxyapatite on titanium substrate. The HA phase stability and morphological evolution of the coated layer when sintered at different temperatures were examined. The main objectives of current research are as follows:

1. To synthesize high quality hydroxyapatite powder derived from bio-waste eggshells using a modified wet chemical technique.
2. To investigate the thermal stability, mechanical properties and microstructural evolution of the eggshell-derived HA at various sintering temperatures.
3. To study the use of electrophoretic deposition technique to coat a thin layer of eggshell-derived HA on titanium substrate.
4. To determine the influence of sintering temperature on the thermal stability and morphological evolution of the coated HA layer at different temperatures.



## 1.4 Thesis Outline

The research is divided into five chapters.

Chapter one includes the background of the research, aim of study, problem statement and main objectives of the work.

Chapter two presents the literature on biomaterials, especially hydroxyapatite, including the different source of calcium used as starting material together with the synthesize techniques. The review on the various sintering methods and coating parameters are also provided in this chapter.

Chapter three describes the research methodology used in this study. The details of powder processing, coating by EPD and the various characterization methods are described in this chapter.

Chapter four presents the results and discussion. The sintering behavior of hydroxyapatite powder and coating are discussed in detail.

Chapter five provides the conclusions of this study and suggestions for future study.

## CHAPTER 2: LITERATURE REVIEW

### 2.1 Introduction

Bone is combination of collagen and apatite which is an active tissue and have supreme ability to regenerate itself. The dominant mineral in the bone is apatite which is almost 70 wt % of the skeletal. The small trace of foreign ions such as, barium, iron, magnesium, potassium, silicon, sodium, strontium, chloride, and fluoride, are observed in the bone lattice structure which are all beneficial to the bone. For instance, a study by Akram et al. (2014) discussed on the need of magnesium ion and sodium ion in bone development. They reported that the presence of these ions could improve osteoblast cell activity and bone metabolism. Based on Dorozkhin (2010), mechanical properties of bone is differs in parts of the body and depends on bone orientation and compartment of bone. Meanwhile, the mechanical properties of the bone is also controlled by porosity, level of mineralization, cortical bone thickness and solid matrix organization (Aoki, 1991; Siddharthan et al., 2009; Rho et al., 1998). Figure 2.1 shows the schematic of human bone which indicates that HA is the main constituent making up the structure.

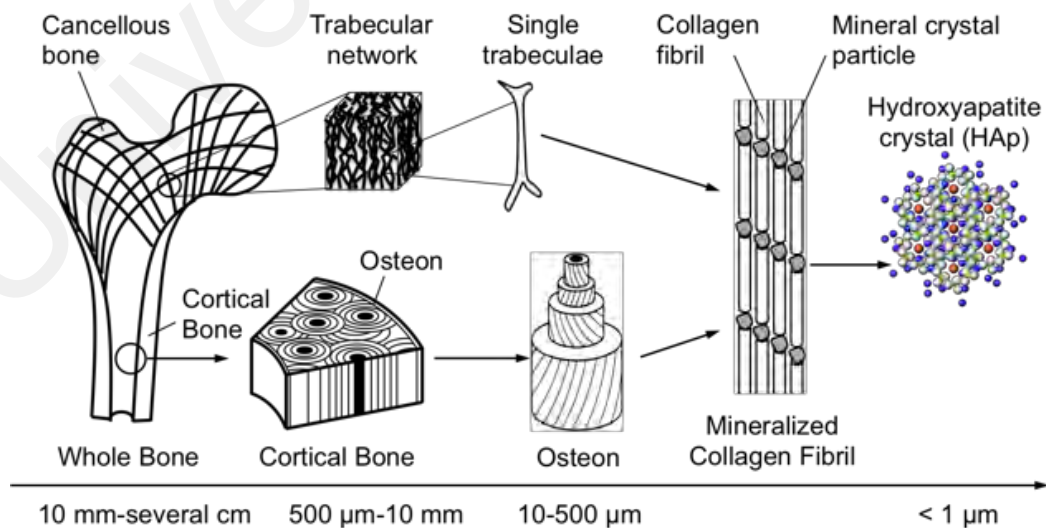


Figure 2.1: Schematic of a human bone structure (Rho et al., 1998).

## 2.2 Bioceramics

Bioceramics which are used clinically in different fields are classified in terms of morphology, composition, applications or behaviour in the human body environment. Bioceramics are classified in different categories such as dental ceramics, biocement, bioinert ceramics, bioresorbable ceramics and bioactive ceramics. Dental ceramics which also known as dental porcelain has been used as artificial teeth or filling material due to their stability in oral environment. Bioinert materials are known as stable ceramics and the one which do not have harmful response in human body. Bioactive material are known as the material which bond straight to bone with no fibrillary connective tissue between the bone and bioceramic. In contrary to bioinert ceramics which remain as foreign implant in the body for lifetime, bioresorbable material will be gradually resorbed in the body. Bioceramics for medical treatment, dental implant, artificial auditory ossicle, bone reconstruction material, artificial tooth root and artificial hip joint are listed as the main examples and application of bioceramics. Although the major limitations of ceramics material are their workability due to their brittle nature and low mechanical properties, but generally, bioceramics demonstrate superior tissue response in compare to metals or polymers. Table 2.1 shows the different classification of bioceramics and popular examples of each categories (Ishikawa et al., 2015; Niakan et al., 2017).

**Table 2.1: Bioceramics classification (Ishikawa et al., 2015).**

<b>Bioceramics Types</b>	<b>Example</b>
Bioinert ceramics	Alumina, Zirconia, Carbon
Bioactive ceramics	Calcium phosphate, Hydroxyapatite, Bioactive glass
Bioresorbable ceramics	Calcium carbonate, Carbonate apatite, Calcium sulphate, $\beta$ – TCP
Dental ceramics	Dental porcelain, Dental cement, Zinc phosphate cement
Biocement	Apatite cement, Bioactive glass cement, Bioactive resin cement

### 2.2.1 Calcium Phosphate

Calcium phosphate is a group of materials which contains calcium ions and phosphate anions or in some cases, oxides and hydroxides as well. Although there are various forms of phosphate such as orthophosphate, pyrophosphate or metaphosphate, but the calcium salt of orthophosphate is the one which is used in biomedical application. Hydroxyapatite, also called apatite, hydroxylapatite and calcium apatite, is in a group of calcium phosphate mineral. Apatite are the main component of hard tissues such as bone and teeth. This mineral known as bioactive ceramic due to its excellent osteoconductivity and good tissue response in human body (Pramanik et al., 2007; Ramesh et al., 2015). Table 2.2 presents the different forms of calcium phosphate together with their chemical formula and Ca/P ratio.

**Table 2.2: Different forms of calcium phosphates compounds (Eanes, 1988).**

Calcium Phosphate	Acronym	Chemical Formula	Ca/P molar ratio
Amorphous calcium phosphate	ACP	$\text{Ca}_3(\text{PO}_4)_2 \cdot 3\text{H}_2\text{O}^a$	0.5
Calcium metaphosphate ( $\alpha$ , $\beta$ , $\gamma$ )	CMP	$\text{Ca}(\text{PO}_3)_2$	0.5
Monocalcium hydrate monohydrate	MCPM	$\text{Ca}(\text{H}_2\text{PO}_4)_2 \cdot \text{H}_2\text{O}$	0.5
Tetracalcium dihydrogen phosphate	TDHP	$\text{Ca}_4\text{H}_2\text{P}_6\text{O}_{20}$	0.65
Heptacalcium phosphate	HCP	$\text{Ca}_7(\text{P}_5\text{O}_{16})_2$	0.7
Calcium pyrophosphate dihydrate	CPPD	$\text{Ca}_2\text{P}_2\text{O}_7 \cdot 2\text{H}_2\text{O}$	1.00
( $\alpha$ , $\beta$ , $\gamma$ ) -Calcium pyrophosphate	( $\alpha$ , $\beta$ , $\gamma$ ) -CPP	( $\alpha$ , $\beta$ , $\gamma$ ) - $\text{Ca}_2\text{P}_2\text{O}_7$	1.00
Dicalcium phosphate dihydrate	DCPD	$\text{CaHPO}_4 \cdot 2\text{H}_2\text{O}$	1.00
Dicalcium phosphate anhydrous	DCPA	$\text{CaHPO}_4$	1.00
Octacalcium phosphate	OCP	$\text{Ca}_4\text{H}(\text{PO}_4)_3 \cdot 3\text{H}_2\text{O}$	1.33
( $\alpha$ , $\beta$ , $\gamma$ ) -Tricalcium phosphate	( $\alpha$ , $\beta$ , $\gamma$ ) -TCP	( $\alpha$ , $\beta$ , $\gamma$ ) - $\text{Ca}_3(\text{PO}_4)_2$	1.5
Oxyapatite	OXA	$\text{Ca}_{10}(\text{PO}_4)_6\text{O}$	1.67
Hydroxyapatite	HAp	$\text{Ca}_5(\text{PO}_4)_3(\text{OH})$	1.67
Tetracalcium phosphate	TTCP	$\text{Ca}_4\text{O}(\text{PO}_4)_2$	2.0

### 2.2.2 Hydroxyapatite

Hydroxyapatite with the chemical formula  $[\text{Ca}_5 (\text{PO}_4)_3 (\text{OH})]$  is a subcategory of bioceramics and known as one of the bioactive ceramic that mimics the composition of natural bone. It has been well documented that hydroxyapatite is the most stable apatite in calcium phosphate group and the nanoparticles of hydroxyapatite (HA) can significantly enhance the bioactivity and biocompatibility of synthetic bioceramics (Sadat-Shojai et al., 2013; Ryabenkova et al., 2017). HA has shown significant potential for use in biomedical application such as dental prostheses or coating on metallic orthopedic implants (Koch et al., 2007). The biocompatibility of hydroxyapatite along with its similarity to the bone, promotes osseointegration and ability to integrate with surrounding hard tissue, thus making it an interesting material for use in clinical applications (Chew et al., 2015; Chlup & Hadaraba, 2009; White et al., 2007; Niakan et al., 2014). Table 2.3 shows the general information and physical properties of hydroxyapatite.

**Table 2.3: General information of hydroxyapatite (Zhang, 2013).**

<b>Category</b>	Phosphate mineral, Apatite group
<b>Formula</b>	$\text{Ca}_5(\text{PO}_4)_3(\text{OH})$
<b>Formula Mass</b>	502.31 g/mol.
<b>Crystal System</b>	Hexagonal
<b>Color</b>	Colorless, white, gray, yellowish green
<b>Cleavage</b>	Poor
<b>Fracture</b>	Conchoidal
<b>Tenacity</b>	Brittle
<b>Diaphaneity</b>	Transparent, Translucent, Opaque
<b>Hardness(mohs)</b>	5
<b>Specific Gravity</b>	3.14-3.21 (measured),3.16(calculated)

As mentioned earlier, beside calcium ions ( $\text{Ca}^{2+}$ ) and phosphorus which are the main components of hydroxyapatite, the small trace of external ions such as; sodium ( $\text{Na}^+$ ), potassium ( $\text{K}^+$ ), magnesium ( $\text{Mg}^{2+}$ ), fluoride ( $\text{F}^-$ ) and chloride ( $\text{Cl}^-$ ) are also observed in the bone lattice structure as well as enamel and dentine. The comparison of hydroxyapatite ceramic composition vs human bone, dentine and enamels are given in Table 2.4. The present of these ions can improve bone development and enhance osteoblast cell activity which is important to prevent bone loss and fragility (Akram et al., 2014; Kehoe, 2008; Driessens & Verbeeck, 1998).

**Table 2.4: Comparison of hydroxyapatite ceramic composition vs human bone, dentine and enamel (Ishikawa et al., 2015).**

<b>Component (wt %)</b>	<b>Enamel</b>	<b>Dentine</b>	<b>Bone</b>	<b>Hydroxyapatite</b>
<b>Calcium (<math>\text{Ca}^{2+}</math>)</b>	36.5	35.1	34.8	39.68
<b>Phosphorus (P)</b>	17.722	17	15.27	18.45
<b>Ca/P molar ratio</b>	1.63	1.61	1.71	1.667
<b>Sodium (<math>\text{Na}^+</math>)</b>	0.5	0.6	0.9	-
<b>Potassium (<math>\text{K}^+</math>)</b>	0.08	0.05	0.03	-
<b>Magnesium (<math>\text{Mg}^{2+}</math>)</b>	0.44	1.23	0.72	-
<b>Fluoride (<math>\text{F}^-</math>)</b>	0.01	0.06	0.04	-
<b>Chloride (<math>\text{Cl}^-</math>)</b>	0.30	0.01	0.12	-
<b>Carbonate (<math>\text{CO}_3^{2-}</math>)</b>	3.5	5.6	7.4	-
<b>Total inorganic</b>	97.0	70.0	65.0	100
<b>Absorbed <math>\text{H}_2\text{O}</math></b>	1.5	10.0	10.0	-

Although hydroxyapatite is highly biocompatible and have good bioactivity but its low mechanical properties limits the usage of this material in load bearing application. Table 2.5, compares the physical and mechanical properties of hydroxyapatite with enamel and human bone. As can be noted in the table, sintered hydroxyapatite have higher density ( $3.156 \text{ g/cm}^3$ ) than natural bone ( $1.5\text{-}2.2 \text{ g/cm}^3$ ) and enamel ( $2.9\text{-}3.0 \text{ g/cm}^3$ ), whilst it has lower fracture toughness ( $0.7\text{-}1.2 \text{ MPam}^{1/2}$ ) when compared to  $2.2 - 4.6 \text{ MPam}^{1/2}$  for bone. The mechanical properties of synthetic hydroxyapatite is dependent on various factors such as the starting precursors, synthesize process and sintering method. For instance, grain size and Ca/P ratio have been reported to have direct effect on the mechanical properties such as fracture toughness and these parameters can be controlled by adjusting the synthesis parameters and sintering condition (Ishikawa et al., 2015; LeGeros, 1993; Muralithran & Ramesh, 2000).

**Table 2.5: Comparison of physical and mechanical properties of hydroxyapatite, enamel and bone (LeGeros, 1993).**

<b>Physical/Mechanical Properties</b>	<b>Bone</b>	<b>Enamel</b>	<b>Hydroxyapatite</b>
<b>Density (<math>\text{g/cm}^3</math>)</b>	1.5-2.2	2.9-3.0	3.156
<b>Relative Density (%)</b>	-	-	95-99.8
<b>Grain Size (<math>\mu\text{m}</math>)</b>	-	-	0.2-25
<b>Bending Strength (MPa)</b>	100-200	-	80-250
<b>Compressive Strength (MPa)</b>	140-300	250-400	270-900
<b>Tensile Strength (MPa)</b>	20-114	-	90-120
<b>Young Modulus (GPa)</b>	10-22	40-84	35-120
<b>Hardness (GPa)</b>	0.4-0.7	3.4-3.7	3.0-7.0
<b>Fracture Toughness (<math>\text{MPam}^{1/2}</math>)</b>	2.2-4.6	-	0.7-1.2

In general, hydroxyapatite is known as a calcium phosphate base (CaP) biomaterial and can be obtained from a variety of starting precursors and through different synthesis methods. Calcium carbonate ( $\text{CaCO}_3$ ), calcium nitrate [ $\text{Ca}(\text{NO}_3)_2$ ], calcium hydroxide [ $\text{Ca}(\text{OH})_2$ ], calcium chloride ( $\text{CaCl}_2$ ), calcium oxide ( $\text{CaO}$ ) and calcium sulfate ( $\text{CaSO}_4$ ) have been used as calcium source and phosphoric acid ( $\text{H}_3\text{PO}_4$ ), ammonium phosphate ( $\text{NH}_4\text{H}_2\text{PO}_4$ ), diammonium phosphate [ $(\text{NH}_4)_2\text{HPO}_4$ ] and potassium phosphate ( $\text{K}_3\text{PO}_4$ ) have been employed as phosphate source. Based on the literatures, calcium also could also be derived from natural source such as eggshell, seashell, snail shell, coral, and from biowaste like bovine, goat bone, chicken bone, fish scale and also from organic matters such as papaya leaves, potato peels, bamboo, grape skin and orange leaves (Hamidi et al., 2017; Sopyan, 2007; Suchanek & Yushimura, 1988).

Hydroxyapatite extracted from biowaste and natural source are more preferred in biomedical application due to availability and existence of some ions naturally in the structure such as  $\text{Na}^+$ ,  $\text{K}^+$ ,  $\text{Mg}^+$ ,  $\text{F}^-$  and  $\text{Cl}^-$  that also exist in natural bone (Bernard et al., 1999; Sadat-Shojai et al., 2013). Figure 2.2 presents the schematic synthesis of hydroxyapatite from various natural sources which are produced via different processes and resulted in dissimilar properties as well as different structures. It has been reported that the starting precursor is one of the parameters which have direct effect on the properties and structure of the derived hydroxyapatite. For example, the viability of producing hydroxyapatite from bovine, caprine and galline bones were investigated by Ramesh et al., (2018) through a heat treatment process. They found that hydroxyapatite derived from bovine bone showed good thermal stability while those produced from caprine showed higher hardness comparable with human cortical bone and the sintered galline bone sample showed higher porosity levels when compared to the other two bone types.



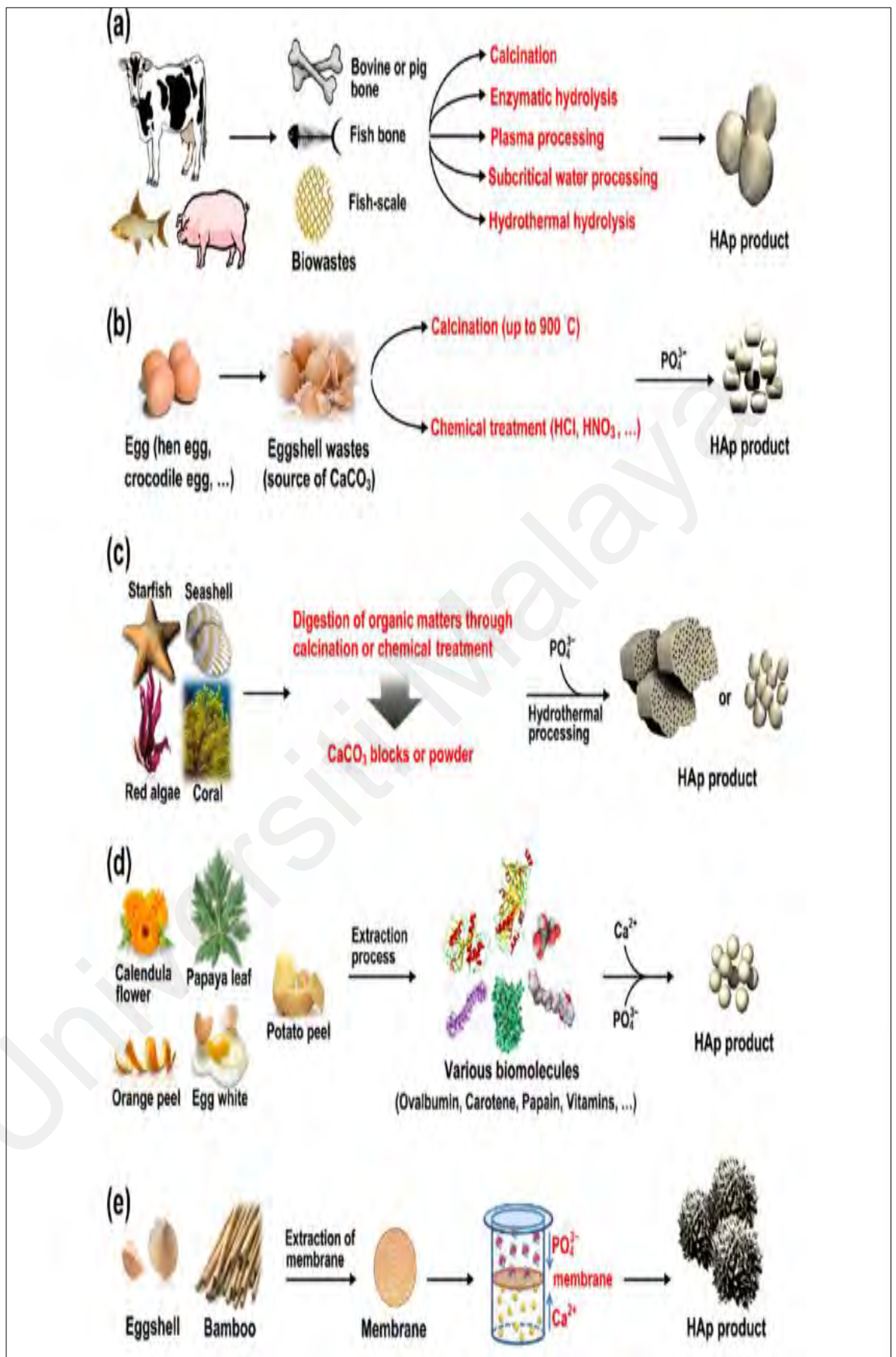


**Figure 2.2: Synthesis of hydroxyapatite via natural sources: (a) animal bone; (b) eggshells bio-waste; (c) exoskeleton of marine organisms; (d) naturally derived biomolecules; and (e) biomemberane (Sadat-Shojai et al., 2013).**












### 2.3 Synthesis of Hydroxyapatite

Over the past years, hydroxyapatite nanoparticles have been synthesized and extensive efforts have been focused on developing production techniques. Based on the literatures, hydroxyapatite can be synthesized through different synthesis methods including mechanochemical synthesis, sonochemical, hydrolysis, emulsion, solid state reaction, hydrothermal, sol-gel technique, and chemical precipitation methods. All these methods can be classified under two main categories, namely wet chemical and dry chemical synthesis (Ferraz et al., 2004; Gergely et al., 2010; Sadat-Shojai et al., 2012).

It is well known that the stoichiometry of synthetic hydroxyapatite and characteristics of final product are dependent on the fabrication technique (Hassan et al., 2016; Martínez-Castanon et al., 2012).

Different hydroxyapatite structure with modulated shapes and sizes according to different synthesis techniques are presented in Table 2.6. According to the literatures, various structure such as irregular, nanosphere, needle like, plate, nanorods bundle, flower like, flake type, fibers bundles, porous microsphere, bowknot and dumbbell structure with particle size range of 5 nm to 200  $\mu\text{m}$  could be produced by employing various synthesis routes (Rad et al., 2014; Hoepfner & Case, 2003; Sadat-Shojai et al., 2012). The most common methodologies to synthesize hydroxyapatite are discussed in following sections.

**Table 2.6: Different hydroxyapatite structure with modulated shapes (Sadat-Shojai et al., 2013)**

Shape	Names in literature	Approx. size range	Synthesis method*
	Irregular, formless, sphere	5nm-200 $\mu\text{m}$	ss, mch, hl, sg, hth, em, sch, cp
	Sphere, microsphere, nanosphere, ball	10nm-1000 $\mu\text{m}$	mch, sg, hth, em, sch, cp
	Rod, needle, tube, filament, fiber, wire, whisker, prism, worm, hexagonal prism, platelet, lath, strip	Length: 10nm-150 $\mu\text{m}$ , diameter: 3nm-50 $\mu\text{m}$ , aspect ratio: 2-1200	ss, mch, hl, sg, hth, em, sch, cp
	Plate, flake, sheet	Length 40nm-50 $\mu\text{m}$ , width: 20nm-35 $\mu\text{m}$ , thickness: 5nm-3 $\mu\text{m}$	hth, cp
	Self-assembled nanorods, bundles of nanorods, oriented bundle, oriented raft, enamel prism like structure, clusters of nanotubes, oriented array of bundled needles, packed nanorods	Length: 200nm-80 $\mu\text{m}$ , width: 100nm-50 $\mu\text{m}$ , diameter: 10nm-12 $\mu\text{m}$	hl, hth, cp
	Dandelion, chrysanthemum, flower, feathery structure, bundle of fibres, self-assembled nanorods, rosette	1-8 $\mu\text{m}$ , organized nanorods of 80-500nm diameter and 600nm-5 $\mu\text{m}$ length	hth, em, cp
	Leaf, flake, sheet, plate	800nm-10 $\mu\text{m}$ , organized nanoplates of 20-100nm thickness	hl, cp
	Flower	700nm-60 $\mu\text{m}$ , organized petals: of 200nm-10 $\mu\text{m}$ width and 180nm-50 $\mu\text{m}$ length	cp, hth
	Porous microsphere, mesoporous sphere	0.5-7 $\mu\text{m}$ , pores of 20-150nm	hth, cp
	Bowknot, self-assembled nanorods	1.5-2.5 $\mu\text{m}$ , organized nanorods of 100-150 nm diameter and 1-2 $\mu\text{m}$ length	cp
	Dumbbell	2-3 $\mu\text{m}$ , organized nanoparticles of $\approx$ 50nm	cp

\* ss- solid state reaction, mch-mechanochemical synthesis, hl- hydrolysis, sg- sol-gel, hth- hydrothermal, em- emulsion, sch- sonochemical, cp- chemical precipitation.

### 2.3.1 Wet Chemical Synthesis

Wet chemical synthesis method is a water base technique with low processing cost and low contamination probability. It is very sensitive process and requires high control on the synthesis process parameters. Hydrothermal method which is generally used to synthesize materials at high temperature, sol-gel technique, hydrolysis, and precipitation are listed as examples of wet chemical synthesis techniques. Stoichiometric hydroxyapatite can be synthesized via mentioned methods. The physical properties of synthesized powder such as particle size and shape are different and depend on the employed method (Afshar et al., 2003; Kweh et al., 1999). For instance, Ramesh and co-workers (2015) produced needle-like particles of hydroxyapatite with an average size of 60–100nm by using the wet chemical precipitation technique. In contrast, while employing the sol-gel as synthesis method the authors produced globular shape particles with an average size of 70-200nm as shown in Figure 2.3.

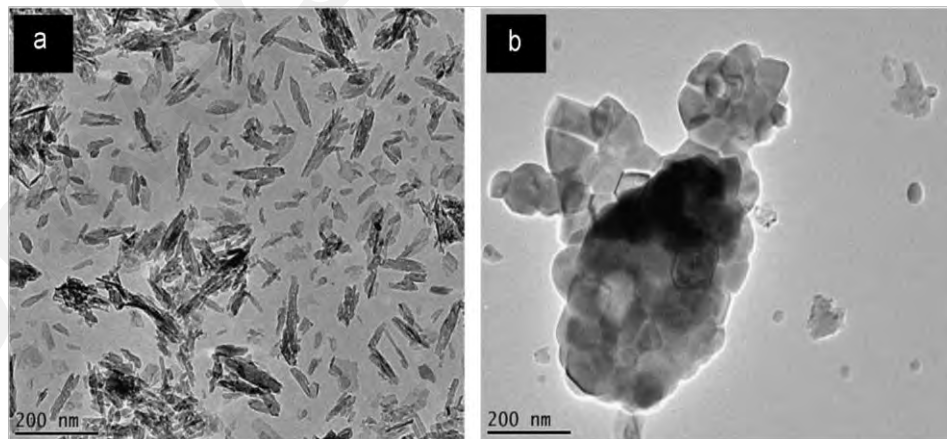


**Figure 2.3: TEM images of synthesized HA powders derived from (a) wet chemical precipitation and (b) sol-gel synthesis (Ramesh et al., 2015).**

In the wet chemical synthesis procedure, even a slight difference in reaction conditions such as reaction temperature, pH, rate of mixing the reactant, stirring rate, reactant concentration, aging time, drying condition and drying temperature can affect the properties of the final powder. The reaction pH is one of the important parameters which should be controlled in synthesizing HA via wet chemical precipitation technique. Orlovskii et al. (2002) used sodium hydroxide or ammonium hydroxide into the HA suspension as adjustment agent, in order to prepare an alkaline medium. Based on the literatures, pH of the solution during synthesis process significantly affected the phase purity, Ca/P ratio, morphology, particle size and mechanical properties of final powder. According to previous researches, the best pH to synthesize phase pure hydroxyapatite via wet chemical method is 9-11. The presence of secondary phase such as tricalcium phosphate have been reported in those studies with lower pH in their HA suspension (Orlovskii et al., 2002; Inthong et al., 2013; Wang et al., 2010). Sadat-Shojai et al. (2012) studied the influence of pH on the properties of calcium phosphate powder. Chemical precipitation followed by hydrothermal processing were employed in their study to synthesize hydroxyapatite. Figure 2.4 summarized their findings on the effect of pH on the phase, particle size and morphology of produced calcium phosphate powder. As can be seen in the Figure 2.4, hydroxyapatite was produced at higher pH level only, and increasing pH values resulted in finer particle size.

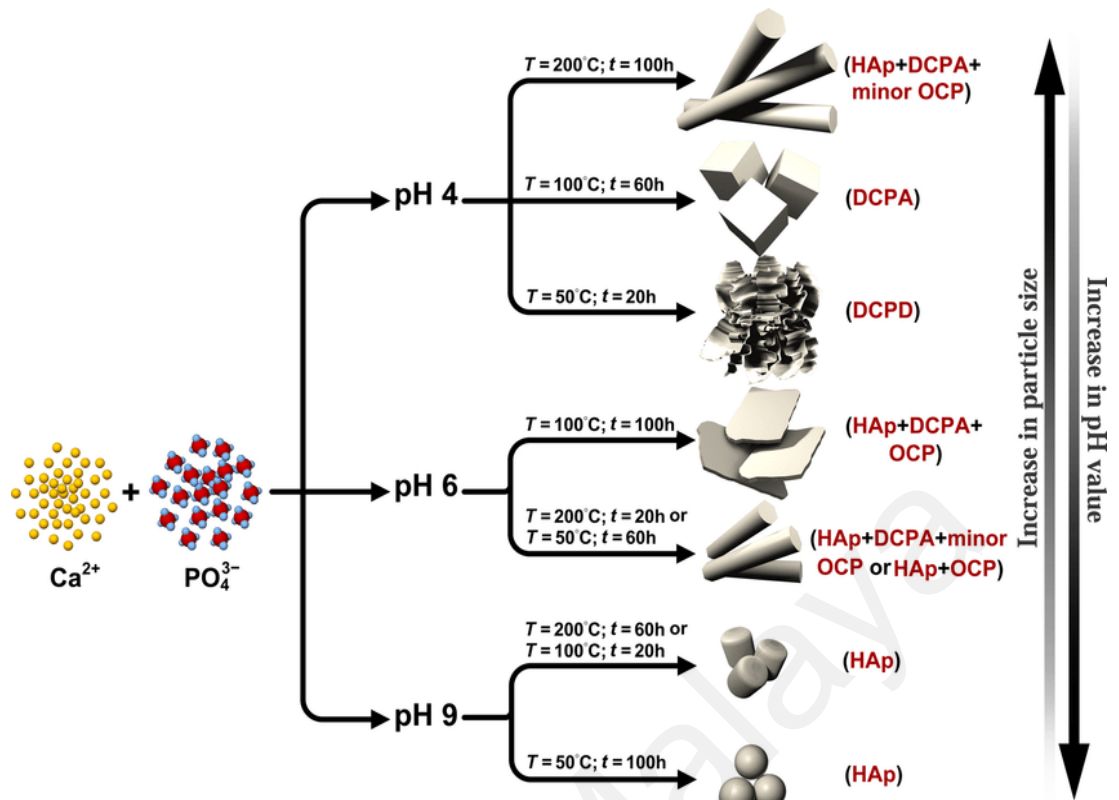


**Figure 2.4: Influence of reaction pH, process temperature, and duration of hydrothermal treatment on morphology, phase, and particle size of the calcium phosphate powder (Sadat-shojai et al., 2012).**

Table 2.7 presents the effect of pH on the mechanical properties of hydroxyapatite synthesised by wet chemical method. Based on the data in this table, density increased with increasing pH from 5 to 9 while the increasing trend in grain size started in the sample with the pH of 6 and continued up to pH of 9. The hardness trend was similar to grain size and reached maximum value when the pH was 9. Based on these results, the authors confirmed that the optimum range of pH (9-10) resulted in desirable properties (Inthong et al., 2013).

**Table 2.7: Influence of pH on mechanical properties of hydroxyapatite (Inthong et al., 2013).**

pH Value	Density (g/cm <sup>3</sup> )	Grain Size (μm)	Hardness (GPa)
5	2.75	2.19	3.12
6	2.82	1.64	3.39
7	2.83	1.72	3.5
8	3.00	5.97	4.63
9	3.04	6.81	6.06
10	2.98	4.34	4.68
11	3.02	2.38	4.67

### 2.3.2 Dry Chemical Synthesis

Dry chemical synthesis methods such as solid state reactions and mechanochemical synthesis are defined by the absence of solvent in hydroxyapatite preparation. In contrary to wet chemical synthesis method which requires high control on the procedure, dry chemical synthesis method does not need precise control condition, hence it is suitable for mass production of crystalline hydroxyapatite (Dorozkhin, 2010; Kehoe et al., 2008; Rhee et al., 2002). High predictability is known as the advantage of dry chemical synthesis methods while long heat treatment time, high calcination temperature and high risk of contamination during milling are main drawbacks of this method. The quality of the initial reagent have a significant influence on the overall characteristic and quality of final product and play an important role in determining the HA phase. Particle shape and size are among the important factor which have a direct effect on density and mechanical properties of the product (Gergely et al., 2010; Hamidi et al., 2017; Ho et al., 2013; Singh, 2011).

## 2.4 Sintering of Hydroxyapatite

Sintering is one of the main techniques for consolidation of hydroxyapatite and producing bulk form of this material (Prokopiev & Sevostianov, 2006). Beside the raw materials and synthetic conditions, the morphology and characteristic of sintered body of hydroxyapatite are also effected by thermal treatment conditions such as sintering method, firing temperature, holding time, heating profile and sintering environment. For instance, based on the researches, the heating time during the sintering process have an effect on density, porosity and grain size. Dasgupta et al. (2013) reported that increasing sintering time led to grain growth and this adversely affected on the mechanical properties such as fracture toughness. It was also reported that the sintering conditions such as the environment and cooling period are very important to prevent oxidation or possible thermal shock (Fang et al., 1994; Ramesh, 2001; Leenakul et al., 2016).

Table 2.8 shows the thermal effects on hydroxyapatite at different heating temperature. Since the reaction temperature is depend on the characteristic of the synthesized materials and firing environment, hence, the heating range is given for each steps instead of exact reacting temperature. As can be seen in the table, heating hydroxyapatite could lead to four observations, I.e. evaporation of water (25 °C-600 °C), dehydroxylation (800 °C-900 °C), decomposition ( $\geq 1050$  °C) and melting of the sintered body which occur at above 1550°C. It is noteworthy that decomposition rate of hydroxyapatite is slowed down when sintered in high humidity atmosphere by preventing dehydration of the OH<sup>-</sup> group from hydroxyapatite matrix (Levingstone, 2008; Berndt et al., 2014; Ramesh et al., 2007).



**Table 2.8: Thermal effects on hydroxyapatite (Levingstone, 2008; Berndt et al., 2014).**

Temperature	Reaction
25 °C-200 °C	Evaporation of absorbed water
200 °C-600 °C	Evaporation of lattice water
600 °C-800 °C	Decarbonation
800 °C-900 °C	Dehydroxylation of hydroxyapatite forming partially or completely dehydroxylated oxyhydroxyapatite
1050 °C-1400 °C	Hydroxyapatite decomposes to $\beta$ – TCP and tetracalcium phosphate
< 1120 °C	$\beta$ – TCP is stable
1120 °C-1470 °C	$\beta$ – TCP is converted to $\alpha$ – TCP
1550 °C	Melting temperature of hydroxyapatite
1630 °C	Melting temperature of tetracalcium phosphate ,leaving behind calcium oxide
1730 °C	Melting of tricalcium phosphate

Conventional pressureless sintering and microwave sintering are known as the main thermal treatment techniques to prepare a solid and dense body of hydroxyapatite which resulted in different density and morphology at the same sintering temperature. Both methods have some advantages and disadvantages, and have been employed based on the applications. Microwave sintering technique is rapid and fast process which preferred in industry for the advantage of energy saving while simplicity and practicality of conventional pressure sintering are the main advantages of this sintering method (Kumar et al., 2012; Meejoo et al., 2006; Nath et al., 2006; Yang et al., 2004). Tan et al. (2015) investigated the effect of sintering techniques on the structure of hydroxyapatite. Figure 2.5 compares the morphology of sintered body of hydroxyapatite at 1050 °C via conventional sintering technique, and microwave sintering method. A relative density of 97% has been reported in their study for sample sintered by microwave method while the conventional sintering showed a lower density of 90.85%. The arrows in the Figure 2.5

are referring to the porosities on the structure of HA sintered via conventional sintering and microwave method.

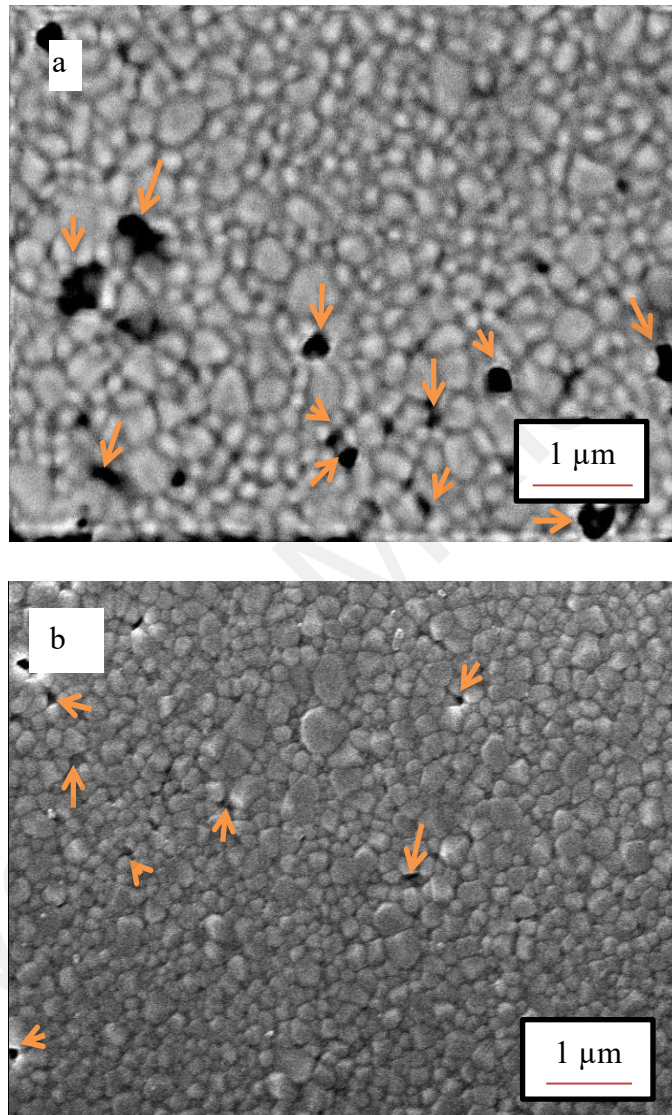


**Figure 2.5: SEM images of hydroxyapatite sintered by (a) conventional sintering and (b) microwave sintering at 1050 °C (Tan et al., 2015).**

Hot Isostatic Pressing (HIP) is one of the method used to produce a dense ceramic by applying simultaneous pressure and temperature. According to literatures, multi direction pressure load on the workpiece applied by HIP resulted in a homogenous structure and uniform properties when compared of uniaxial pressing sample (Palacio, 2017; Laker & Larker, 1991). Porosity and density are important factors in biomedical application. It is known that pores allows cell attachment and bone regeneration in compare to a dense structure which leads to better mechanical properties (Hung et al., 2017; Niakan et al., 2017).

Fu and Batchelor (1998) investigated the effect of hot isostatic pressing on plasma sprayed hydroxyapatite on titanium substrate. Their result showed that HIP was useful to improve the mechanical and physical properties of the coated film. In another study, Hero et al. (1994) inspected the bonding strength of HA coated film on titanium after hot isostatically pressed at 850 °C and 1000 bar with no holding time. The comparison of the coated specimen before and after HIP showed that, by using HIP the bond strength was improved and the HA phase was stable, although some micro cracks was observed after sintering.

## **2.5 Coating Technique**

Hydroxyapatite is a preferred biomaterial for medical application such as orthopaedic and dental use due to its desirable bioactive properties and similar composition to human skeletal. Beside all mentioned advantage of this biomaterial, poor mechanical properties of HA like strength, toughness and brittleness, limited the usage of HA in bulk form. On the other hands, titanium based alloy which are the most common material that used as implants, exhibited excellent mechanical properties and corrosion resistant. Non-toxicity and ability of forming in different shapes also can be listed as the reasons of using this material. Deposition a thin film of HA on bio-substrate has been suggested by researchers

to take the advantage of both material. Some of the most popular techniques for coating, HA onto titanium based alloys are reviewed in this section.

### 2.5.1 Dip Coating

Dip coating is known as a low cost process with simple steps which is able to fabricate high quality coating in few seconds. A uniform coating layer can be deposited even on complex shape substrate in this system. Hence, this method is among the popular deposition technique in laboratory application and industry. The process of dip coating is shown in Figure 2.6. As can be seen in the diagram, the whole process is summarized by immersing substrate into solution, holding there and withdrawing. The process would be complete by drying the wet liquid film which was deposited on substrate and finished by sintering if necessary.

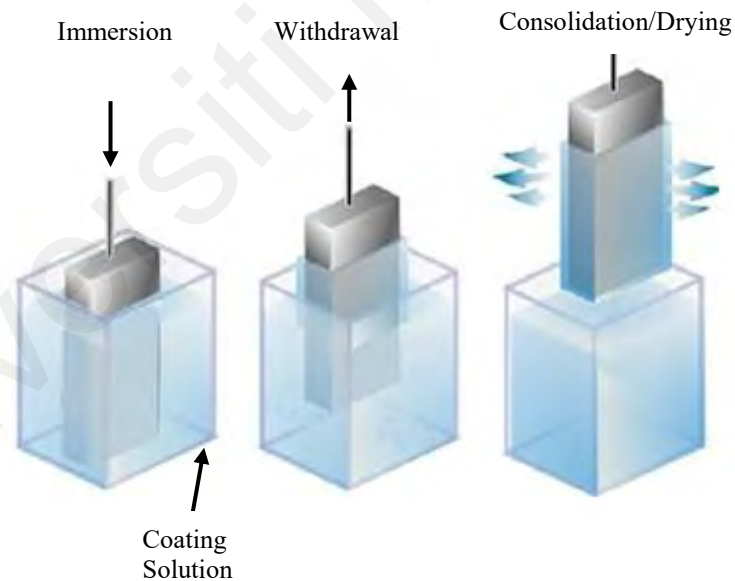


**Figure 2.6: Schematic diagram of dip coating process (Kunst et al., 2015).**

Deposition of hydroxyapatite can be done through dip coating technique. The formation of homogenous thin film of hydroxyapatite on metal substrate has been reported with thickness ranging from 50 $\mu$ m to 500 $\mu$ m (Mohseni et al., 2014). The

thickness of coated layer can be controlled by changing the concentration of HA solution, and also by changing the speed rate of deposition process (immersion-withdrawal). For instance Li et al. (1996) reported a thickness of 10  $\mu\text{m}$  by using a solution having 1.5 wt% HA concentration while the thickness increased significantly up to 200  $\mu\text{m}$  by increasing the concentration of HA in solution to 10 wt.%. The researchers studied the bone tissue reaction of dip coated hydroxyapatite on titanium as bone replacement. For this purpose they had coated hydroxyapatite on titanium and implanted the samples into dog femur. After four weeks of implantation they have found that new bone formation was observed around the coated material. The coated HA produced by dip coating method needs further heat treatment at high sintering temperature, thus the appearance of crack formation in deposited film in some reports could be due to the mismatch of thermal expansion between coated surface and substrate. Mavis and Tas (2000) studied the characteristic of HA deposited film on metal substrate. They reported that, there was no sign of decomposition in the coated layer or reaction between deposited layer and substrate despite applying high sintering temperature. It is worth mentioning that the necessity of applying high temperature would induced grain coarsening and hence lowers the mechanical properties of the final coating (Lacefield, 1988; Li et al., 1996; Choudhury & Agrawal, 2012).

### **2.5.2 Electrophoretic Deposition**

Electrophoretic coating technique which is also known as electrophoretic deposition (EPD), is an electrical based coating method to produce ceramics thin film on metallic substrates. This technique is one of the most attractive coating technique for researchers especially in biomedical applications due to its simple setup, cost effective process, ability to apply on complex shape and ability to apply on large size parts. The possibility to coat different materials beside high rate of control on coating parameters, which leads to achieving desirable structure of final products, can be listed as the benefits of using this

coating method. The electrophoretic deposition technique has innumerable applications and have been employed to fabricate layered ceramics. Deposition of thin and thick film coating of different category of materials such as nanocomposite, hybrid materials and fiber reinforced composite have also been done via this technique (Anne et al., 2006; Besra et al., 2007; Boccaccini et al., 2002; Boccaccini et al., 2008). Figure 2.7 shows the schematic diagram of electrophoretic deposition process. As can be seen in the image, the mechanism of this coating process is based on the migration of suspended nanoparticles of a colloidal solution from charged electrode, and deposition on cathode as substrate by using a direct current power supplier to produce a layer of suspended nanoparticles as coating film (Ferrari & Moreno, 1998; Boccaccini et al., 2010; Corni et al., 2008; Khanaki et al., 2015).

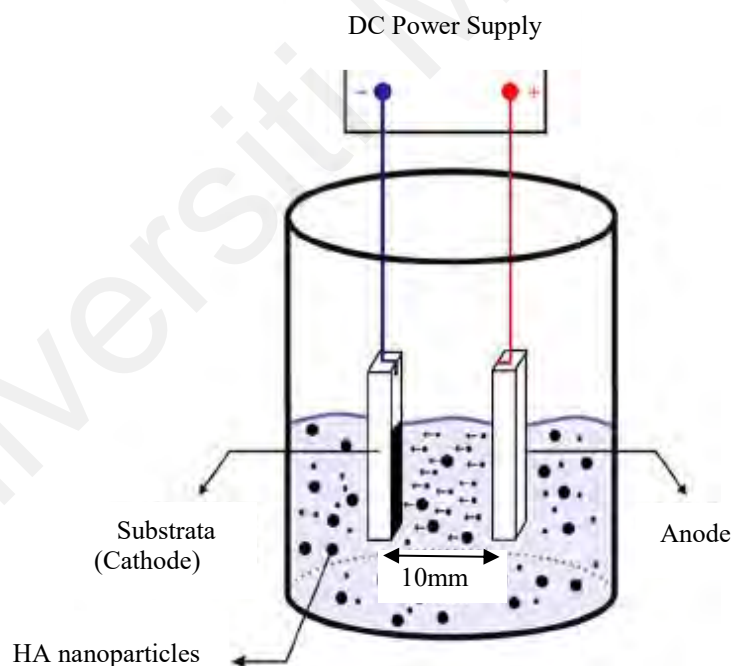


**Figure 2.7: Schematic diagram of electrophoretic deposition method (Khanaki et al., 2015).**

There are many parameters that can affect the quality and structure of final coatings. The setup such as the electrodes distance, as well as solution concentration, solvent type,

pH, coating time, drying process, post heat treatment process, coating material density and particle size, conductivity of electrodes together with electrical parameters such as applied voltage or current are highlighted in the literatures as the main parameters controlling the characteristics and properties of deposited film. All of the mentioned parameters should be optimized to attain a uniform and well bonded coating product (Zhitomirsky & Gal, 1997; Kruger et al., 2004; Moreno et al., 1998; Moritz, 2006). Besides these parameters which are mainly related to preparation stage and setup of deposition process, the physical properties of coating material also should be considered in the coating process. Physical properties of the coating material such as particle size, particle shape, size distribution and density of the powder are amongst the parameters that influence the mobility of charged particles and powder flowability in the precipitating slurry. The physical properties of hydroxyapatite are depended on the synthetize route parameters such as, calcination temperature, reaction pH, or even drying temperature of synthesized powder. For instance, Inthong et al. (2013) synthesized hydroxyapatite via wet chemical process. They found that low pH value of 5 resulted in lower sintered density of about  $2.75\text{g/cm}^3$  while they obtained density of  $3.02\text{g/cm}^3$  by increasing the pH value to 11. The improvement density also resulted in an overall improvement in the mechanical properties of the synthetic hydroxyapatite (Inthong, 2013; Keohe et al., 2008; Presscott et al., 2000). Some of the variables which could influence on the powder behavior in the slurry are summarized in Table 2.9.

**Table 2.9: Effective parameters on powder flowability (Freeman, 2007).**

<b>Powder/Particles variables</b>	<b>External factors influencing powder behavior</b>
Particle size	Flow rate
Powder/Particle size distribution	Compacting condition
Particle shape	vibration
Surface texture	Temperature
Cohesivity	Humidity
Surface coating	Electro-static charge
Particle interaction	Aeration

It is known that the coating thickness of thin film is one of the important factors in coating process which have a direct effect on the quality of coated layer. Based on literature, thicker coating film showed better mechanical properties in comparison to thinner film; however increasing the thickness could cause delamination or weak bonding between the substrate and deposited film. Hence, possibility of producing a uniform thin layer at a wide range of thickness via EPD makes this technique more desirable especially in orthopaedic or dental application. Figure 2.8 presents a typical thickness range of biomaterial coated film obtained by various coating methods in comparison with electrophoretic deposition technique. Based on the graph, electrophoretic deposition technique is able to produce a wide range of thickness which is more relevant for orthopaedic applications when compare to other deposition methods (Oetzen & Clasen, 2006; Boccaccini et al., 2015; Drevet et al., 2016).



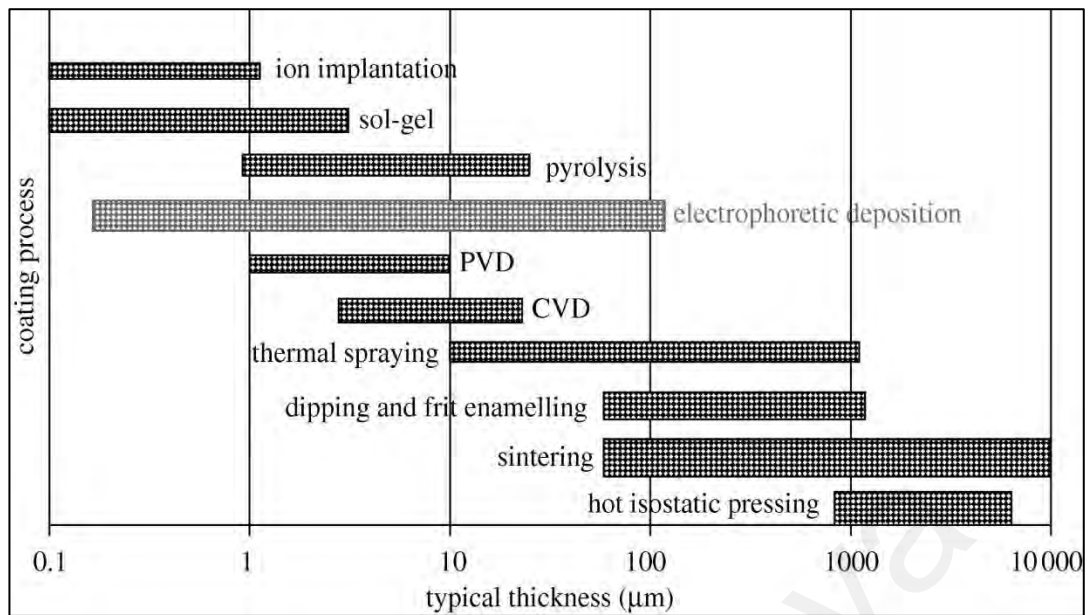


**Figure 2.8: Thickness of coating thin films achieved by various deposition techniques (Boccaccini et al., 2015).**

Various dispersing media such as water, acetone and ethanol are commonly used as solvent in electrophoretic deposition process, which can affected the homogeneity and uniformity of deposited film due to their effect on coagulation rate (Sardar et al., 1993; Zhang et al., 1994). A wide range of metallic substrate such as titanium, titanium alloys, stainless steel, aluminium and brass have been considered for electrophoretic deposition of hydroxyapatite but titanium base substrate is more preferred as implant material due to the lower thermal expansion when compared to other mentioned material (Andreiotelli et al., 2009; Soballe et al., 1992; Thair et al., 2011). The process of coating via electrophoretic deposition method has been done at room temperature, hence, some post thermal treatment such as annealing or sintering is needed to densify the coated layer and improve the mechanical properties of the fabricated product. On the other hand, thermal treatment of deposited specimen at high sintering temperature would resulted in cracks formation on the deposited thin film due to thermal expansion mismatch between the metallic substrate and coated material (Gleiter, 1992; Siegel et al., 1988; Yamashita et al.,

1998). Overall, electrophoretic deposition of hydroxyapatite on metallic substrate can be mentioned as a good candidate to fabricate implants for biomedical applications accordingly to high rate of control on coating parameters when using electrophoretic coating deposition technique compared with other coating methods.

### **2.5.3 Ion Beam Deposition**

Ion beam deposition (IBD) technique is a bombardment base technique of physical vapor deposition system and used for surface modification of ceramics and metals. The combination of ion beam bombardment with specific energy ion beam is done in a vacuum chamber for the purpose of coating via ion beam assisted deposition technique. There are many parameters such as ion energy, ion beam current density, ion species, coating material, sputtering rate or evaporation rate which can influence the structure, chemical properties, mechanical properties and also composition of the deposited coating thin film. IBD is also introduced as an alternative technique for plasma spray coating method to produce more permanent bone bonding hydroxyapatite coating (Park et al., 2005; Cui et al., 1997; Choi et al., 2000; Nelea et al., 2002).

### **2.5.4 Plasma Electrolytic Oxidation**

Plasma electrolytic oxidation (PEO) is an electrochemical coating method to deposit a thin film of bioceramics such as hydroxyapatite onto metallic implant surface. The schematic of PEO system is shown in Figure 2.9. Electrochemical parameters such as current, voltage, density, electrolyte composition and immersion time can affect the properties of the final coating produced by PEO method. Based on the literatures, reasonable adhesion strength, controllable thickness and capability to apply on complex shape implants can be listed as advantage of this coating technique for use in biomedical application. Moreover, coating of hydroxyapatite on titanium implant via this technique can result in a thick layer of HA with acceptable porosity which favour its use in dental

surgery (Lugovskoy & Lugovskoy, 2014; Clyne et al., 2018; Adeleke et al., 2018). Hwang et al. (2018) found that the pore size of HA coating could also be controlled by using PEO and was dependent on the electrolyte concentration and the particle size of coated powder.

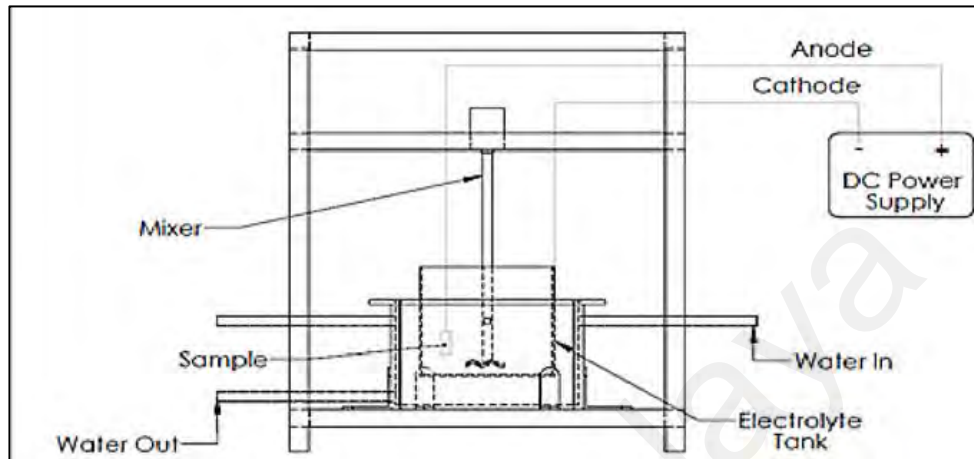


**Figure 2.9: Schematic diagram of plasma electrolytic oxidation technique (Adeleke et al., 2018).**

In another research, PEO method was employed to coat hydroxyapatite on titanium substrate increasing immersion time which led to increasing the amount of apatite induced at the PEO coated surface (Durdu et al., 2016). Similarly, Dzhurinskiy et al. (2016) prepared HA coated titanium via PEO technique. They reported that a porous network HA layer was formed uniformly over the entire surface of the substrate. The PEO HA coated sample resulted in higher corrosion resistance compared to the uncoated sample and could provide a bioactive layer to enhance implant surface bioactivity and osseointegration.

### 2.5.5 Plasma Spraying

Plasma spray coating is the most frequently investigated technique that has been employed for the fabrication of hydroxyapatite coating. Coated HA via plasma spray coating method is reported as biocompatible and also able to bond directly to the bone. According to De Groot et al. (1987), in vivo study of plasma-coated HA implant exhibited similar histological reaction when compared to bulk hydroxyapatite material (Sun et al.,

2001). In plasma spray coating system, the ionized inert gas is used to melt the metal or ceramic powder which is used as coating precursor, and in second stage of coating process, the molten material is sprayed onto the substrate surface (Herman, 1988). There are many parameters such as working distance between nozzle and surface which can affect the coated layer characteristics. For instance, Vahabzadeh et al. (2015) found that a low crystalline HA phase with high solubility was formed by decreasing the working distance between the spray nozzle and substrate surface from 100 mm to 90 mm. A multilayer coating could also be produced by plasma spraying technique. Hahn and Palich (1970) have designed a double layer coating to prevent coating delamination and to provide a strong adherent bond to the hydroxyapatite. They employed plasma spray technique in their study to combine titanium alloy and hydroxyapatite as coating material while the first layer of porous titanium and a second layer of hydroxyapatite were deposited on implant and placed in sheep femora for 26 weeks. They found that the Interface shear strengths increased when compared to uncoated implant. Other advantages of plasma spraying include quick deposition rate and ease of application makes it a favorable choice among others available coating techniques (Herman, 1988; Lemons, 1988; Rakchat et al., 2017; Landor et al., 2007).

#### **2.5.6 Sputter Coating**

Deposition of thin film on substrate can be done thru different coating process which are based on physical, chemical or electrical principals. Sputter coating is a type of physical vapor deposition technique which is used for sputtering to deposit a layer of coating material on substrate. A schematic diagram of sputter coating is shown in Figure 2.10. As can be seen in the diagram, the operation of this procedure involves ejecting material from a source which is called target by utilizing inert gas such as argon, neon, krypton or xenon, and sputtering onto substrate to deposit a thin film coating.

Homogenous thin film coating with uniform thickness in the range of  $0.02\ \mu\text{m}$ – $3\ \mu\text{m}$  can be deposited via sputter coating technique (Tarafdar et al., 2015; Mohseni et al., 2015)

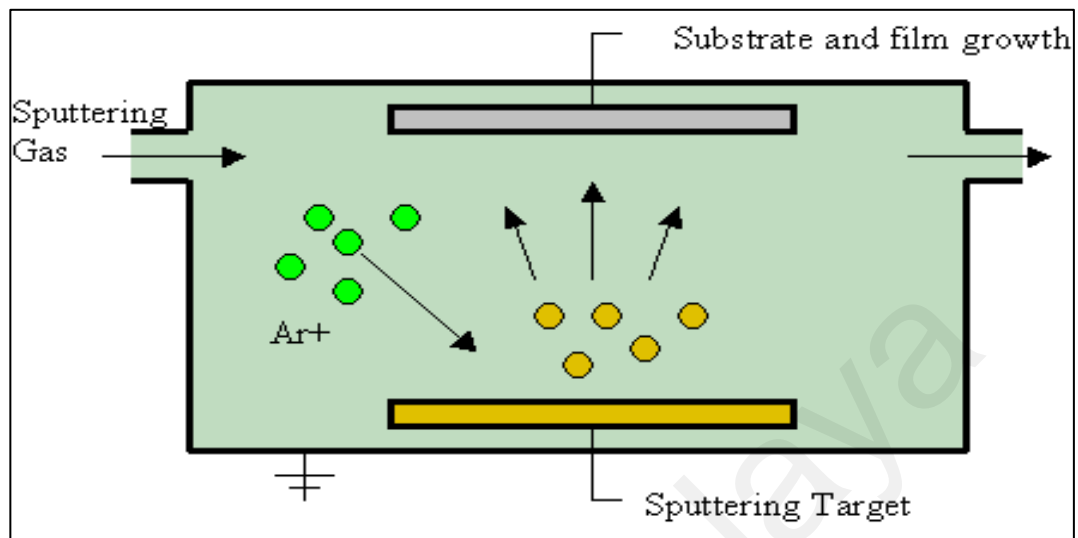


**Figure 2.10: Schematic of sputter coating method (Tarafdar et al., 2015).**

Successful deposition of hydroxyapatite thin film on titanium was reported in the literatures, however for some of the ceramic targets such as hydroxyapatite and other calcium phosphate materials, difference in chemistry of deposited layer and bulk target was also reported after coating process (Lacefield et al., 1990; Ong et al., 1991; Ozeki et al., 2000).

From the findings in the literatures, although the deposition of hydroxyapatite on titanium substrate was reported to have highest adhesion strength amongst other coating methods. The low crystallinity of deposited hydroxyapatite which resulted in higher dissolution rate of the coated film in the body is a disadvantage of this coating process (Mohseni et al., 2015). Some factors such as thermal treatment and discharge radiofrequency power can also affect the deposited film characteristics. Van Dijk et al. (1995) prepared amorphous thin film by sputter coating at low-discharge radiofrequency power, while crystalline hydroxyapatite thin film was attained when high-discharge

radiofrequency power was utilized. Other researchers have shown that post-deposition treatment on sputtered hydroxyapatite coatings can also improve the osseointegration rate with hard tissues (Yang et al., 2005; Ivanova et al., 2016).

### 2.5.7 Pulse Laser Deposition

Pulse laser deposition is another type of physical vapor deposition which use laser as source of energy to deposit nanoparticles from a target onto substrate in a vacuum chamber. This technique is known to be clean and rapid process to coat single layer or multilayer thin films on substrate by ejecting material from target under controlled condition. The surface modification can be done by optimizing the process parameters such as substrate temperature, laser parameters and surface temperature. The schematic diagram of pulsed laser deposition technique is given in Figure 2.11. The process of pulsed laser deposition is include plasma creation, laser interaction with the bulk target material, ablation of the coating material, deposition of ablated particles on substrate and growth of the deposited thin film on the surface (Mroz et al., 2015; Koch et al., 2007).

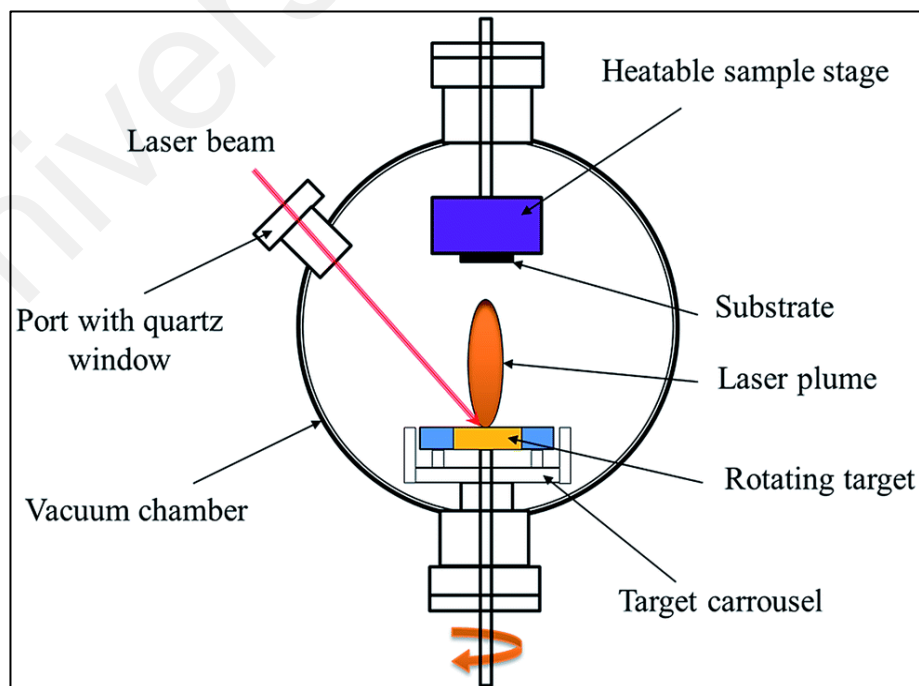


**Figure 2.11: Schematic diagram of pulse laser deposition technique (Azadmanjiri et al., 2016).**

The major issue of pulse laser deposition technique is splashing of the particulates deposition on the coated layer while producing multilayer coating using different materials as well as ability to control the coating parameters and fabricating of high crystalline film are benefits of employing this technique for coating (Kuppuswamy, & Ganesan, 2016). Nishikawa and Umatani (2017) investigated the effect of the pulse repetition rate of the ablation on surface density of coated film. Based on the topographical analysis, they have concluded that the lower pulse repetition rate led to decreased in surface protrusion density.

Other study by Wang et al. (1997) discussed on similar stoichiometry of hydroxyapatite in terms of coated thin film and bulk target. They employed pulse laser deposition technique to coat hydroxyapatite on titanium alloy substrate. They commented that the stoichiometry of the coated film was similar to the target, suggesting that the hydroxyapatite was stable after deposition.

Based on the literatures, pulse laser deposition technique have been used to coat hydroxyapatite on metallic substrate and found to be favorable due to easy control on the structure of the material. Moreover, the surface roughness and adhesion of hydroxyapatite thin film attained by employing this coating method, together with high crystallinity of the deposited layer makes it a suitable choice in coating dental and orthopedic implants (Blind et al., 2005; Chen et al., 2018). According to current researches, the amorphous structure of hydroxyapatite thin film can be transformed to crystalline structure by applying post heat treatment on the sample to improve the bioactivity and mechanical properties of the coated layer. For instance, Dinda et al. (2009) deposited hydroxyapatite on titanium alloy substrate and they restored the crystalline structure of HA by annealing the as-deposited amorphous film at 300 °C.

### **2.5.8 Sol-gel Coating**

Sol-gel method is one of the most prevalent techniques employed to coat hydroxyapatite on metallic implants due to their ability to deposit a well adherence coating film and ease in processing. These parameters have positive effect on the coating performance and the surface topography. The process of deposition via sol-gel coating technique is based on the formation of solid material from a homogenous solution, and can be generally compared with dip coating method. The stages in sol-gel coating method includes: (a) preparation of a solution which is a mixture of precursor and solvent, (b) using a reagent like water to convert the solution to a sol form shape and adding condensation agent in order to make a gel form which is an important stage in coating of hydroxyapatite, (c) shaping the thin film from the gel and sintering the coated film. Chemical composition of the starting material, calcination temperature, number of coated layer and substrate type, are the parameters that have an effect on the characteristics of final product (Kunst et al., 2015; Olding et al., 2001; Ramesh et al., 2015; Troczynski et al., 2001). Gross et al. (1998) employed sol-gel technique to coat hydroxyapatite on titanium substrate and achieved HA coating with average grain size of 50 nm after heat treatment. Based on their finding, oxidation and phase transformation of the substrate was started when sintered at 800 °C. Based on their finding, biocompatibility of resulted coating and adhesion strength were mentioned as the major issues of using sol-gel coating.

### **2.5.9 Thermal Spray**

Generally, the purpose of coating is to improve the performance of substrate by providing functional surface with coated material. Thermal spray technique can be used to coat different types of material such ceramics or metal and different forms of materials such as powder, wire and rod form. Figure 2.12 shows the schematic diagram of thermal spraying deposition method. A typical thermal spray system consists of spray gun, feeder,



and media supply (gas), and control consoles. Noted coating technique is based on heating coated material to a molten state and spraying toward the substrate surface which can be generally compared with plasma spraying deposition technique. The type of energy source that used for heating coated material is different in these two methods. Many types of thermal spraying process such as electrical arc spraying, flame spraying, plasma arc spraying, warm spraying, high velocity air fuel coating spraying and detonation spraying are identified to date. Thermal spray coating is more known for industrial application as a technique to increase corrosion, erosion, abrasion, cavitation, wear, heat and chemical resistance of fabricated parts (Heimann, 2006; Yang et al., 2005; Liang et al., 2004). Thermal spraying of hydroxyapatite on implants with different parameters values can result in different quality of coated film. Many parameters such as spraying distance, powder feeding rate, and inert gas composition are highlighted in the literatures as important factors in thermal spray coating procedure which could affect the quality of final product (Shunyan et al., 2000; Hamdi et al., 2000; Hsiung et al., 2012). Liu et al. (2018) employed this technique to deposit hydroxyapatite on titanium substrate and produced potentially bioactive bone-regeneration implants. The thermal sprayed hydroxyapatite coating film was reported biocompatible and adhered well to the substrate. Although, the appearance of cracks and lack of uniformity in coated film is reported as limitation of using this technique for biomedical application, but, the in vitro test in their study demonstrated, that the coating of porous thin film with this method was enhance cell attachment and increased the cell proliferation on hydroxyapatite thin film when compared to uncoated implants (Liu et al., 2018; Mohseni et al., 2014).

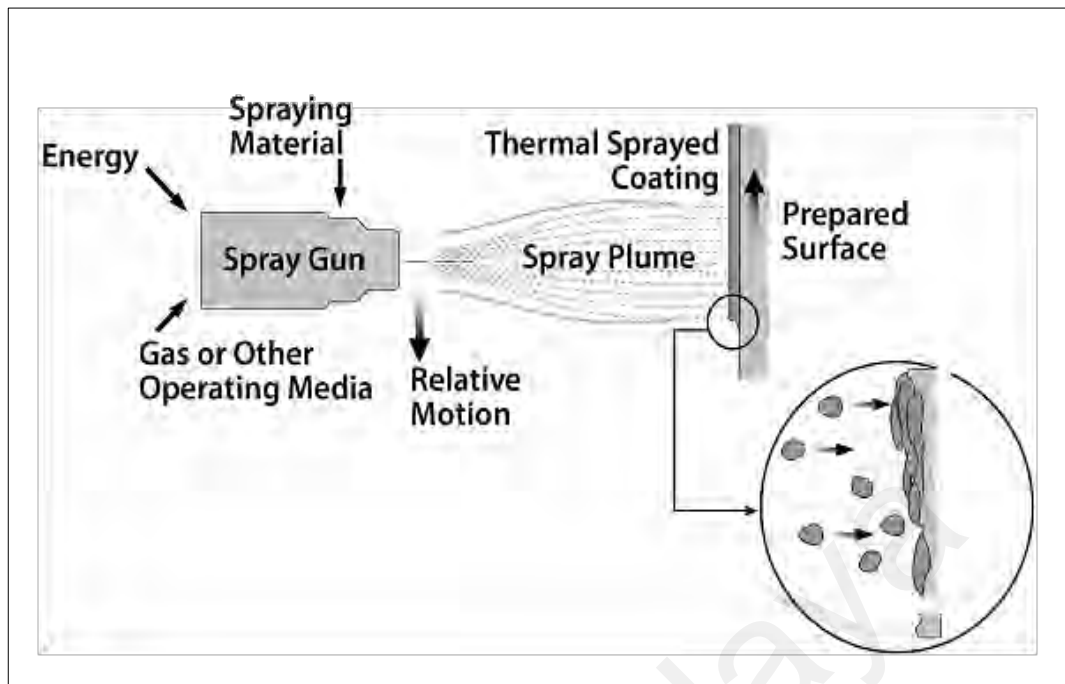


**Figure 2.12: Schematic of thermal spray deposition technique (Ahmad et al., 2016).**

## 2.6 Comparison of Coating Techniques

Several coating techniques have been used to deposit hydroxyapatite on metal implants, but some of them are more popular due to the application and quality of final product. Common techniques such as, dip coating, electrophoretic deposition (EPD), ion beam deposition (IBD), plasma electrolytic oxidation (PEO), plasma spraying, pulsed laser deposition (PLD), sputter coating, sol-gel technique and thermal spraying method, which are more prevalent to deposit hydroxyapatite on titanium implant were reviewed. Each of these methods reported to have some benefits such as low process cost, ease in processing or homogeneity of coating film or limitation like difficulty to produce crack free thin film. The advantages and disadvantages of each methods together with the thickness range of deposited film, are summarized in Table 2.10 (Mohseni et al., 2015; Choudhury & Agrawal, 2012).

**Table 2.10: Advantages and disadvantages of different coating techniques to deposit hydroxyapatite on titanium implants (Mohseni et al., 2015; Choudhury & Agrawal, 2012).**

<b>Coating Technique</b>	<b>Thickness</b>	<b>Advantages</b>	<b>Disadvantages</b>
<b>Dip Coating</b>	0.05 mm – 0.5 mm	Inexpensive, high surface homogeneity, rapid and fast coating procedure, applicable on complex substrate	Appearance of cracks, requires secondary thermal treatment at high sintering temperatures, thermal expansion mismatch
<b>Electrophoretic Deposition</b>	0.02 mm – 2.0 mm	Simple setup, low cost, uniform coating thickness, high degree of control on coating thickness and morphology, rapid deposition rate, applicable on complex substrate, high adhesion, good mechanical strength	Difficult to produce crack-free coatings, requires high sintering temperatures, decomposition of hydroxyapatite during sintering
<b>Ion Beam Deposition</b>	<0.03 $\mu$ m	Low temperature process, high adhesion, high reproducibility and reliability	Appearance of cracks on coated surface
<b>Plasma Electrolytic Oxidation</b>	20 -200 $\mu$ m	Cheap, simple process setup, can apply on complex shape, high wear resistance, corrosion resistance	Long treatment time and high polarization frequencies needed to get HA phase,
<b>Plasma Spraying</b>	<20 $\mu$ m	Rapid deposition, fast bone healing, sufficiently low cost, less risk for coating degradation	Unable to produce complete crystalline HA coating, high temperature procedure, grain growth of substrate and phase transformation due to high temperature, poor adhesion, non-homogeneity in coating density, alteration of hydroxyapatite structure due to coating process

<b>Pulse Laser Deposition</b>	0.05 $\mu\text{m}$ – 5 $\mu\text{m}$	Uniform coating thickness on flat substrates, dense and porous coating, ability to produce multilayer coating with different material, ability to produce high crystalline HA coating, high degree of control on deposition parameters	expensive, need surface pre-treatment, lack of uniformity
<b>Sputter Coating</b>	0.02 $\mu\text{m}$ – 3 $\mu\text{m}$	Homogenous coating, high adhesion, uniform deposition thickness, high adhesion, dense coating,	Line of sight technique, cannot coat complex substrates, produces amorphous coatings, expensive, low crystallite which accelerate the fil dissolution in the body
<b>Sol-gel</b>	0.1 -2 $\mu\text{m}$	simple deposition method, can coat complex shapes, high purity, low processing temperatures, relatively cheap, high corrosion resistant, good adhesion	Some processes require controlled atmosphere processing, hard to control porosity, not suitable for industrial scale, expensive raw materials, high permeability, low wear resistance,
<b>Thermal Spray</b>	30 $\mu\text{m}$ – 200 $\mu\text{m}$	Low cost, high deposition rates	Crack appearance, lack of uniformity, delamination of coated film, low porosity, line of sight technique, high temperatures induce decomposition, rapid cooling produces amorous coating

**Table 2.10, 'continued'**

## 2.7 Summary

This literature gathers the brief overview of biomaterials, especially hydroxyapatite, including various synthesize techniques and also discussed on different calcium source as starting material together with the parameters which affected on final product. Besides that, various process of synthesizing hydroxyapatite such as wet methods or dry method along with thermal treatment process and the effect of varying the parameters on phase stability and sinterability of produced hydroxyapatite powder has explained. A review on the methods used for coating HA has been presented in this chapter.

Universiti Malaysia

## CHAPTER 3: MATERIALS AND METHODS

### 3.1 Introduction

As mentioned earlier, this research is involve two main parts. The synthesis of hydroxyapatite from natural source and sintering at different temperature and the coating of derived HA on titanium substrate via electrophoretic deposition method. Samples were evaluated by physical and mechanical properties, such as density and microhardness and also by structural and thermal analysis like FESEM and TGA/DTA. Detail of materials specification and techniques of each steps as well as characterization methods are presented in this chapter. The flowchart showing the experimental procedure adopted in this research is given in Figure 3.1.

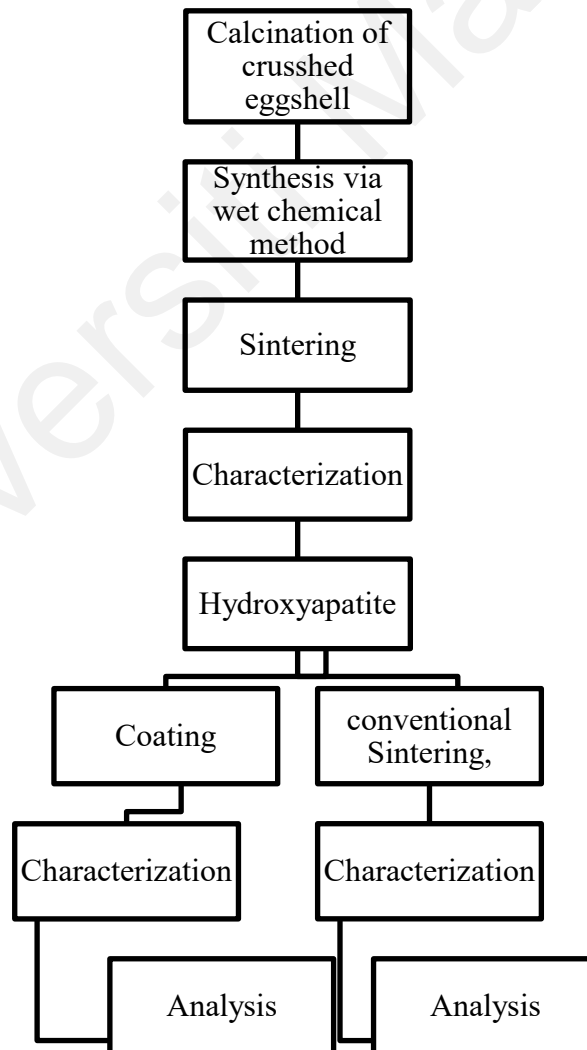


**Figure 3.1: Summary of all process.**

### **3.2 Materials**

Eggshell and phosphoric acid were used as calcium and phosphate source in this experiment. Synthesized hydroxyapatite, ethanol and titanium are the materials which were used in the coating procedure. All materials which have been used in this study, together with their characteristic, supplier name and their role in the experiment are given in Table 3.1.

Universiti Malaya

**Table 3.1: List of employed materials and their characteristics.**

<b>Process</b>	<b>Material</b>	<b>Characteristic</b>	<b>Role in the experiment</b>	<b>Supplier</b>
<b>Wet chemical precipitation</b>	Calcium oxide	Pure calcium oxide confirmed by XRD	Calcium precursor in synthesis process	Extracted from eggshell via calcination method
	Orthophosphoric Acid	85% Purity	Phosphate source in synthesis process	Merck
	Ammonium hydroxide	25% Solution	pH adjustment reagent in synthesis process	Sigma Aldrich
<b>Electrophoretic deposition</b>	Synthesized hydroxyapatite	Pure hydroxyapatite, confirmed by XRD	Deposited layer in coating procedure	Produced via wet chemical technique
	Hydrochloric Acid	1mol/liter concentration	Dispersing agent in coating procedure	Fluka Analytical
	Ethanol	95% Purity	Solvent in coating procedure	HMBG Chemical
	Titanium sheet	Grade 2	Substrate in coating procedure	Esteel company
	Stainless steel sheet	Grade 316L	Electrode in coating procedure	Esteel company



### 3.3 Powder Preparation Method

The preparation route of green powder from eggshell waste into bio-based hydroxyapatite including, calcination and synthesis procedure will be presented in next section.

#### 3.3.1 Conversion of Eggshell to Calcium Oxide via Calcinations Method

First step of synthesis was to convert eggshell to calcium oxide, which is the base material of wet chemical precipitation route. In this part, chicken eggshells were washed to eliminate all contamination. The inner layer of eggshells which is the organic part were removed and cleaned. The clean eggshell was washed with distilled water and put in dryer at 60 °C for 24 hours. Cleaned and dried eggshell was crushed manually by using mortar and pestle. Next step was to calcine eggshell powders which was done in a box furnace at 900 °C for one hour with heating and cooling rate of 10 °C per minute to burn the organic parts of the shell and convert calcium carbonate of the shell to calcium oxide. Figure 3.2 shows the temperature curve of the calcination process.

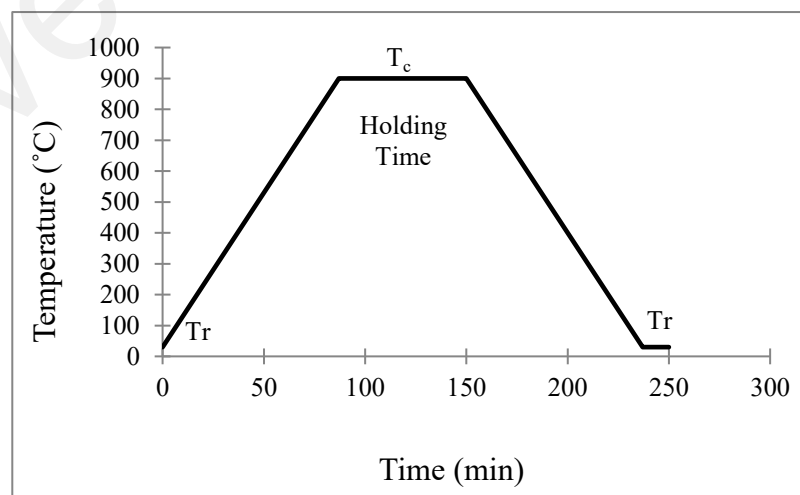


**Figure 3.2: Temperature curve of calcinations process. T<sub>r</sub>= room temperature and T<sub>c</sub>= calcination temperature.**

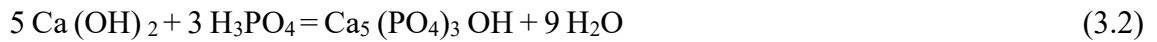
Powder was weighted before and after heating obtained the percentage of calcium oxide. The extracted powder was examined by X-Ray diffractometer and FTIR to confirm the composition of calcium oxide and any impurity such as organic parts etc. The reacted calcium oxide was sieved using a 212  $\mu\text{m}$  sieve.

### 3.3.2 Synthesize HA via Wet Chemical Precipitation Method

The calcium oxide powder was added to distilled water to produce calcium hydroxide  $[\text{Ca}(\text{OH})_2]$  solution. The mixture was stirred using magnetic stirrer (Heidolph MR 3001-Germany) at 80 rpm for 15 minutes, followed by ultra-sonication (Power Sonic 410) at 30  $^\circ\text{C}$  for three hours. Upon completion of sonicating, the stirring of the solution was done once again for another 15 minutes. Concurrently, orthophosphoric acid ( $\text{H}_3\text{PO}_4$ ) which was used as phosphate source, was added to distilled water followed by stirring for 15 minutes before titration. The second solution which was the blend of orthophosphoric acid and distilled water was added to calcium hydroxide solution at a rate of 20 drops per minute. Total amount of calcium oxide and phosphoric acid was calculated based on 1.67:1 molar ratio.

The pH of suspension was controlled regularly during titration process and it was kept above 11 by adding ammonium hydroxide ( $\text{NH}_4\text{OH}$ ) if the pH drops below 10. The solution was stirred for one hour after titration process and the final pH was obtained.

The final liquid mixture was left to age overnight followed by filtration and washing using distilled water. Synthesized hydroxyapatite cake was placed in an oven (Memmert UF110-Germany) at 60  $^\circ\text{C}$  for 24 hours. After the drying the powders were crushed and sieved to obtain HA powders. The reactions for the above processes are given in Equations 3.1 and 3.2.



### **3.4 Samples Fabrication**

#### **3.4.1 Compacting of Green Powder**

Compaction was performed to produce a disc sample using a uniaxial hydraulic press and cylindrical metal mould. The green powders were added into the die and the powder surface was smoothed out flat to produce disk sample. Then, pressure load of 10 MPa was applied to compact the powders to form a disc having 20mm in diameter and about  $10 \pm 2$  mm in height. The green samples were subjected to cold isostatic pressing (Riken Seiki, Japan) at 200 MPa for 1 minute.

#### **3.4.2 Convectional Sintering**

Sintering of green samples was done using a box furnace at different temperatures ranging from of 900 °C-1400 °C to evaluate the best sintering temperature based on phase stability of synthesized HA. Sintering profile was kept the same for all samples with 1 h holding time at the firing temperature using the ramp rate of 10 °C per minute for both heating and cooling process. For FESEM investigation, thermal treatment was done on sintered samples after polishing in order to delineate the grain boundaries. For thermal etching, the samples were heated for 30 minute in the box furnace while the heating and cooling rate were set to 10°C /min. The etching temperature was 50°C lower than the sintering temperature.

### **3.4.3 Grinding and Polishing**

The samples were ground and polished using a grinder polisher machine before phase and structural analysis. Grinding was performed at speed of 100 rpm by using SiC abrasive paper number 600 (rough) continued by 800, 1000, 1500, 2000 and 2500 (fine) successively. Polishing of the samples was done using 3  $\mu\text{m}$  and 1  $\mu\text{m}$  diamond paste to obtain a mirror surface.

### **3.5 Electrophoretic Coating Process**

The principal of electrophoretic deposition procedure can be summarized in migration of colloidal particles suspended in a liquid medium onto an electrode and deposited on it, under the effect of electron field. The electrophoretic system is very sensitive and influent by many factors, such as suspension condition, applied electrical parameters and process setup. The routes of suspension preparation, geometrical and electrical setup, as well as thermal treatment parameter are presented below.

#### **3.5.1 Powder Preparation**

For this purpose green powder was calcined using a box furnace at 900  $^{\circ}\text{C}$  for one hour, while heating and cooling rate was set at 10  $^{\circ}\text{C}$  per minute. The calcined powder was mixed with ethanol in an alumina jar of a planetary ball mill for four hours at 100 rpm to achieve a homogeneous mixture. The mass ratio of zirconia balls to the powders was equal to 4. The blended suspension was placed in an oven at 60  $^{\circ}\text{C}$  for 24 hours to be fully dried. The dried powder was sieved using 212 $\mu$  sieve to reach uniform powder prior to the coating process.

### **3.5.2 Suspension Preparation**

The calcined hydroxyapatite powder was weighted and added to the solvent which is ethanol. To control the motion of particles in the colloid, hydrochloric acid was used as dispersing agent and added to the mixture followed by sonification for 20 minutes. The pH of the solution was checked before applying on the substrate and kept at  $3 \pm 0.2$ .

### **3.5.3 Substrate and Electrode**

One of the advantages of electrophoretic technique is the applicability on complex shape. Titanium grade two was used as substrate in this study which has higher strength in comparison to titanium grade one and more formability when compared to titanium grade three. Titanium sheet was cut to small pieces of 10 mm width, 20 mm length and 2 mm height.

Stainless steel was chosen as the electrode in this study. The electrode was also cut to a square shape while the length size was equal to 20 mm. Double size electrode was selected to reduce the aggregation of particles at the edge of the samples which mostly happen when using same size electrode as the substrate.

Both substrate and electrode were ground lightly using abrasive paper number 600,800 and 1000. After grinding was completed, the sheets were washed with distilled water, then submerged in acetone liquid and placed in an ultrasonic bath for 15 minute prior to coating to remove all contaminations.

### **3.5.4 Deposition Procedure**

In order to find the best coating surface, electric parameters were tested by different values to find optimum numbers. The electrode and substrate were placed in the suspension and left for one minute to be settled. The voltage, current, power and time were varied. By applying the voltage, the deposition process started. Preparation of

double layered sample followed the same route as single layered samples, but the procedure was repeated once again after five minute. Deposited samples were dried at room temperature for 24 hours. By completion of drying, samples were compacted using cold isostatic press (Riken Seiki-Japan) for one minute at 200 MPa. Details of coating parameters and their values which were examined thru deposition procedure in order to find the best coating surface are summarized in Table 3.2.

**Table 3.2: Examined coating parameters.**

<b>Examined Parameters</b>	<b>Examined values</b>
<b>Hydroxyapatite Powder</b>	As-Synthesized HA powder, Calcined HA powder (900°C)& (1100°C)
<b>pH</b>	1, 2, 3±0.5, 4, 5, 6, 7
<b>Weight(g)</b>	0.01, 0.02, 0.03, 0.04, 0.05, 0.055±0.005, 0.06, 0.07, 0.08, 0.09, 0.1, 0.11, 0.12
<b>Solvent Type</b>	Acetone ,Ethanol
<b>Sonicating Time (min)</b>	5, 10, 15, 20, 25
<b>Applied Voltage(V)</b>	10, 15, 20, 25, 30, 35, 40, 45, 50, 55, 60, 65, 70, 75, 80, 85, 90
<b>Deposition time (min)</b>	1, 2, 3, 4, 5, 6, 7, 8, 9, 10
<b>Deposition type</b>	Single layer. Double layer
<b>Distance between electrodes</b>	0.5 cm,1cm,2cm
<b>Roughness of substrate</b>	Abrasive paper No: P1000,P800,P600
<b>Electrode Size</b>	Same size with substrate and Double size
<b>Applied binder</b>	Triethanolamine
<b>Sintering temperature</b>	900°C, 950°C, 1000°C, 1050°C, 1100°C

### 3.5.5 Sintering

Last step of sample preparation is sintering. Samples were fired in a tube furnace using argon gas to prevent oxidation of substrate. Thermal treatment can affect the final product, so sample were sintered using different temperature and profile to find the optimum sintering profile.

The samples were placed in the middle of furnace at room temperature. The air in the tube furnace was removed and replaced with argon gas (99.99% purity). The heating was maintained at a constant rate of 10 °C/min until 600 °C and maintained for five minutes at this temperature. Heating was continued at a rate of 5 °C until it reached the firing temperature. Then the samples were cooled at a constant rate of 10 °C/min to room temperature. Figure 3.3 shows the temperature curves of conventional sintering process of sample sintered at 1000 °C.

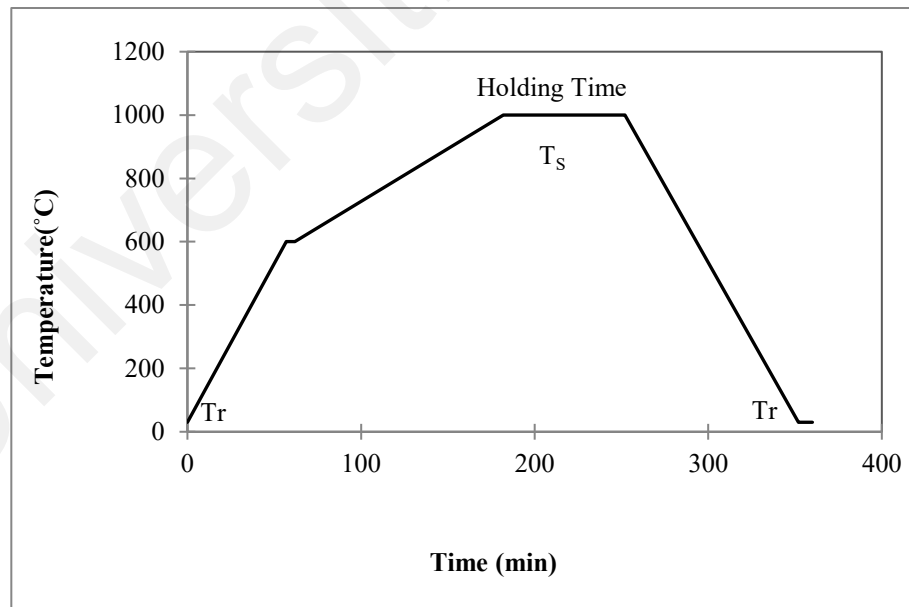


**Figure 3.3: Temperature curve of conventional sintering, employed for coated sample sintered at 1000 °C. T<sub>r</sub>=room temperature and T<sub>s</sub>=sintering temperature.**

### **3.6 Characterization**

Compositional and structural characterizations as well as the products' physical and mechanical properties were investigated after synthesis and sintering. Based on the products of each stage, different inspection methods were employed to evaluate the samples at the end of each process.

#### **3.6.1 Fourier Transforms Infrared Spectroscopy (FTIR)**

Functional groups of  $\text{CaCO}_3$  in eggshells, calcined eggshells, as-synthesized and sintered HA at  $1250\text{ }^\circ\text{C}$  were characterized by Fourier Transform Infrared Spectroscopy (FTIR, Perkin Elmer, Spectrum 100 Series-USA) using the KBr pellet in the  $4000\text{--}400\text{ cm}^{-1}$  wave number range with a  $4\text{ cm}^{-1}$  spectral resolution.

#### **3.6.2 Thermogravimetric Analysis**

Differential thermal analysis (DTA) and thermogravimetric analysis (TG) were conducted on the eggshells and as-synthesized HA by using the TG/DTA instrument (Perkin Elmer, Pyris Diamond TG/DTA-USA) with  $5\text{ }^\circ\text{C}/\text{min}$  heating rate from room temperature up to  $1000\text{ }^\circ\text{C}$ .

#### **3.6.3 Particle Shape and Size Analysis**

Imaging of synthesized hydroxyapatite particles as starting material was carried out using transmission electron microscopy (TEM, Carl Zeiss, Libra-Germany). For this purpose, hydroxyapatite powder was mixed with ethanol and sonicated for one hour followed by two days aging. A small amount of suspension was applied on a copper grid and kept for two days to be dry prior to analysis.

#### **3.6.4 Optical Microscopic Inspection**

Samples were evaluated visually to assess the resulting and surface quality. The macroscopic parameters such as cracks, pinhole, aggregation and overall coverage of



green samples were evaluated. Optical microscope was used for evaluation of coated samples before sintering.

### 3.6.5 X-Ray Diffraction (XRD)

X-Ray Diffraction is an important method of characterizing crystalline materials and evaluating the existing phases in the sample. It can be used powders, thin film and dense samples. The XRD phase analysis and crystallinity of as received eggshell, calcium oxide, synthesized and sintered eggshell HA were carried out by X-Ray Diffractometer (EMPYREAN.PANAlitical.Netherland). The samples were scanned using Cu-K $\alpha$  ( $\lambda=1.5406\text{\AA}$ ) at a scan speed of  $0.5^\circ\text{min}^{-1}$  step size of  $0.02^\circ$  and monochromatized radiation from  $2\theta=20^\circ$  to  $2\theta=60^\circ$ . The relative intensities and diffraction peaks of XRD patterns were studied by Xpert-High Score Plus software. Existing phases in each samples were checked by reference codes referring to the JCPDS database (Joint Committee on Powder Diffraction Standards) supplied by the International Centre for Diffraction Data (ICDD). The JCPDS cards numbers of the studied phases in this research are listed in Table 3.3.

**Table 3.3: JCPDS data reference codes.**

Component Name	Formula	JCPDS Cards Numbers
Carbonated Calcium	CaCO <sub>3</sub>	00005-0586
Calcium Oxide	CaO	0000-40-777
Hydroxyapatite	Ca <sub>5</sub> (PO <sub>4</sub> ) <sub>3</sub> OH	0000-90-432 & 010-740-565
TCP	Ca <sub>3</sub> (PO <sub>4</sub> ) <sub>2</sub>	9800-97-500
Titanium	Ti	980043-733

### **3.6.6 Field Emission Scanning Electron Microscope (FESEM)**

Field emission Scanned electron microscope (FESEM) (Hitachi TM3030, Japan) was employed for microstructural evaluation of the samples. The FESEM micrographs were taken at different magnifications from the typical points of each sample for better illustration. Grains size, grains shape, porosity size and distribution, homogeneity and the arrangement of grains, are parameters that can be obtained from microstructure evaluation.

### **3.6.7 Energy Dispersive X-Ray Spectroscopy (EDX)**

The elemental composition of products was determined by Energy Dispersive X-Ray Spectroscopy technique. The detailed composition of grains was investigated by EDX to evaluate the homogeneity or heterogeneity of the composition at various points. The EDX and FESEM tests were done using the same equipment.

### **3.6.8 Atomic Force Microscopy**

Roughness of the samples are among the important items should be considered and evaluated for biomedical applications. Topography of coated sample was investigated using atomic force microscope (AFM-Bruker-USA). In this method a mechanical probe was touched on the specimen and dragged across the surface of the sample. Surface topography information of the sample such as histogram analysis including roughness and average height as well as dimension analysis can be detected from the 2d and 3d scanned images.

### **3.6.9 Cross Sectional Analysis**

Cross sectional analysis was done to study the interaction between hydroxyapatite and titanium substrate after sintering and also to check the thickness of coated layer. For this purpose, sample was mounted using a mixture of epoxy resin and hardener at portion of 5:1 and kept for 24 hours. Mounted sample was cut using linear precision saw (Isomet

5000-Buehler-USA) at speed of 3000 rpm and feeding rate of 0.5 mm per minute. Before submitting samples to FESEM viewing, the samples need to be ground, and to be polished to a mirror finish surface. FESEM micrographs of sample were taken at 200 x and 400 x magnification, in order to determine the coating thickness and deposition quality. Thickness size of deposited layer was measured using digimizer software.

### 3.6.10 Density

Density of samples was evaluated using Archimedes' principle. In this test, the samples were weighed ( $W_d$ ) and submerged in water and weight of immersed specimen ( $W_w$ ) were measured. According to the data, density was calculated using the formula given in Equation 3.3. The theoretical density of hydroxyapatite was taken as 3.156 g/cm<sup>3</sup>. Table 3.4 entails descriptions of the symbols used in the density formulas.

**Table 3.4: Descriptions of symbols utilized in density formula.**

Symbol	Description
$\rho$	Density of specimen
$W_d$	Weight of specimen in dry state
$W_w$	Weight of specimen when submerged in water

$$\rho = \frac{W_d}{W_d - W_w} \quad (3.3)$$

Porosity (P) of samples were obtained using Equation 3.4.

$$P = 1 - \rho \quad (3.4)$$

### 3.6.11 Micro Hardness and Fracture Toughness

Hardness of the samples was measured by a Vickers hardness machine (Shimadzu-Japan). The mechanism of the machine entails applying a vertical load by a pyramidal indenter on a sample's surface, holding it for enough time which set based on sample rigidity, and then removing the load. The hardness was calculated by measuring the diameter of the indent in two directions. The load was selected, so that the full shape of the indent could be seen. The formula used to calculate the Vickers Hardness is given in Equation 3.5.

$$HV = 1.854 \frac{F}{d^2} \quad (3.5)$$

Where  $HV$  is Vickers Hardness,  $F$  is load and  $d$  is mean of the two diagonals.

The fracture toughness ( $K_{Ic}$ ) of samples was measured using the Niihara equation (Niihara, et al., 1982).

$$K_{Ic} = 0.203 \left(\frac{c}{a}\right)^{-1.5} Hv(a)^{0.5} \quad (3.6)$$

Where  $a$  is the half diagonal of the indent and  $c$  is represents the crack length. Hydroxyapatite sample were examined under 0.3 kg load for 5 second. At least five measurements were performed to find the average Vickers Hardness (HV) and fracture toughness of each sample.

### **3.6.12 Nanoindentation**

The nanoindentation test of coated hydroxyapatite, was conducted using a Triboscope system with a Berkovich indenter (Hysitron TI950; Bruker; USA) according to the ISO 14577. The maximum indentation load of 4000  $\mu\text{N}$  was applied by an indenter probe on the surface of each sample while the loading/unloading and holding time were set at 30 s and 10 s, respectively. At least five measurements were done at different sites of deposited film to find the average hardness of each sample.

### **3.6.13 Bioactivity Test (Wettability)**

The surface hydrophobicity or hydrophilicity of the coated specimens were determined by sessile & captive drop method using a video based optical contact angle measuring device (Optical Contact Angle 15EC; Data Physics instrument; Germany).

In order to check the wettability of the hydroxyapatite film, 5  $\mu\text{l}$  of deionized water dropped on the surface at dropping rate of 2  $\mu\text{l}$  per second. The contact angle ( $\theta$ ) of nanostructured layer calculated by SCA20 software from the captured image throughout the measurement.

## CHAPTER 4: RESULTS AND DISCUSSIONS

In this chapter, the result and discussion of the research will be presented in three parts. First part focused on the evaluation of eggshell powder as calcium precursor, characterization of derived calcium oxide through thermal treatment and properties of hydroxyapatite powder synthesized via wet chemical precipitation technique.

The second part of discussion focused on the sintering behavior of eggshell-derived HA at different sintering temperatures will be discussed in terms of phase stability, microstructural analysis and mechanical properties.

Comparison of green samples in different conditions of coating process, as well as, thermal phase analysis and characteristic of bio-based hydroxyapatite deposited on titanium which were fired at various firing temperatures, are presented in the last part of this chapter.

### 4.1 Characterization of Crushed Eggshell as Raw Material

The bio-waste chicken eggshell was used in this study as base material. The chicken eggshell was characterized to investigate the composition and to determine the firing temperature for the purpose of calcination.

#### 4.1.1 XRD Analysis of Chicken Eggshell

The XRD pattern of chicken eggshells is shown in Figure 4.1. Based on presented diffractogram and JCPDS data reference (05-0586), the dominant detected peaks corresponded to  $\text{CaCO}_3$ , which is the main constitutive components of chicken eggshells. The highest intensity peak of the graph situated at a  $2\theta$  angle of  $29.56^\circ$  which correlated with Miller indices of (1 0 4). Other observed peaks at  $2\theta$  angles of  $36.3^\circ$ ,  $39.7^\circ$ ,  $43.47^\circ$ ,  $47.9^\circ$  and  $48.82^\circ$  also matched the JCPDS code for  $\text{CaCO}_3$  and were in good agreement with other researchers (Rivera et al., 1999; Kumar et al., 2012; Sanosh et al., 2009).

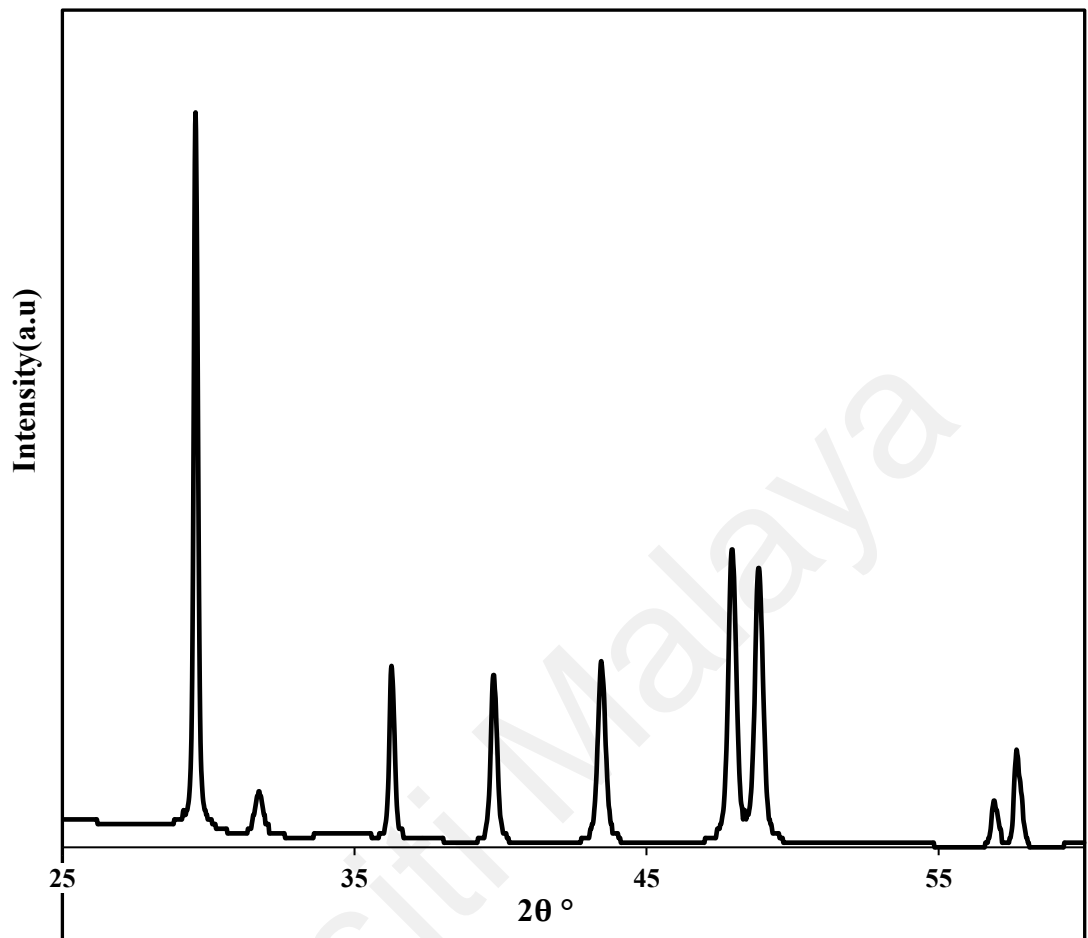


**Figure 4.1: XRD pattern of chicken eggshells revealing phase pure  $\text{CaCO}_3$ .**

#### 4.1.2 FTIR Analysis of Chicken Eggshell

The FTIR spectroscopy of crushed eggshell is presented in Figure 4.2. The significant characteristic peaks of carbonate phase are clearly observed at the spectrum of chicken eggshell powder. Eggshell is known as biowaste material which is contained of 94% calcium carbonate, 4% organic matter, 1% calcium phosphate and minor quantity of other components such as K, Mg, Na and Sr, which are also observed in human bone structure. Existence of these elements does not affect the crystallographic characteristics of hydroxyapatite, but can improve the performance of this biomaterial.

The characteristic peaks at  $712\text{ cm}^{-1}$ ,  $872\text{ cm}^{-1}$  and  $1418\text{ cm}^{-1}$  are attributed to the carbonate group in intrinsic calcium carbonated of eggshell. A broad band started from  $\sim 2700\text{ cm}^{-1}$  to  $\sim 3700\text{ cm}^{-1}$  is ascribed to  $\text{H}_2\text{O}$ . Small frequency bands observed at  $1762\text{ cm}^{-1}$ ,  $2098\text{ cm}^{-1}$ , and  $2532\text{ cm}^{-1}$  are corresponded to the different combination mode of  $\text{CO}_3^{2-}$ . The IR spectrum in this research was in good agreement with previous studies, which reported similar trend of IR spectra for eggshell (Gunasekaran et al., 2006; Wu et al., 2015; Kamalanathan et al., 2014).

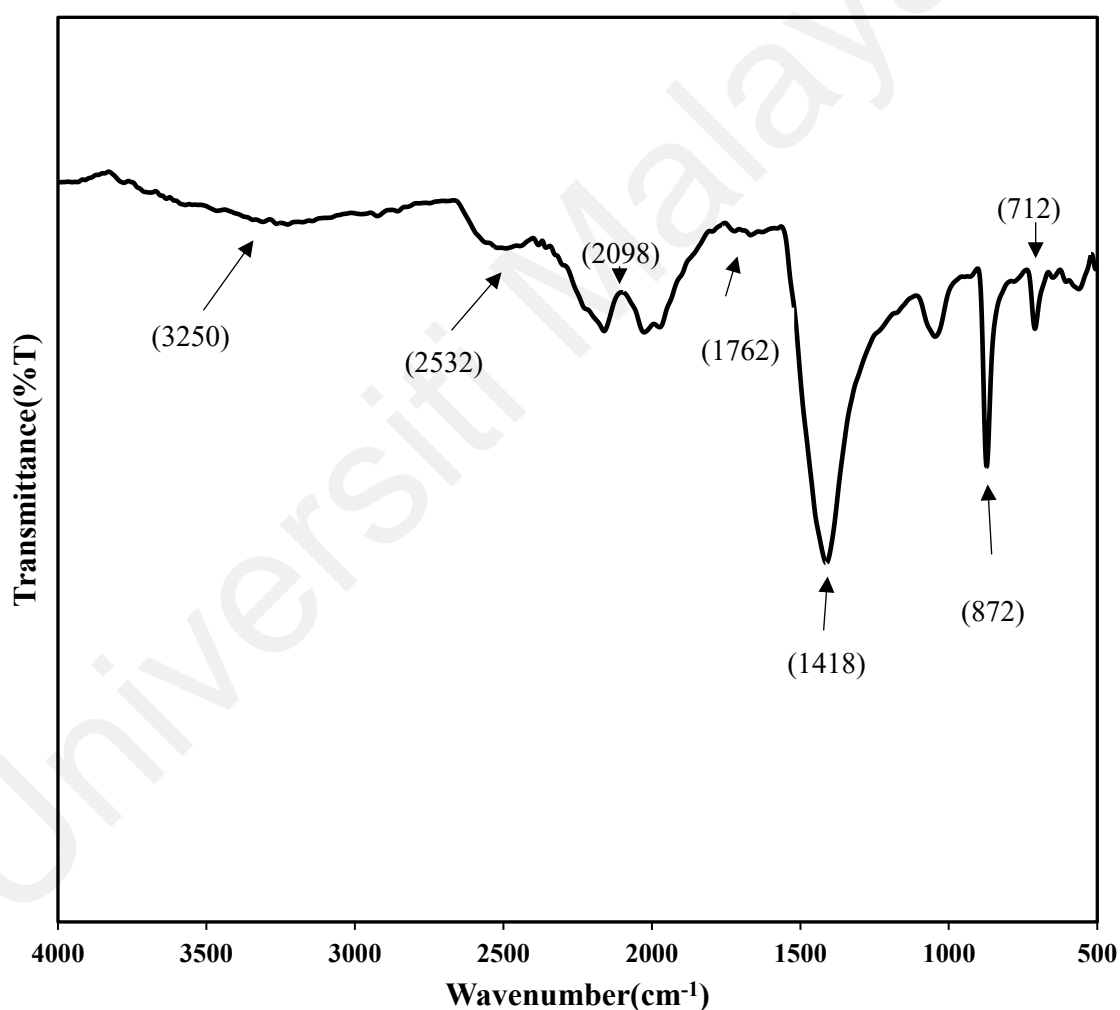


**Figure 4.2: FTIR spectrum of crushed eggshell.**



### 4.1.3 Thermogravimetric Analysis of Crushed Eggshell

Thermogravimetric analysis of eggshell was done to determine the best temperature for calcination process. The TGA curve of crushed eggshell from room temperature to 1000 °C using heating rate of 5 °C/min is shown in Figure 4.3. Based on the curve, two steps of weight lost happened during the heating process. The TGA graphs showed the weight was steady from the room temperature up to 495 °C. The weight loss of about 3% at this range was due to drying up process and vaporization of absorbed water.

The organic portions of eggshells, that remained after the cleaning process was oxidized at temperature range of 495 °C - 505 °C and caused the slight descent of weight lost ( $\approx 4\%$ ). The TGA curve showed the weight was steady up to 700 °C. The remarkable weight loss of about 40% from  $\approx 700$  °C to  $\approx 865$  °C could be attributed to decomposition of  $\text{CaCO}_3$  and released of carbon dioxide. The powder weight remained constant and did not change up to 1000 °C. From the TGA graph, all thermal reaction was completed up to 865 °C, hence, 900 °C was chosen as the calcination temperature in this study, while lower calcination temperature of 700 °C (Elizondo-Villarreal et al., 2012), 800 °C (Ho et al., 2013) and 850 °C (Krishna et al., 2007) were reported in literature.

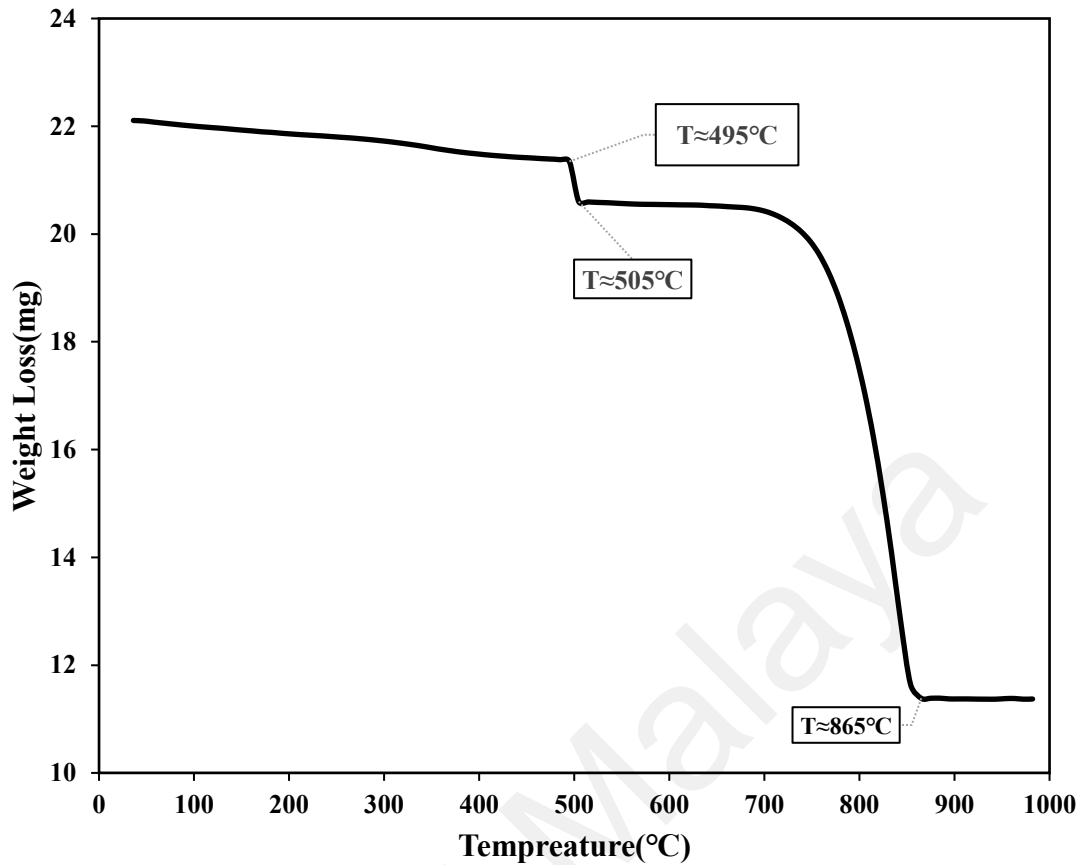


**Figure 4.3: TGA analysis of eggshell powder.**

## 4.2 Characterization of Calcined Eggshell as Calcium Source

The bio-waste chicken eggshell powder were transformed into calcium oxide powder through heat treatment procedure at 900 °C. The achieved calcium oxide powder were characterized to study the composition of the calcine powder and to confirm the conversion of eggshells to pure calcium oxide.

### 4.2.1 XRD Analysis of Calcium Oxide Powder

The XRD trace of Calcium oxide derived from chicken eggshells at calcination temperatures of 900 °C is shown in Figure 4.4. Upon calcination of eggshells waste, the XRD graph shows the crystalline phase formation of calcium oxide. The highest intensity of calcium oxide peak was detected at a  $2\theta$  angle of  $34.2^\circ$ , which matched the JCPDS

data reference (37-1497) correlated with Miller indices of (2 0 0). The conversion of  $\text{CaCO}_3$  into calcium oxide was completed at the calcination temperature of  $900\text{ }^\circ\text{C}$ . The highest crystallinity was obtained at this temperature when compared to recorded data from other studies, which calcined the eggshells at lower calcination temperature (Chaudhuri et al., 2013; Ho et al., 2013; Dahlan et al., 2012).

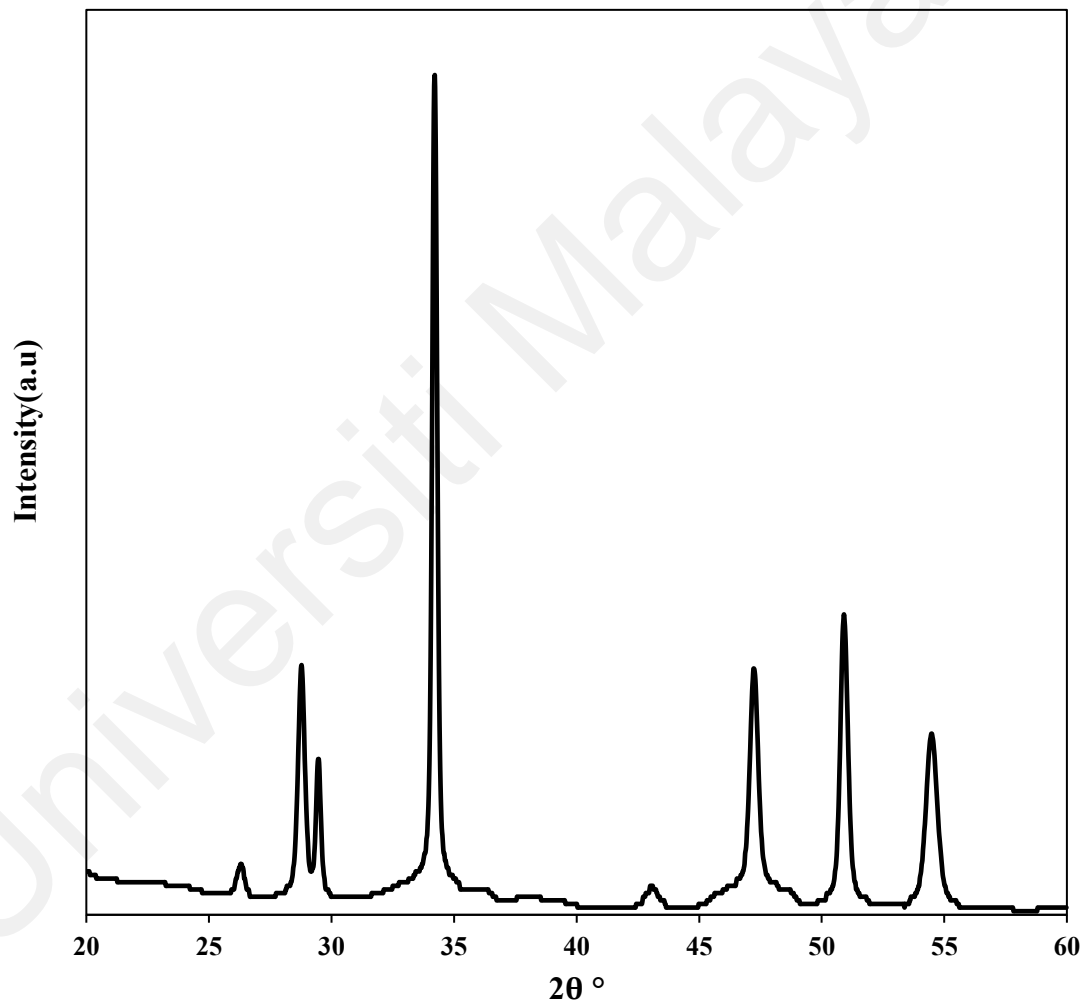


**Figure 4.4: XRD pattern of calcium oxide powder.**

#### 4.2.2 FTIR Analysis of Calcium Oxide Powder

The Fourier transform infrared analysis of chicken eggshell powder after thermal treatment at 900 °C is shown in Figure 4.5. The analysis of calcined eggshell powder demonstrate the complete decomposition of carbonate phase and fully conversion of calcium carbonate to calcium oxide after calcination. The frequency bands inherent to calcium oxide structure can be seen in the IR spectra of calcined eggshell. The sharp peak at 3636  $\text{cm}^{-1}$  corresponded to O-H group and belongs to the stretching vibration of  $\text{OH}^-$  ions. The absorbance of  $\text{CO}_2$  on the surface of calcium oxide resulted in the appearance of C-O stretching band. The broad bands observed at 1074  $\text{cm}^{-1}$  and 1490  $\text{cm}^{-1}$  are attributed to the C-O stretching mode. The comparison of the IR spectra of crushed eggshell (Figure 4.2) and FTIR spectrum of calcined eggshell powder (Figure 4.5) revealed the full transition of eggshells to calcium oxide was complete since the characteristic bands of the  $\text{CO}_3^{2-}$  disappeared and no longer visible in the calcined powder. The high purity of calcium oxide powder used for synthesizing hydroxyapatite in this study as calcium source has confirmed by the XRD trace (Figure 4.4) and FTIR spectrum of calcined eggshell powder (Figure 4.5). These results were in good agreement with those reported in previous studies (Prabakaran et al., 2009; Fukuda et al., 1973; Galvan-Ruiz et al., 2007).

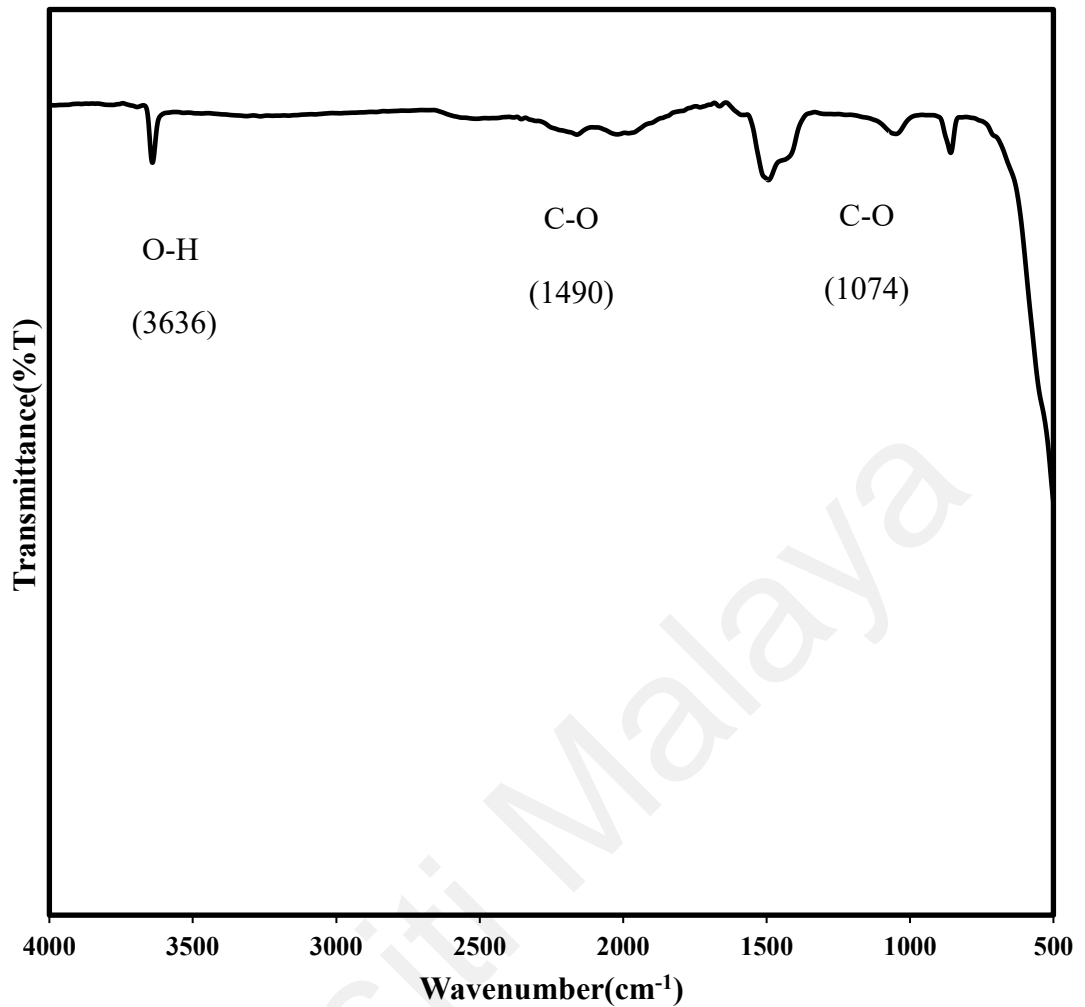


**Figure 4.5: FTIR spectrum of calcium oxide powder.**

### 4.3 Characterization of As-Synthesized Hydroxyapatite

Hydroxyapatite was derived from chicken eggshell via wet chemical procedure. Synthesized powder were characterized to confirm phase formation and to investigate the properties of synthesized powder such as phase purity, Ca/P ratio, particle size or shape. An overview on physical properties of as-synthesized eggshell hydroxyapatite powder is given in Table 4.1.

**Table 4.1: Physical and chemical properties of as-synthesized hydroxyapatite.**

<b>As-synthesized hydroxyapatite powder characteristics</b>	
Calcium (Ca) Wt%	~ 20.96
Phosphorus (P)Wt%	~ 12.54
Average Ca/P ratio	~ 1.671
Particle size(nm)	50±10
Particle shape	Needle like
Colour	white

#### **4.3.1 XRD Analysis of As-Synthesized Hydroxyapatite**

The phase formation and purity of as-synthesized eggshell hydroxyapatite powder was evaluated from XRD graph, which is presented in Figure 4.6. As shown in the X-ray diffraction analysis of as-synthesized eggshell hydroxyapatite powder, all peaks were matched by the standard JCPDS card number 90-432, and corresponded to hydroxyapatite. There is no evidence of secondary phases such as calcium oxide (CaO), tricalcium phosphate (TCP) or tetracalcium phosphate (TTCP) in the X-ray diffraction analysis of synthesized hydroxyapatite powder. The prominent peak at (0 0 2) reflection corresponding to diffraction angle of  $2\theta \approx 25.9^\circ$  and the highest intensity peak of (2 1 1) plane, which is observed at the diffraction angle of  $2\theta \approx 32^\circ$ , confirmed the successful formation of HA single phase from eggshell via wet chemical precipitation route. The XRD pattern of synthesized HA powder was in good agreement with the XRD pattern of

human bone presented by Ramesh et al. (2008), thus the synthesized powder characteristic expected to be similar to properties of the bone mineral (Khalid et al., 2013). The HA single phase was produced in this study while the appearance of calcium oxide, calcium hydroxide or tricalcium phosphate trace were reported by other researchers and these could be related to incomplete reaction which happened due to insufficient usage of either phosphorus or calcium precursors (Gergely et al., 2010; Wu et al., 2013; Hui et al., 2010; Qui et al., 2018).

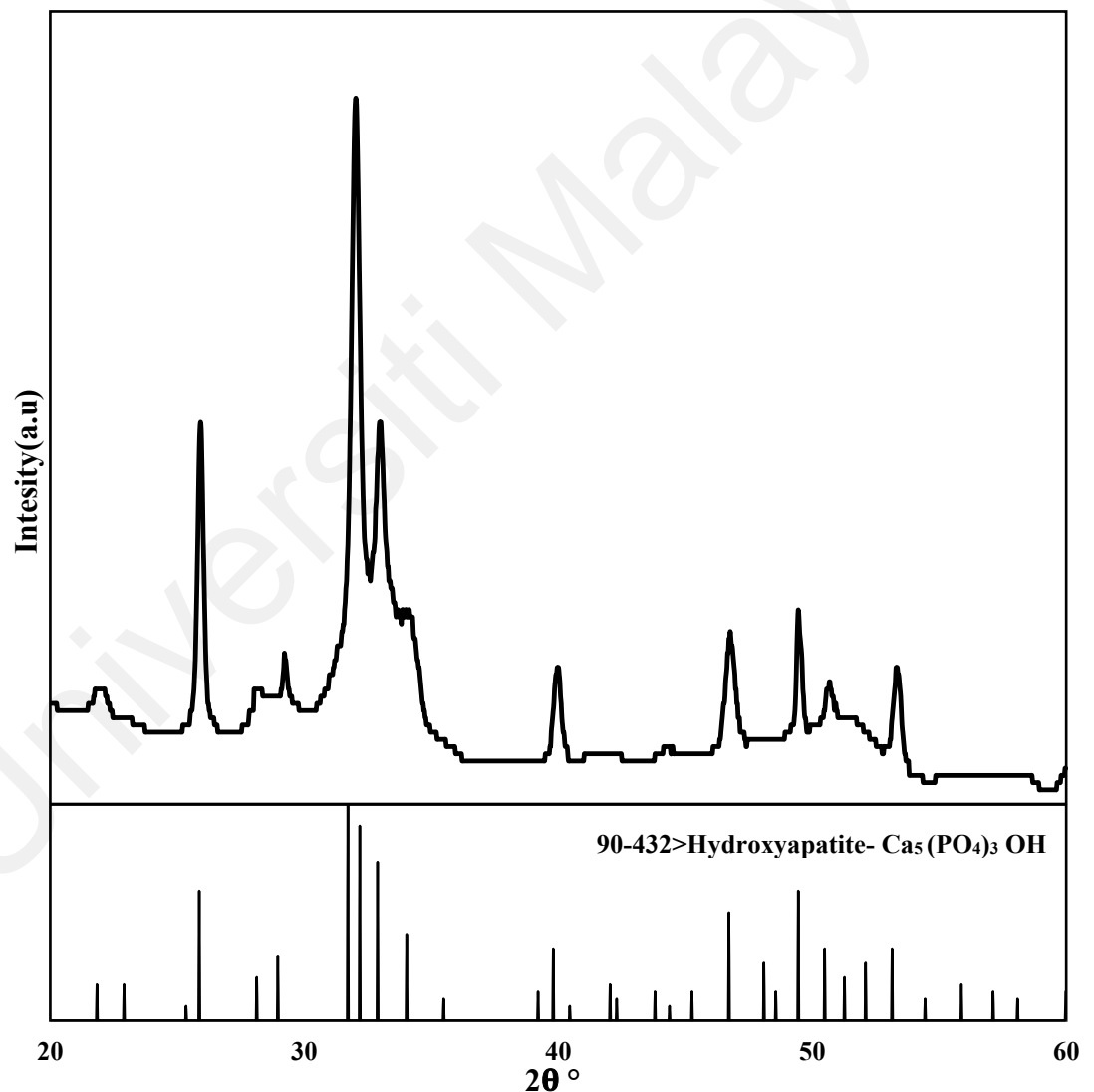


**Figure 4.6:** XRD pattern of as-synthesized hydroxyapatite powder.

### 4.3.2 FTIR Analysis of As-Synthesized Hydroxyapatite

The FTIR spectrum of as-synthesized hydroxyapatite powder is shown in Figure 4.7. The typical characteristic band of hydroxyapatite can be observed at the IR spectrum of synthesized powder. This observation confirmed the presence of hydroxyl and phosphate group. The characteristic bands at  $560\text{ cm}^{-1}$ ,  $614\text{ cm}^{-1}$  together with the maximum absorption at  $1024\text{ cm}^{-1}$  corresponded to  $\text{PO}_4^{3-}$  ion and matched with asymmetrical stretching peak of P-O. A broad band at the range of  $3000\text{ cm}^{-1}$  to  $3600\text{ cm}^{-1}$  belongs to O-H and shows the existence of hydroxyl group. The  $\text{CO}_3^{2-}$  vibration mode at  $1836\text{ cm}^{-1}$ ,  $1484\text{ cm}^{-1}$  and  $948\text{ cm}^{-1}$  which were also observed in previous studies could be related to adsorbed species remaining from aqueous precipitation precursors (Krishna et al., 2007; Landi et al., 2008; Bardhan et al., 2011).

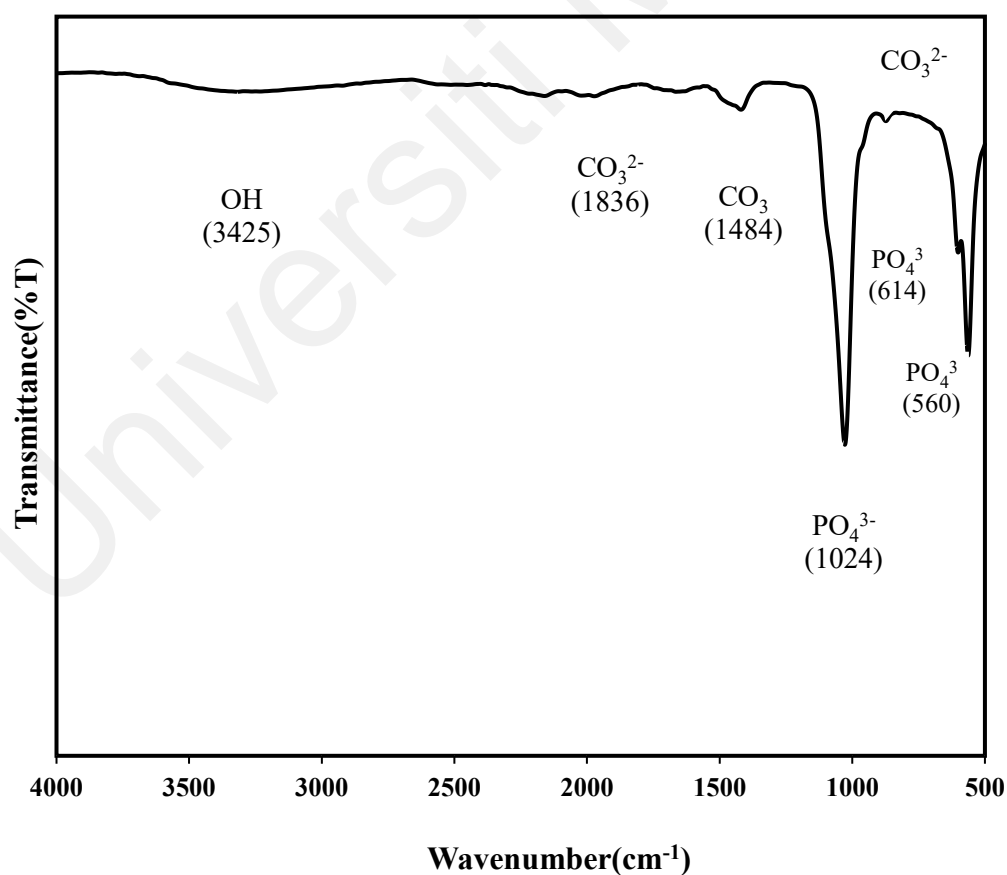


**Figure 4.7: FTIR spectrum of as-synthesized hydroxyapatite powder.**



### 4.3.3 Microstructural Analysis of As-Synthesized Hydroxyapatite

Hydroxyapatite was synthesized successfully from eggshell and synthesized powder was analysed using scanning electron microscope. The FESEM micrograph of as-synthesized hydroxyapatite powder is shown in Figure 4.8. The aggregation of the particles can be seen in the microstructure image, this could be related to the characteristic features of synthesized powder, which was physically moist and sticky after precipitation process. Meanwhile, the high surface energy of nanoparticles increases the Van der Waals interactions and resulted in high tendency of agglomeration (Ferkel & Hellmig, 1999; Ebrahimi et al., 2010). Sadat Shojai et al. (2013) observed that using nano size hydroxyapatite powder resulted in better cell adhesion and bone regeneration due to its higher surface area and surface roughness. It has been reported that the particle size and shape of hydroxyapatite particles can affect the sinterability, solubility and densification of the produced HA powder (Yang et al., 2004; Hamidi et al., 2017; Ramesh et al., 2018).

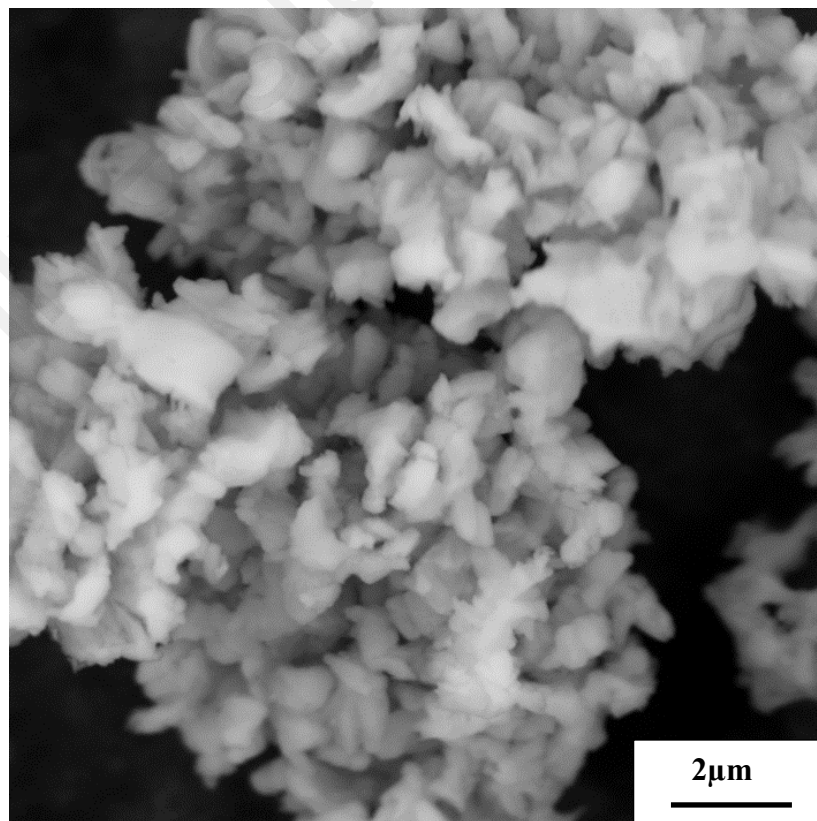


**Figure 4.8: Micrograph of as-synthesized hydroxyapatite powder.**

#### 4.3.4 Thermogravimetric Analysis of As-Synthesized Hydroxyapatite Powder

The DTA/TGA curve of synthesized hydroxyapatite is shown in Figure 4.9. A broad exothermic band starting from 90 °C and centred at about 400 °C was observed and this could be attributed to the crystallization of hydroxyapatite and conversion of amorphous phase to crystalline form. This phenomenon was also accompanied by a sharp weight loss of about 10% at 400 °C and increased further to 12% at 1000 °C, believed to be associated with the loss of hydrated water in the HA lattice (Martinez-Castanon, et al., 2012; Ramesh et al., 2015; Prabakaran et al., 2009). Same thermal analysis trend had been reported by Niakan et al. (2015). In some of researches, DTA curve continued by an endothermic peak after 800 °C which corresponded to decomposition of hydroxyapatite powder (Pramanik et al., 2007).

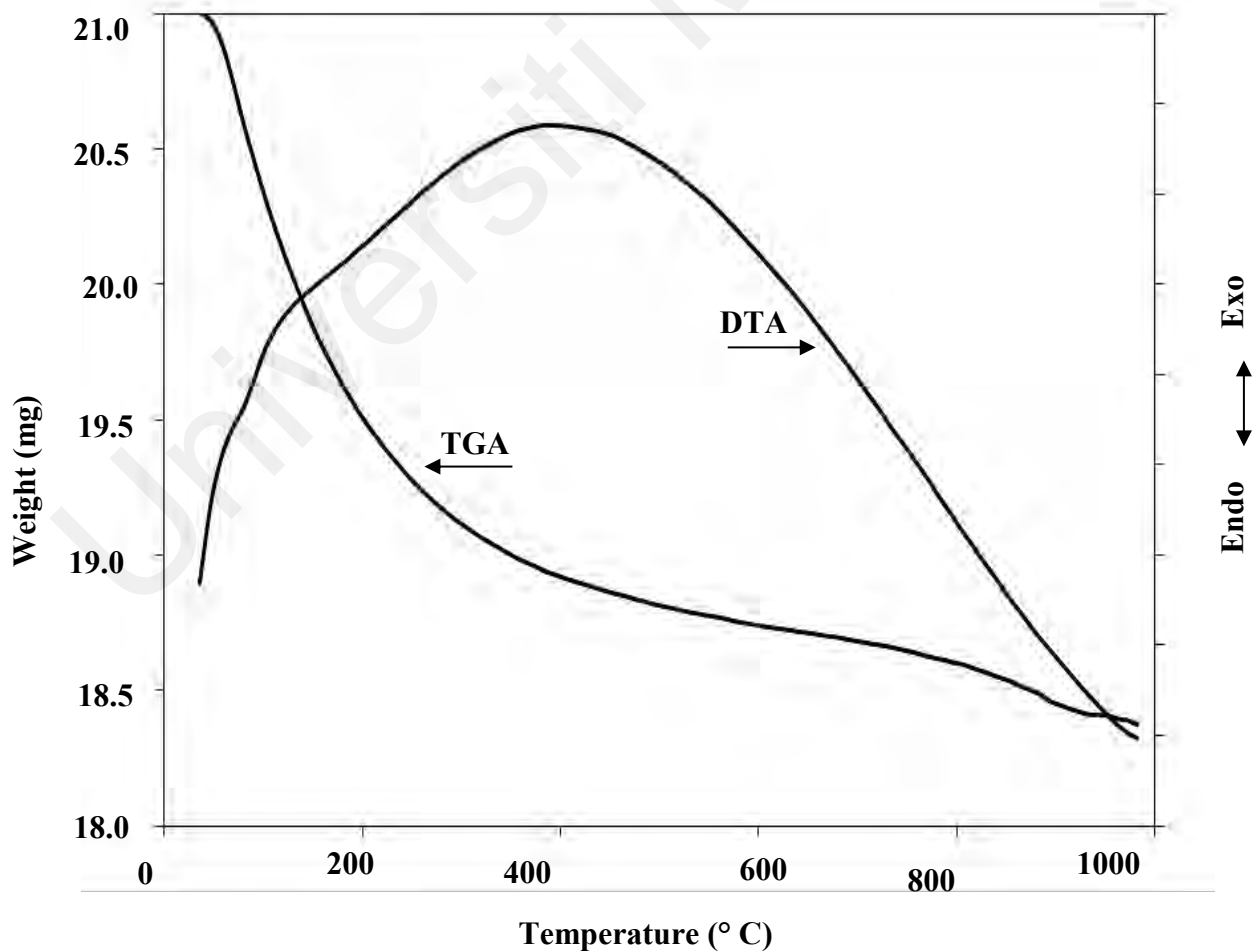
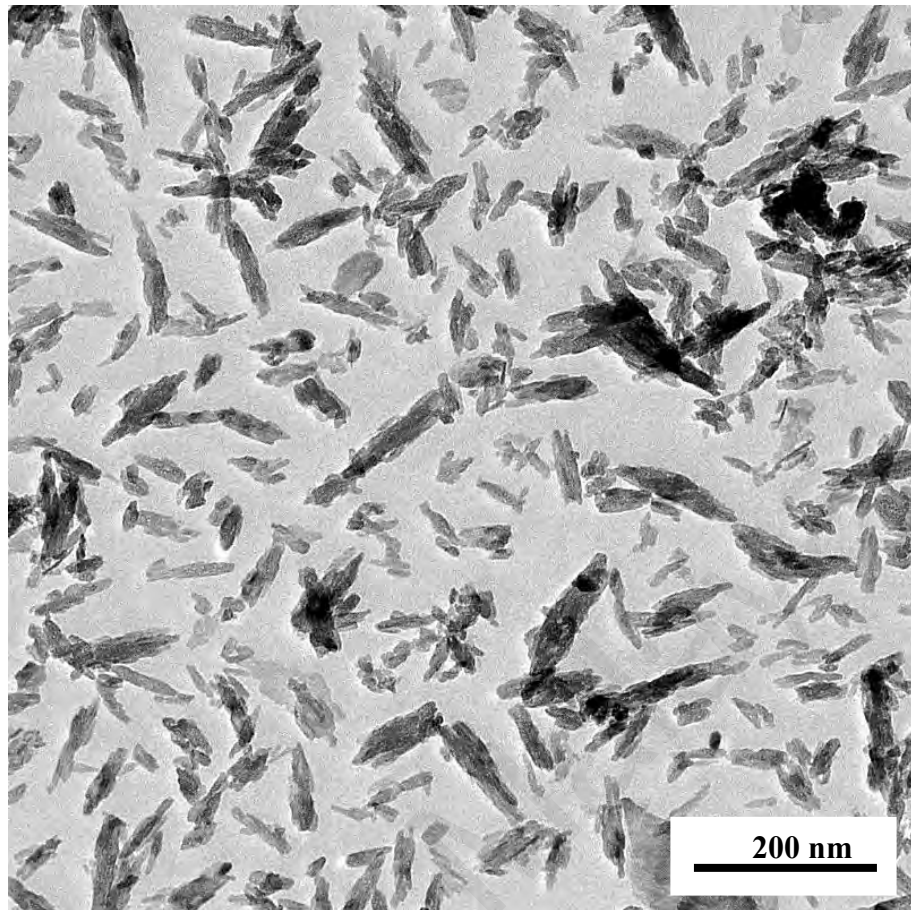


Figure 4.9: TGA/DTA analysis of eggshell-derived hydroxyapatite powder

#### 4.3.5 Morphological Analysis of As-Synthesized Hydroxyapatite Powder

TEM image shown in Figure 4.10, revealed the morphology of synthesized hydroxyapatite particles. The starting hydroxyapatite powder exhibited a needle-like nanostructured particles, with an average size length of  $50 \pm 10$  nm. This morphology is typical for wet-chemical precipitated HA and could vary depending on the powder processing method employed to synthesis the HA (Akram et al., 2014; Chew et al., 2015; Pal et al., 2017). It is believed that different morphology resulted in different characteristic, hence the powder employed for different applications (Sahiner et al., 2012; Sadat-Shojai et al., 2013; Evis et al., 2011). The morphology of the particle has an effect on the mobility of the charged particles and could influence the coating process (Ferrari et al., 1998). Production of different morphology such as needle like, flower like, and spherical reported by researcher through different route. For instance Ramesh et al. (2015) achieved globular shape particles of hydroxyapatite as a result of using a sol-gel method while they reported a needle like particles through wet chemical route. Nevertheless, the needle-like particles has been reported to exhibit better sinterability when compared to other particle morphologies (Zanotto et al., 2012).



**Figure 4.10: TEM micrograph of eggshell-derived hydroxyapatite powder.**

#### **4.4 Characterization of Sintered Eggshell Based Hydroxyapatite**

Hydroxyapatite was produced successfully from chicken eggshell waste through wet chemical method. Synthesized powder was compacted and cold isostatically pressed, then sintered at different firing temperature from 900 °C-1400 °C at heating rate of 10 °C per minute and one hour holding time. The sintered specimens were analysed and characterized in terms of structural, mechanical and physical properties. The sintered samples were observed in perfect shape after sintering without any cracks or other defects.

#### 4.4.1 XRD Analysis of As-Sintered Hydroxyapatite

Figure 4.11 shows the XRD signatures of sintered hydroxyapatite at 900-1300 °C and the XRD traces of sintered hydroxyapatite at 1350-1400 °C is shown in Figure 4.12. Analysis of XRD graphs revealed the formation of pure and high crystalline HA as confirmed by JCPDS card number 010-74-0565. Diffractogram of the sintered samples depicts that, regardless of sintering temperature, all detected peaks corresponded to hydroxyapatite and there is no secondary phase up to 1300 °C. However, the small peaks of tetracalcium phosphate (TTCP) at the position of  $2\theta = 30.6$ , and  $\alpha$ -tricalcium phosphate ( $\alpha$ -TCP) situated at  $2\theta = 48.5$ , were observed for samples sintered at 1350 °C and above (Figure 4.12). The intensity of the highest peak, corresponding to the (211) lattice plane, at  $2\theta = 31.8^\circ$ , increases from 900 °C to 1300 °C revealing a highly crystalline HA structure has been formed. Conversely, the reason of HA peak intensity decrement at higher temperature could be associated with the existence of TCP and TTCP phases, which formed due to decomposition of HA at 1350 °C. The high thermal stability of the HA observed at 1300°C clearly indicated that the eggshell-derived HA was superior than the chemically produced HA as reported by many researchers. According to the literatures, most of the HA derived through the chemical route would be unstable when sintered beyond 1250 °C, resulting in decomposition of the HA phase (Singh et al., 2011; Rapacz-Kmita et al., 2005; Kamalanathan et al., 2014).

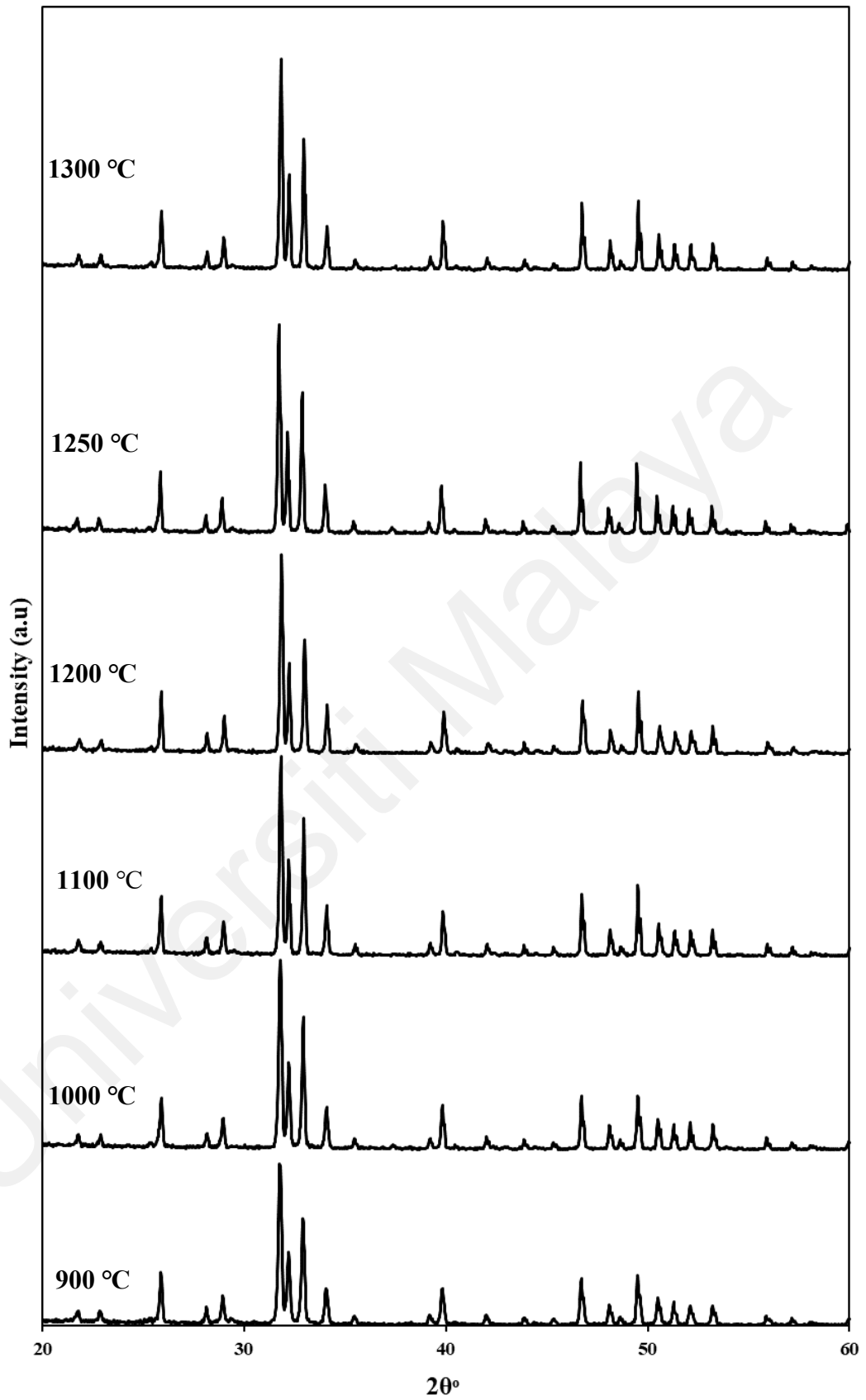


**Figure 4.11: XRD signatures of HA samples sintered at various temperatures, (900 °C-1300 °C) revealing fully HA phase.**

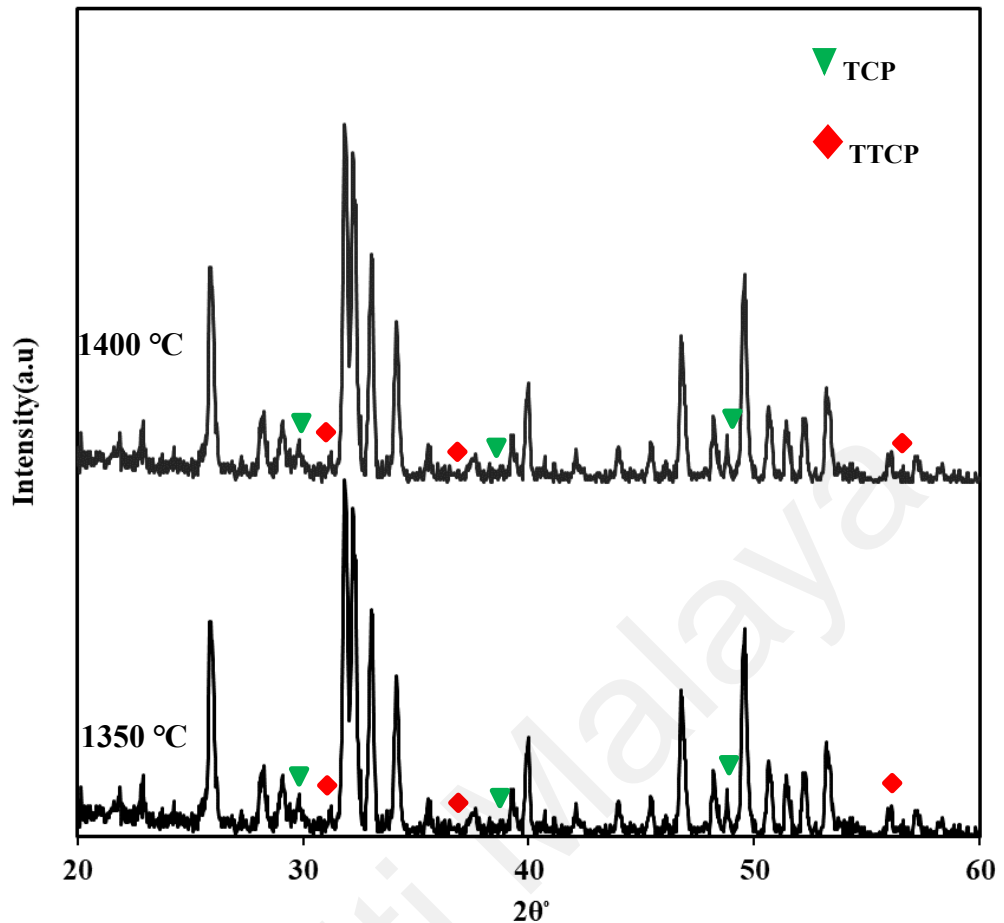


**Figure 4.12: XRD signatures of HA samples sintered at 1350 °C-1400 °C. The unmarked peaks represents HA phase.**

#### 4.4.2 FTIR Analysis of As-Sintered Hydroxyapatite Powder

Figure 4.13 revealed the FTIR spectra of sintered hydroxyapatite at 1250 °C. The typical absorption peaks at the IR spectrum of the sintered powder is corresponded to stoichiometric HA. The IR doublet peak observed at frequencies of  $960\text{ cm}^{-1}$ ,  $1065\text{ cm}^{-1}$  and the most intensive peak at  $1020\text{ cm}^{-1}$  are corresponded to  $\text{PO}_4^{3-}$  vibrations of hydroxyapatite. Moreover, vibrational mode of structural  $\text{OH}^-$  was observed at  $3570\text{ cm}^{-1}$  which is sharper than the detected broad band of OH at same range in the spectra of synthesized HA (Figure 4.7). This phenomena could be related to removal of water as hydroxyl from the crystalline structure of hydroxyapatite.

The obtained FTIR spectrum is in good agreement with XRD analysis of HA in this study and also with reported literatures (Wang et al., 2002; Meejoo et al., 2006).

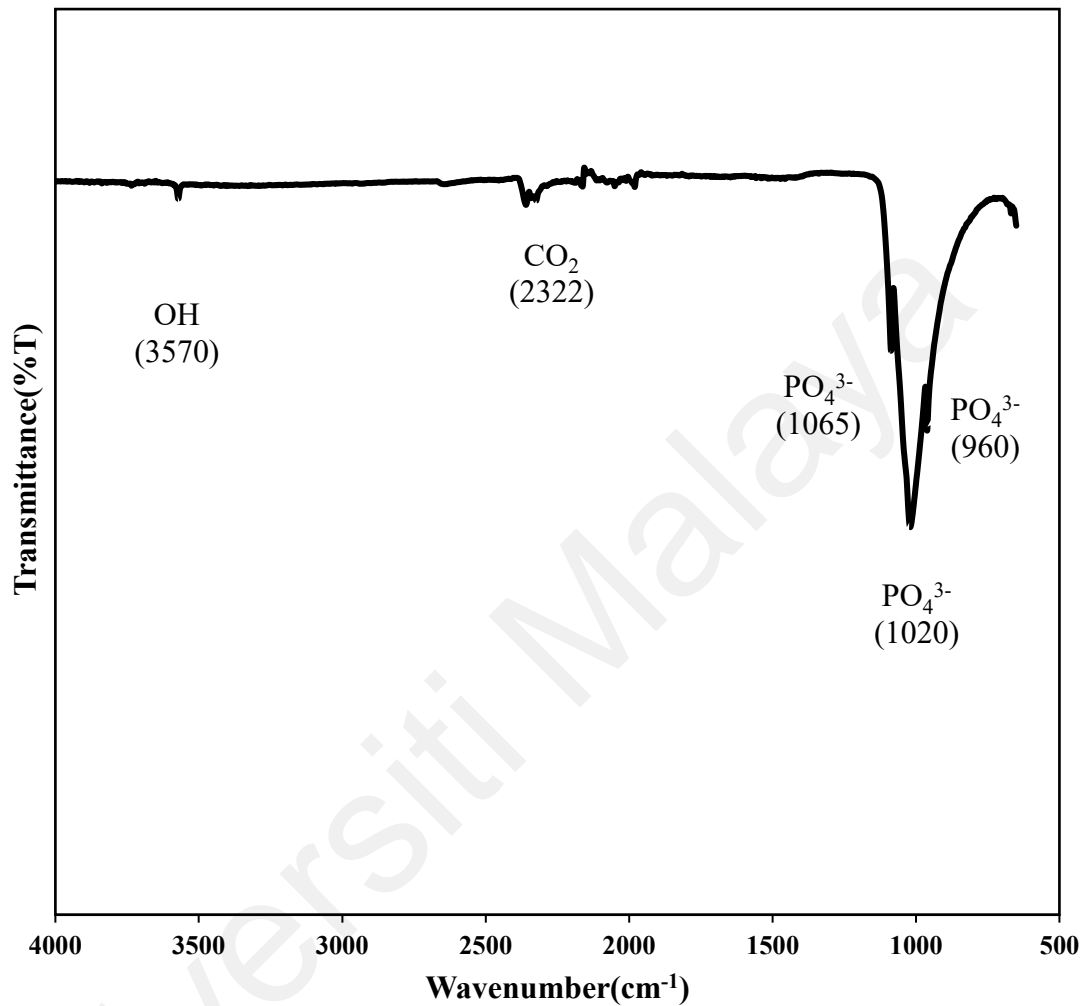


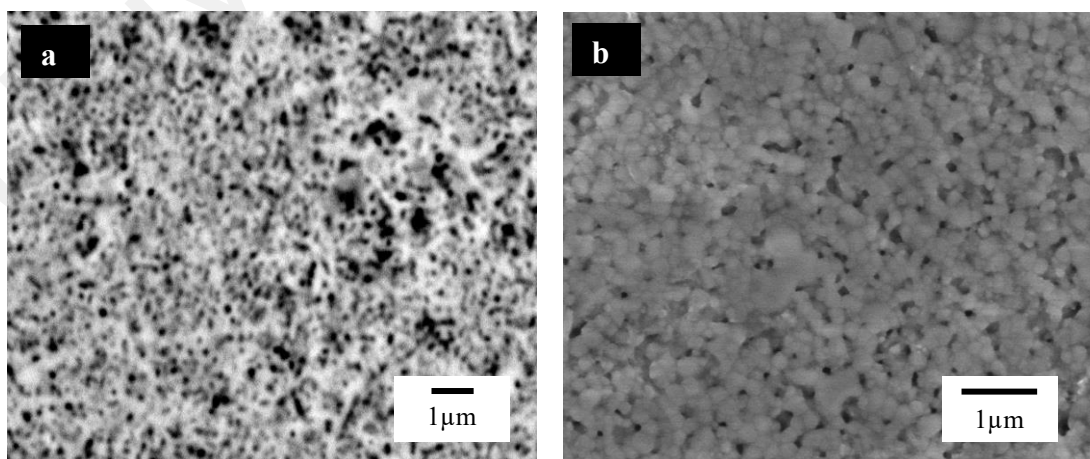
**Figure 4.13: FTIR spectrum of as-sintered hydroxyapatite.**

#### 4.4.3 Microstructural Analysis of As-Sintered Hydroxyapatite

Hydroxyapatite powder was compacted and sintered at the temperature range of 900 °C-1400 °C. The microstructure evolution of sintered samples at different temperatures are shown in Figure 4.14. Regardless of sintering temperature, a homogenous structure with submicron porosity could be observed in the FESEM images of all samples fired above 900 °C. It has been reported that the particle size and surface area of synthesized



powder have an effect on the sinterability of the HA powder. Smaller particle size has a higher sinterability and resulted in higher packing density (Kothapalli et al., 2004, Ramesh et al., 2013). Hence the synthesized powder with small particle size (Figure 4.10) expected to have smaller grain size, higher sinterability and higher packing density. A porous structure can be observed for sample sintered at 900°C when compared to sample sintered at 1000°C. However, as the temperature increased to 1100°C and beyond, this was accompanied by densification (Figure 4.17) and elimination of porosity. A very dense structure can be seen for samples fired at 1200 °C and above which is in contrast with the porous structure of the sample sintered at 900 °C. This could be related to growing of grains along with decreasing the value of porosity which effected by raising temperature. Suchanek and Yushimura (1998) had reported on the correlation between the grain growth at high sintering temperature and densification of HA. It is obvious from Figure 4.14, that the HA grains started to grow as the sintering temperature increased from 1000 °C to 1400°C, (Figure 4.16) resulting in the formation of equiaxed grains having a bimodal grain size distribution.



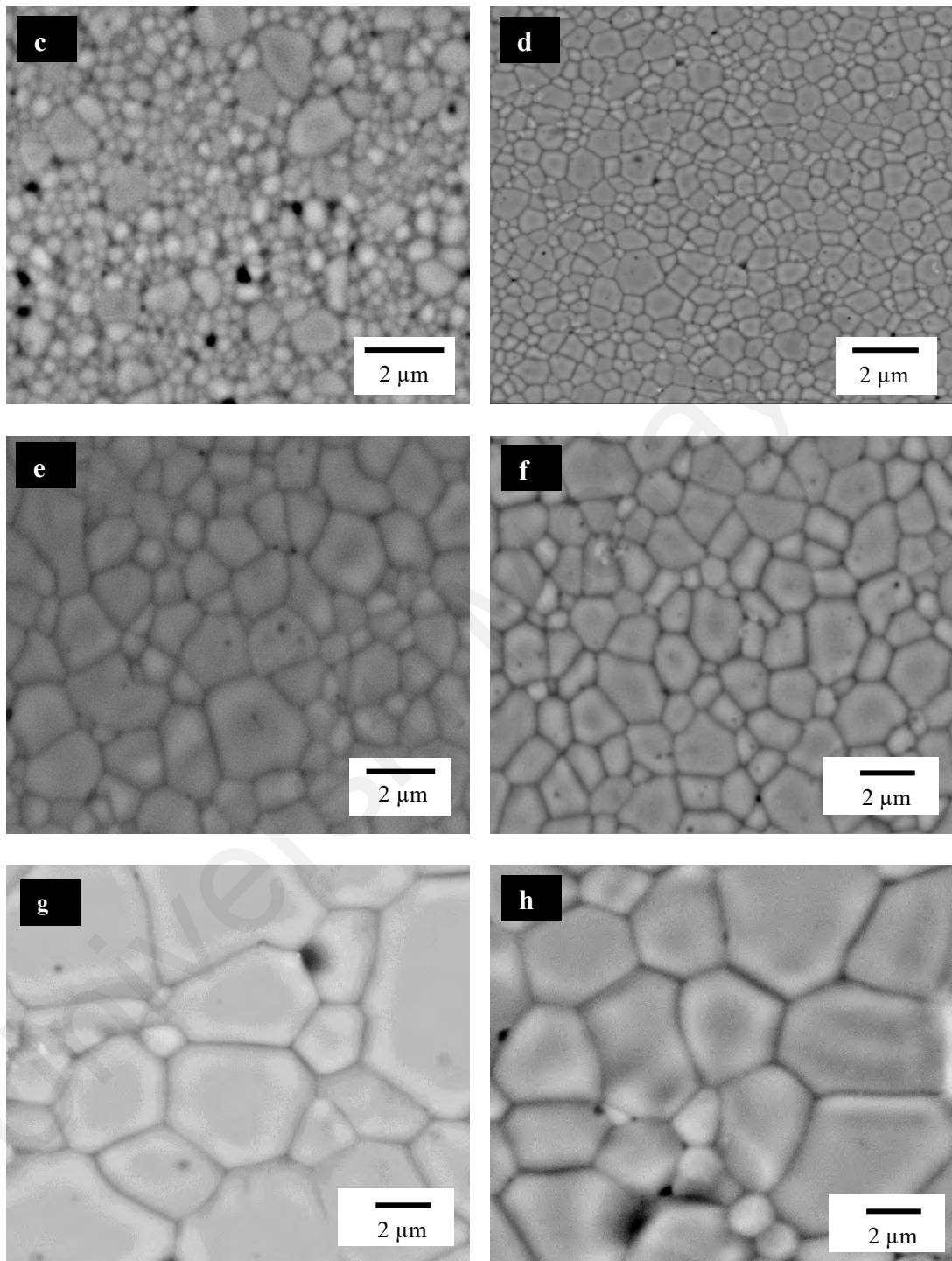


**Figure 4.14: FESEM micrographs of eggshell-derived HA sintered at (a) 900 °C, (b) 1000 °C, (c)1100 °C, (d) 1200 °C, (e) 1250 °C, (f) 1300 °C, (g)1350 °C and (h) 1400 °C.**

#### 4.4.4 EDS Analysis of As-Sintered Hydroxyapatite

Elemental analysis of sintered hydroxyapatite is given in Figure 4.15. EDX analysis of all the sintered samples show two major elements, Ca and P, were present along with other minor elements of Mg, Si and K as typically shown in the graph. These elements present in the HA are believed to originate from the eggshells and are in good agreement with that commonly found in natural bones (Akram et al., 2014; Niakan et al., 2015). The Ca/P ratio as calculated from the EDX data for the sintered HA was about  $1.67 \pm 0.03$  regardless of the sintering temperature and this value correlates well with that of the stoichiometric molar ratio of pure HA. The Ca/P ratio has been reported to have an influence on the properties and reactivity of the HA powder. For instance, if there is less or excess of calcium or phosphate added during the reaction, this would result in a non-stoichiometric Ca/P ratio. Hence, during sintering, decomposition of the HA phase will take place and this in turn would have an adverse effect on the mechanical properties of the sintered body (Raynaud et al., 2001; Raynaud et al., 2002). Different range of Ca/P ratio obtained by other researchers throughout various method. Sintering temperature, firing profile and synthesis condition have affected on Ca/P ratio of final product. For instance, the Ca/P ratio at range of 1.5-1.65 have been reported by Yang et al. (2004) that producing hydroxyapatite with same method and material but at different aging time of 1-24 hour during synthesis procedures (Yang et al., 2004; Raynaud et al., 2002; Al-Qasas & Rohani, 2005).

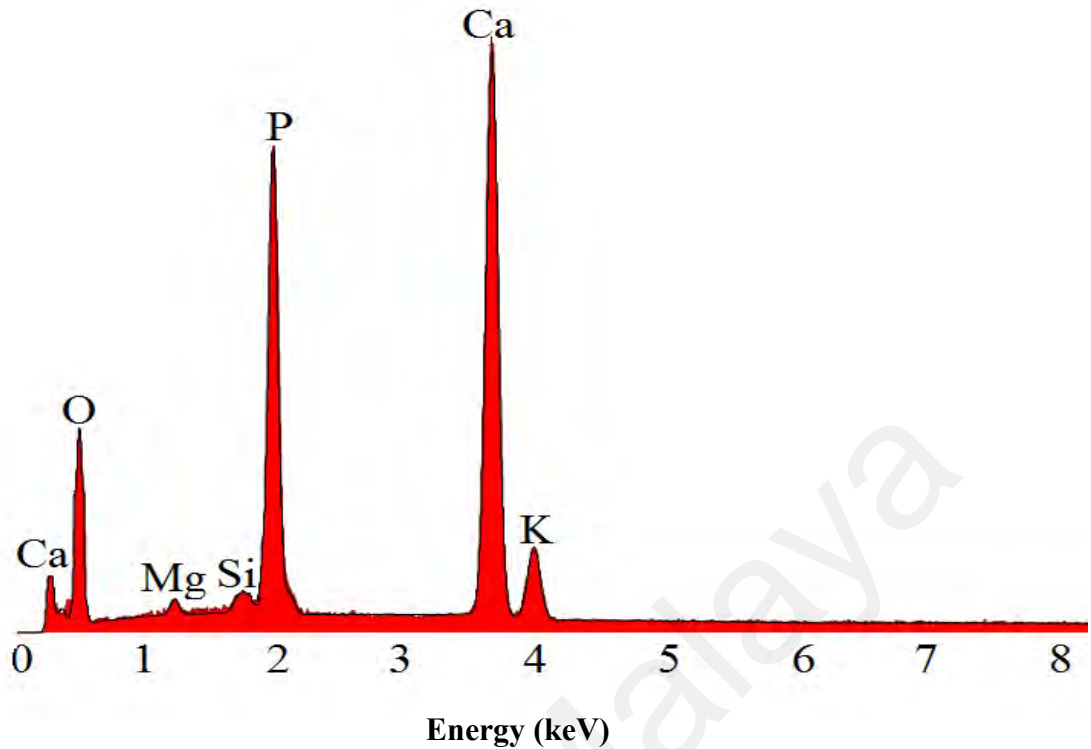


**Figure 4.15: Typical EDX analysis of eggshell-derived HA sintered at 1300°C.**

#### **4.4.5 Grain Size Analysis**

The effect of sintering temperature on the average grain sizes of sintered hydroxyapatite specimens is shown in Figure 4.16. The graph shows that an almost linear relationship exist between grain size and sintering temperature. The smallest grain size of 0.6  $\mu\text{m}$  was measured for the specimen which sintered at 1000  $^{\circ}\text{C}$ , whereas the largest grain size of 2.7  $\mu\text{m}$  was obtained when sintered at 1400  $^{\circ}\text{C}$ . Rapid grain growth was observed on the sintered samples when heat treated between the sintering temperature of 1100  $^{\circ}\text{C}$  and 1200  $^{\circ}\text{C}$ . However, the rate of grain growth noted in the present work was not as significant compared to that observed in the literature (Ramesh et al., 2013) where the HA grain size increased from approximately 2 to 8  $\mu\text{m}$  when sintered from 1200  $^{\circ}\text{C}$  to 1250  $^{\circ}\text{C}$ . This suggests that the eggshell-derived hydroxyapatite in the present study was not susceptible to rapid grain growth, resulting in smaller grain sizes which would be

beneficial for the mechanical properties (Kamalanathan et al., 2014; Heidari et al., 2016).

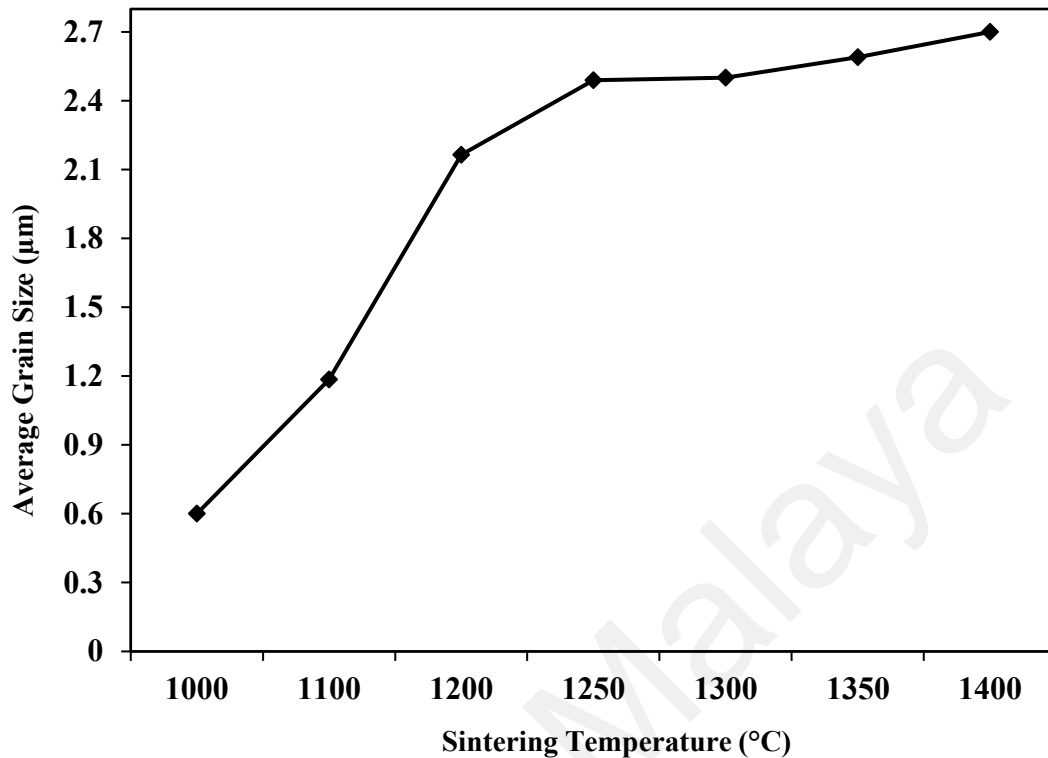


**Figure 4.16: The variation of grain size as a function of sintering temperature.**

#### 4.4.6 Bulk Density Analysis

The effect of sintering temperature on densification of sintered samples is shown in Figure 4.17. Sintering at 900 °C resulted in low relative density of 80% and this is in agreement with the FESEM images (Figure 4.14-a) which confirm the existence of a porous HA structure. The bulk density of the samples raised by increasing temperature from 900 °C-1300 °C at different rate. The fastest densification rate happened between 900 °C-1000 °C, whereas the relative density increased from 80.2% to 90.3%. This alteration occurred due to pore elimination process as can be seen from the FESEM image (Figure 4.14-b). As illustrated in Figure 4.17, the relative density increased rapidly to 97% when sintered at 1100 °C and thereafter fluctuated slightly and attained a maximum

value of 98.5% for sintering at 1250 and 1300 °C. Thereafter, the relative density decreased slightly to 97% at 1400 °C which can be attributed to decomposition of hydroxyapatite which started at 1350 °C as confirmed by XRD analysis (Figure 4.12). The observations resulting from this analysis were in good relation with microstructural observation (Figure 4.14) and grain size variation (Figure 4.16). The results obtained in the present work is considered high when compared to those reported by other researchers where a maximum relative density of 97.4% was reported by Kamalanathan et al. (2014) when sintered under similar conditions at 1250 °C (Ramesh et al., 2008; Ramesh et al., 2016; Niakan et al., 2015).

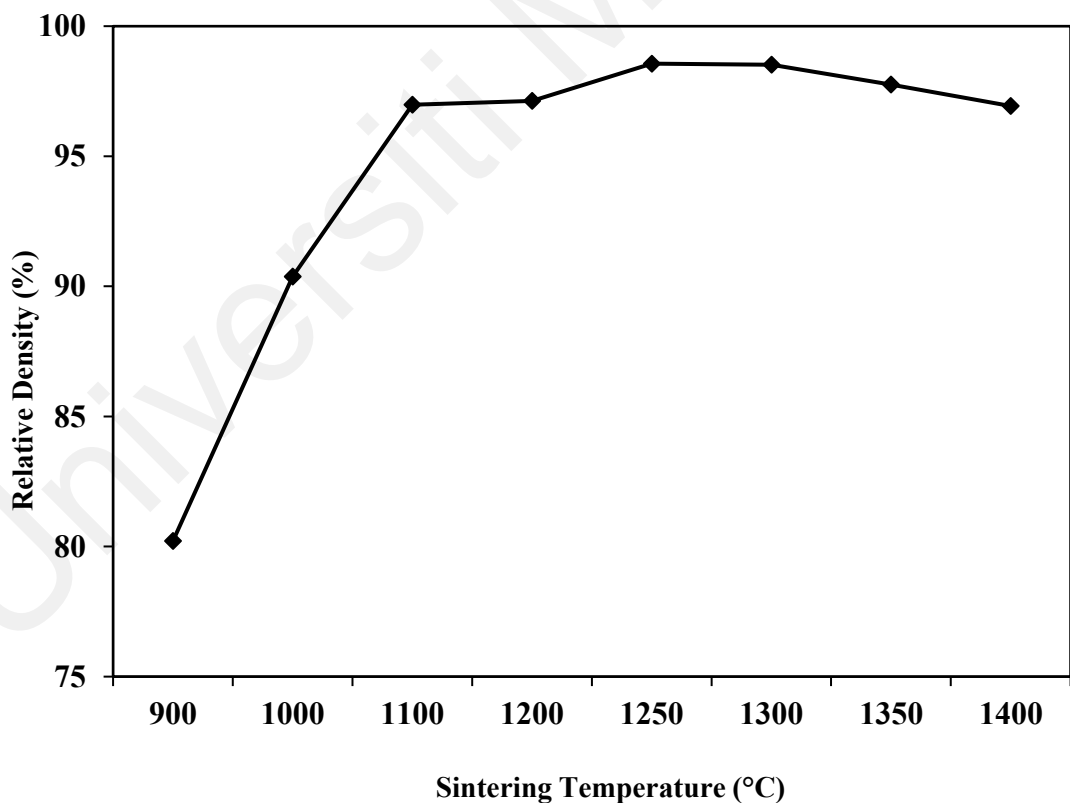


**Figure 4.17: Variation in relative density of eggshell-derived HA samples sintered at various temperatures.**

#### 4.4.7 Linear Shrinkage Analysis

The variation of linear shrinkage at different sintering temperature is shown in Figure 4.18. The linear shrinkage of the cold isostatically compacted specimens were measured based on length change of the samples, before and after sintering. The average shrinkage of the samples were found to be enhanced linearly by increasing temperature from 900 °C to 1300 °C and almost steady thereafter. It's believed that heat treatment profile such as the sintering temperature and firing time can affect the shrinkage of the fired HA. It has been reported that shrinkage could be correlated to densification of sintered body, losing of volatile species such as structural water and pore elimination process (Kutty et al., 2015; Bandyopadhyay et al., 2007). As expected from the density graph of sintered samples (Figure 4.14) and the TGA curve of synthesized HA powder (Figure 4.9), significant increment in shrinkage should proceed up to 1100 °C. As can be seen in the graph, the shrinkage of about 22% is recorded at 1100 °C and raised by about 2% up to 1400 °C. These results are in good agreement with the researches who used the same starting material and method and found the similar rate of ~ 24% shrinkage (Natasha et al., 2016; Gibson et al., 2001). However the present results are not in agreement with the finding of Tan et al. (2015) who reported a linear shrinkage of ~ 14% and ~ 34% by Tan et al. (2008). The different range of HA shrinkage could be related to the different sintering behavior and the synthesized powder which are factors of physical characteristic of synthesized powder such as particle size and shape.

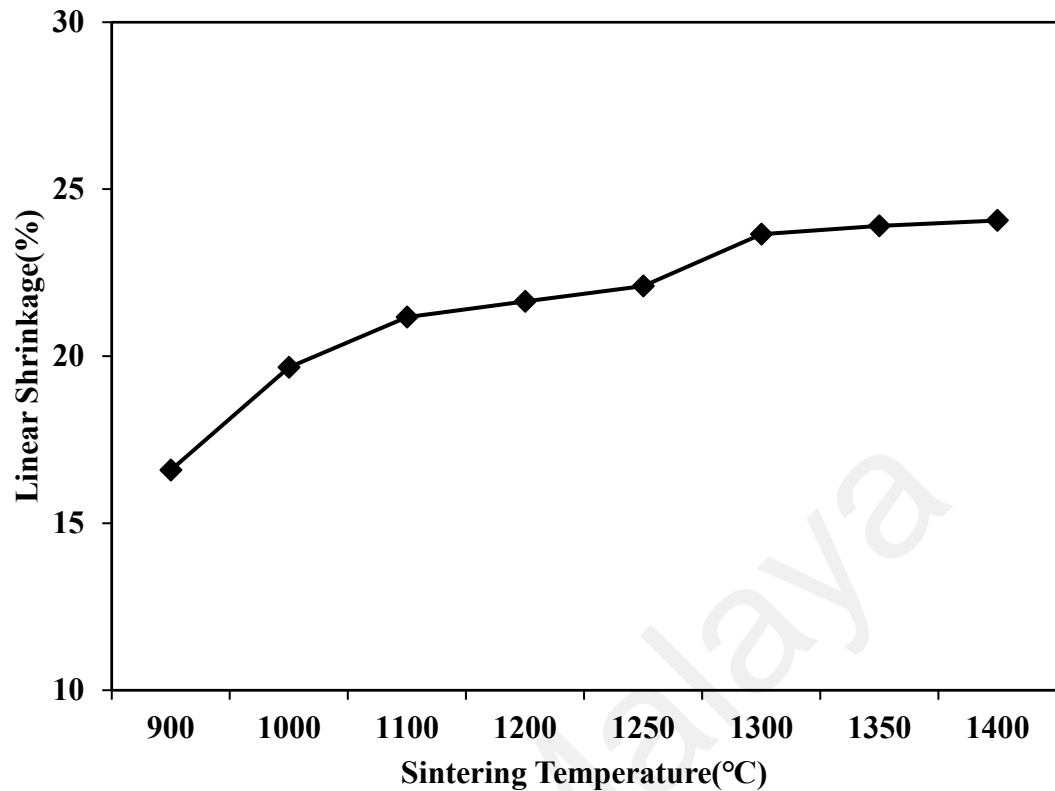


**Figure 4.18: Variation in linear shrinkage of eggshell-derived HA samples sintered at various temperatures.**

#### 4.4.8 Vickers Hardness Analysis

The influence of sintering temperature on the Vickers hardness of eggshell-derived HA is shown Figure 4.19. The results obtained in the present study shows that the microhardness value of sintered samples initially increased almost linearly by increasing temperature from a minimum value of 1.9 GPa at 900 °C to a maximum value of 5.9 GPa at 1250 °C and 1300 °C. The graph shows that the Vickers hardness exhibited a similar trend as that observed for the relative density (Figure 4.17). A low hardness of 1.9 GPa was measured at 900 °C and this can be attributed to the low bulk density of the sintered sample. However, as the sintering temperature was increased, this was accompanied by a steady increased in the Vickers hardness from 3.7 GPa at 1000 °C to reached a maximum of 5.9 GPa when sintered at 1250 °C and 1300 °C. The slight descent can observed with



further increased of sintering temperature up to 1400 °C which could be related to starting of HA phase decomposition at 1350 °C. This behaviour is in good agreement with the increased in the relative density (Figure 4.17). The comparison of Figure 4.17 and Figure 4.19 show that the result of microhardness and relative density were found to be relevant to each other and both attained the max value at the same temperature (Muralithran et al., 2000).

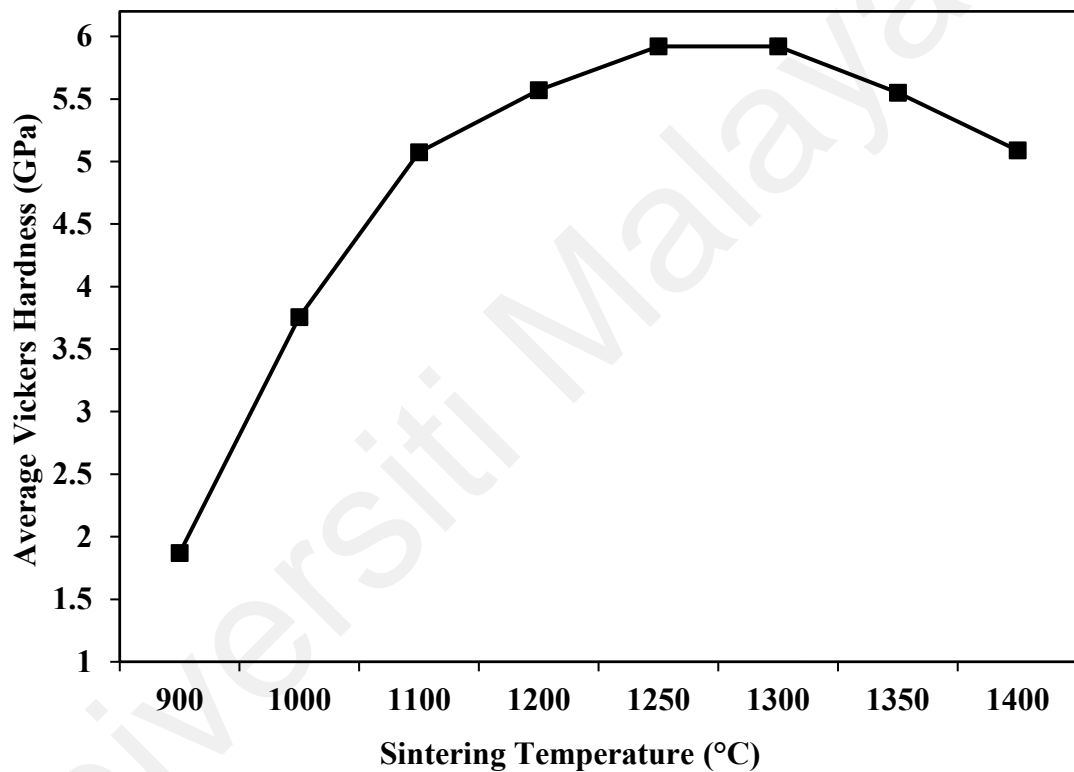


**Figure 4.19: The effect on sintering temperatures on the Vickers hardness of eggshell-derived HA.**

#### 4.4.9 Fracture Toughness Analysis

The fracture toughness variation with sintering temperature for the eggshell-derived HA is shown in Figure 4.20. As can be noted from the Figure 4.20, the graph shows that the fracture toughness increased sharply from 0.71 MPam<sup>1/2</sup> at 900°C to 0.93 MPam<sup>1/2</sup> at

1000°C. Thereafter, the fracture toughness fluctuated slightly between 1.06 – 1.09 MPam<sup>1/2</sup>. The maximum value of 1.09 MPam<sup>1/2</sup> obtained at 1000 °C which is higher than most reported literature of <1 MPam<sup>1/2</sup> could be related to the different synthesized powder (Lin et al., 2012; Wang et al., 2009; Mazaheri et al., 2009). The difference in fracture toughness at first interval could be related to the transition of a porous structure to a packed structure from 900-1000 °C (Figure 4.14) which also affected on the density (Figure 4.17). The values of fracture toughness then dropped slightly up to 0.95 MPam<sup>1/2</sup> at 1400 °C. A similar trend was also observed by other researchers (Tan et al., 2015; Kamalanathan et al., 2014; Natasha et al., 2016).

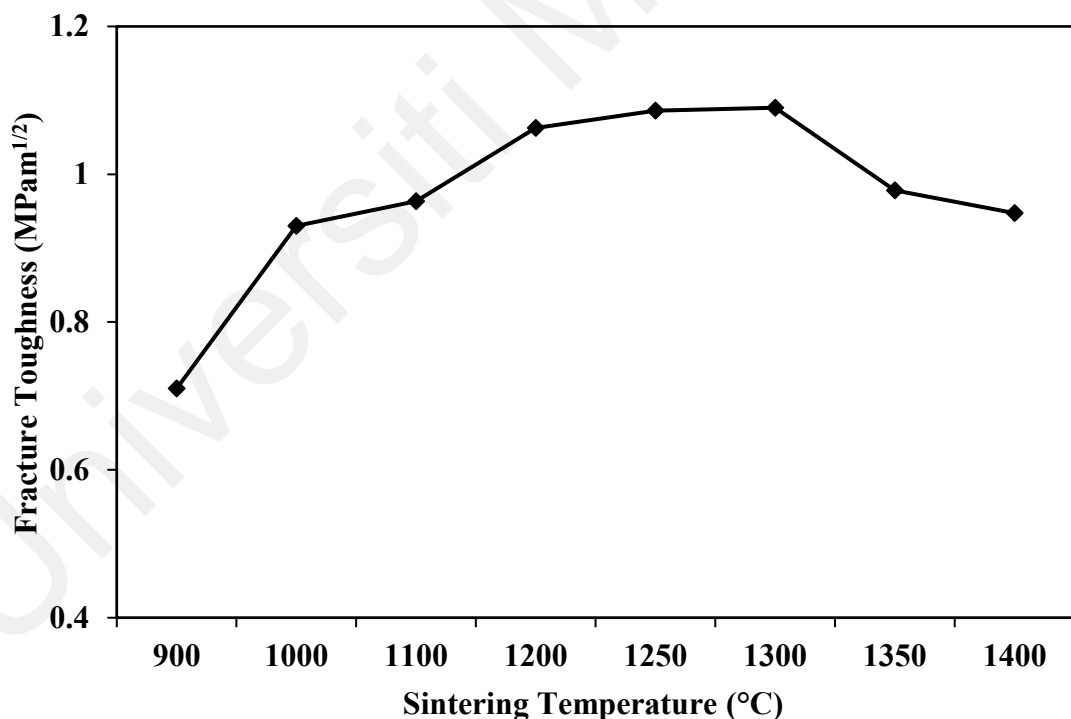


**Figure 4.20: Fracture toughness variation with sintering temperature for eggshell-derived HA.**

#### **4.5 Characterization of Deposited Film of Hydroxyapatite on Titanium Substrate**

Hydroxyapatite powder was derived from eggshell bio-waste through wet chemical method. The synthesized HA powder was applied on titanium substrate via electrophoretic deposition technique. There are many factors which can affect the quality of final product in coating process, such as suspension preparation elements, geometric setup, electrical parameters, electrodes condition and heating process. Many items from mentioned categories were tested to improve the quality of coated layer. Some of them are summarized in Table 4.2. The bold and underlined items in the table are optimized value of each parameter which are finalized and used in sample preparation process.

Universiti Malaysia

**Table 4.2: Examined parameter during deposition process.**

<b>Examined Parameters</b>	<b>Examined values</b>	<b>Remarks</b>
<b>Hydroxyapatite Powder</b>	As-Synthesized HA powder  <b><u>Calcined HA powder (900°C)</u></b> & (1100°C)	As-Synthesized HA powder = comb pattern cracks  <b><u>Calcined HA powder at 900°C</u></b> =crack free, better adhesion
<b>pH</b>	1, 2, <b><u>3±0.5</u></b> , 4, 5, 6, 7	Change mobility of particles=change surface quality  Higher pH=lower mobility=Incomplete coverage substrate by HA  Lower pH=increasing mobility of particles= surface was not homogenous(Particle aggregation)
<b>Weight(g)</b>	0.01, 0.02, 0.03, 0.04, 0.05, <b><u>0.055±0.005</u></b> , 0.06, 0.07, 0.08, 0.09, 0.1, 0.11, 0.12	Less amount of HA=Incomplete coverage  Weak joining between substrate and coated layer after deposition.(formation of a thick layer and different drying rate of film)
<b>Solvent Type</b>	Acetone, <b><u>Ethanol</u></b>	Rapid vaporization of acetone caused cracks on surface
<b>Sonicating Time (min)</b>	5, 10, 15, <b><u>20</u></b> , 25	More sonicating duration caused better surface. There were not too much difference between 20 and 25min, So 20min was chosen as optimum time.
<b>Applied Voltage(V)</b>  (higher voltage applied on minimum time and weight)	10, 15, 20, <b><u>25</u></b> , 30, 35, 40, 45, 50, 55, 60, 65, 70, 75, 80, 85, 90	Low voltage= appearance of pinholes,  High voltage= high turbulence effect on accumulation rate

‘Table 4.2, continued’

Examined Parameters	Examined values	Remarks
<b>Deposition time (min)</b>	1, 2, 3, 4, 5, <u>6</u> , 7, 8, 9, 10	Short times=very thin layer Long time= Ruptured and appearance of deep cracks
<b>Deposition type</b>	<u>Single layer</u> . Double layer	Chipping and weak joining in double layer specimen
<b>Distance between electrodes</b>	0.5 cm, <u>1cm</u> , 2cm	Distance between electrodes effect on surface quality
<b>Roughness of substrate</b>	Abrasive paper No: P 1000, P800, <b>P600</b>	Higher roughness=Better joining
<b>Electrode Size</b>	Same size with substrate and <b>Double size</b>	Bigger electrode= Less aggregation
<b>Applied binder</b>	Triethanolamine	High viscosity = Surface quality was not good: Less smoothness
<b>Sintering temperature</b> (Holding Time: 70minute)	900°C 950°C 1000°C 1050°C 1100°C	1100°C: Laminated

The first step of coating process is suspension preparation which is a factor of solvent nature, sonication time, pH of medium, suspension concentration and hydroxyapatite particles. Ethanol and acetone were tested as solvent in this study. More cracks were observed on the samples when using acetone compared to ethanol base suspension. It is known that the evaporation rate of acetone is higher than ethanol, hence this would be the reason of rapid drying and appearance of cracks on deposited film. The suspension was sonicated in order to attain a homogenous suspension. Various sonication time of 5 min-25 min were tested. More sonicating duration resulted in a more uniform and better surface. The pH of medium was adjusted by adding different amount of hydrochloric acid. The pH of suspension effects the mobility of particles, surface charging level and density of deposited layer (Besra et al., 2007; Kruger et al., 2004). Higher pH level resulted in a porous layer of hydroxyapatite on substrate and lower pH level resulted in agglomeration of coated layer. The pH level of  $3\pm 0.5$  was found to be optimum in this study. Different amount of hydroxyapatite was added to solvent to optimize the concentration of suspension. A very thick and unstable coating film was formed when tested in high concentration level while partial coverage of hydroxyapatite powder on substrate was observed in lower concentration level.

The geometrical setting up of the coating elements was the second step in deposition procedure. Electrodes condition such as roughness, size and position also played an important role in this stage of coating process. Two electrodes should be situated carefully and fixed in front of each other in same direction. The optimum distance and constant direction of electrodes allowed to form a dense particle packing of hydroxyapatite on titanium substrate with less aggregation during coating process. The sizes of electrodes also affect the surface quality. Using the same size of electrode and substrate resulted in the condensation of the particles at the edge of coated specimen, while using double size

electrode with smaller substrate showed more homogenous thickness (Fleckenstein et al., 2012).

Electrical parameter such as the power can affect the thickness, smoothness and density of formed layer as well. The coating process is based on migration of particles in a suspension toward electrode and deposited on substrate under electrical field. The migration rate of particles and the speed of the process can be controlled by adjusting the applied voltage and deposition time throughout coating procedure. The voltage of 10-90v at deposition time of 1 min-10 min were applied on titanium to find the optimum range. Higher voltage increases turbulence intensity of particles (Boccaccini et al., 2008), so accumulation rate of hydroxyapatite powder on substrate was raised and resulted in a non-uniform layer of deposited film. Deposition time is another factor that should be controlled in coating process. The coating of hydroxyapatite in different period, showed increasing of coating duration time would ruptured the deposited film and caused the appearance of deep cracks on coated layer due to it higher thickness.

Final stage of sample preparation is the heating process. After optimizing of coating parameters, deposited specimens should be heat treated prior to characterization. Heating profile such as sintering temperature, heating and cooling rate, firing time and furnace atmospheres were optimized to produce perfect shape and crack free coating film of hydroxyapatite on titanium substrate. Oxidizing of the layers, crack, and pinhole, were the observed defects which were solved by adjusting heating profile and furnace environment.

#### 4.5.1 Microscopic Evaluation of Coated Surface

The surface of deposited hydroxyapatite was inspected using optical microscope. Figure 4.21 shows the microscopic view of coated film in different condition. The first deposition of HA on titanium substrate with basic parameters is shown in Figure 4.21a. As discussed earlier, many items such as solvent type, suspension concentration and deposition time, were examined during the coating process to make improvement on the deposited HA film. Figure 4.21(b) presented the outcome of double layer deposition. Coating of hydroxyapatite in two steps, resulted in a non-uniform film and expected to be laminated after sintering because of weak connection between the layers. The highlighted colours show the difference between upper and inner layer. Rupturing of HA film and appearance of deep micro cracks on deposited film (Figure 4.21 c) was observed after using triethanolamine as binder. Although adding the binder to solution was suggested by researchers to make the particles more suspended and to improve the adhesion of deposited layer to substrate, but it also increased the viscosity of the suspension and caused the formation of a thick layer (Maleki-Ghaleh et al., 2012; Karimi et al., 2016). Based on previous studies, it has been assumed that the different rate of drying between the inner part and top surface of coated film resulted in the forming of honeycomb pattern cracks (Jankovic et al., 2016; Sun et al., 2011). A crack free HA coating film (Figure 4.21d) was produced after optimizing the various coating factors. The optimized coating factors are listed and highlighted in Table 4.2.



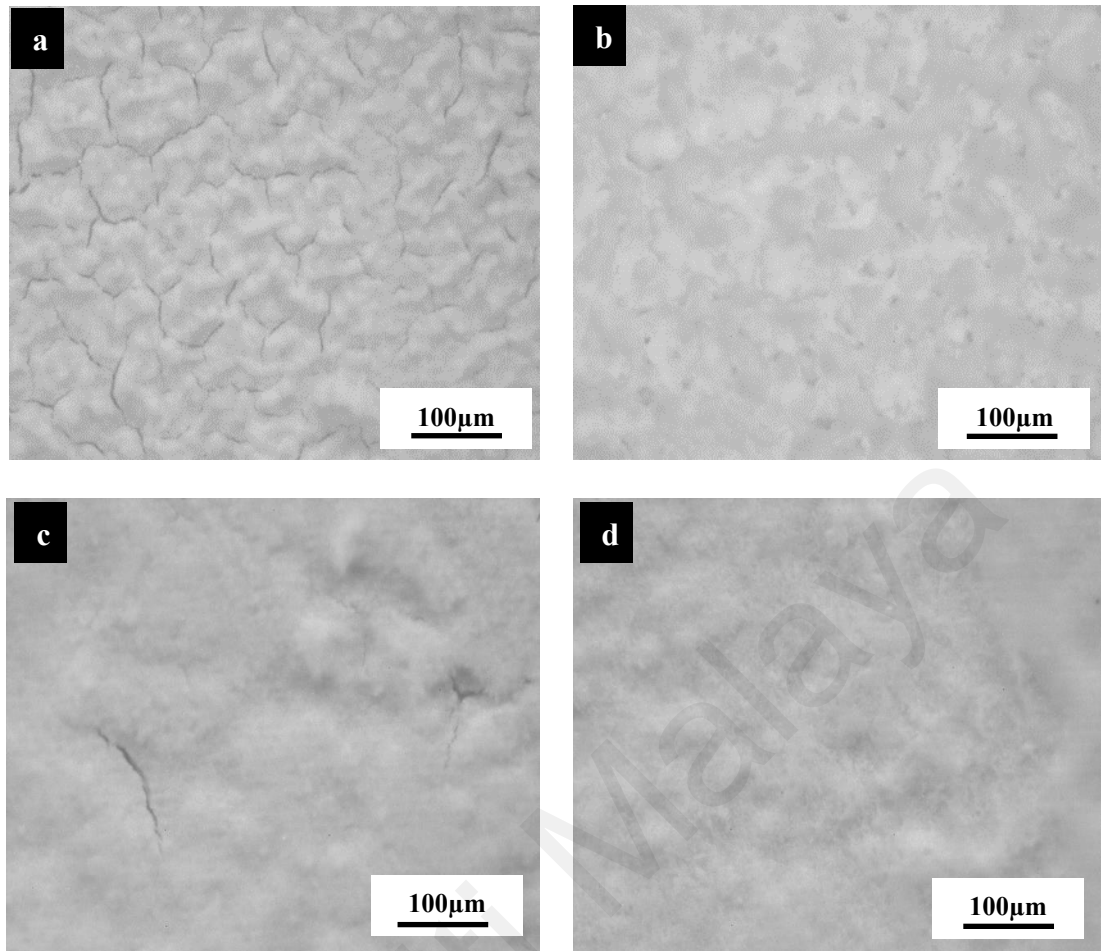


**Figure 4.21: Microscopic images of deposited film of hydroxyapatite on titanium substrate via EPD before heat treatment.**

The microscopic image of sintered specimen before (a) and after (b) modification is shown in Figure 4.22. One of the unfavourable defects of ceramics after sintering is cracks of sintered body or surface. Figure 4.22(a) shows a network of crack on the sintered body, which was happened due to the different thermal characteristic of hydroxyapatite and titanium. As discussed in section 4.4.7, the synthesized hydroxyapatite in this study which was used as coating material, exhibited about 16% linear shrinkage when sintered at 900 °C (Figure 4.18).

Thermal expansion of titanium along with shrinkage of hydroxyapatite caused mismatch between the contact areas and lead to network cracks after sintering. It was reported that, calcination treatment on hydroxyapatite delays the initiation of sintering, and also decreases the shrinkage rate, thus the material will reach the final stage of sintering at higher temperature (Juang & Hong, 1996; Wei et al., 1999). Hence as-synthesized hydroxyapatite powder was calcined at 900 °C prior to deposition process and resulted in a crack free coated film (Figure 4.22 b) after heat treatment process.

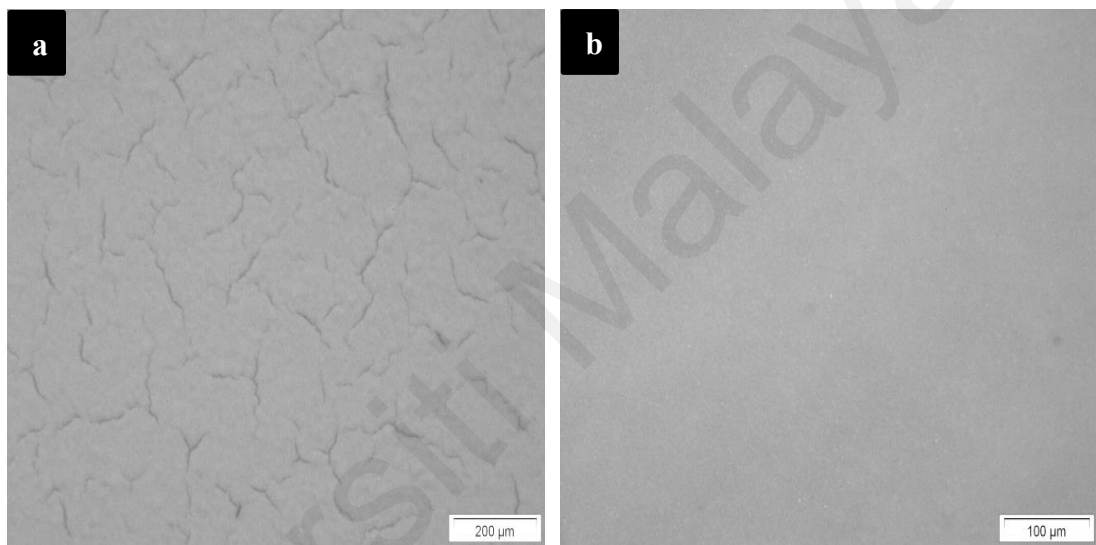


**Figure 4.22: Microscopic images of sintered specimen before (a) and after (b) modification.**

#### **4.5.2 XRD Analysis of Sintered HA Coating**

Visual observation of the sintered coated substrates indicated that sintered at 1100 °C was detrimental as it resulted in the delamination of the HA coating. Hence, subsequent analysis was focused on substrates sintered up to 1050 °C.

The XRD signatures of sintered substrates at 900 °C to 1050 °C are shown in Figure 4.22. The XRD analysis of coated hydroxyapatite on titanium revealed the formation of pure and highly crystalline hydroxyapatite as confirmed by comparing to the standard

JCPDS reference card number (00-009-0432) for hydroxyapatite. There was no secondary phase formation such as tricalcium phosphate or tetracalcium phosphate. The intensity of all peaks including the highest peak at  $2\theta=31.78^\circ$  corresponding to (2 1 1) lattice plane, increased with increasing sintering temperatures. The changing of the broad peaks to sharp peaks at higher temperatures was associated to phase transition from amorphous to crystalline which is believed to start at 400 °C based on the DTA analysis (Section 4.3.4 - Figure 4.9).

Based on the XRD analysis, sintering of deposited sample at 1050 °C has been identified as the optimum sintering temperature as the coating composed of highly crystalline hydroxyapatite phase which is favourable for biomedical application.

In general, the synthesized HA derived from eggshell in the present work exhibited good thermal stability when sintered up to 1050 °C when compared to that reported by other researchers who noted the decomposition of hydroxyapatite proceeded at about 930 °C in their studies (Zhitomirsky & Gal, 1997; Rapacz-Kmita et al., 2005).

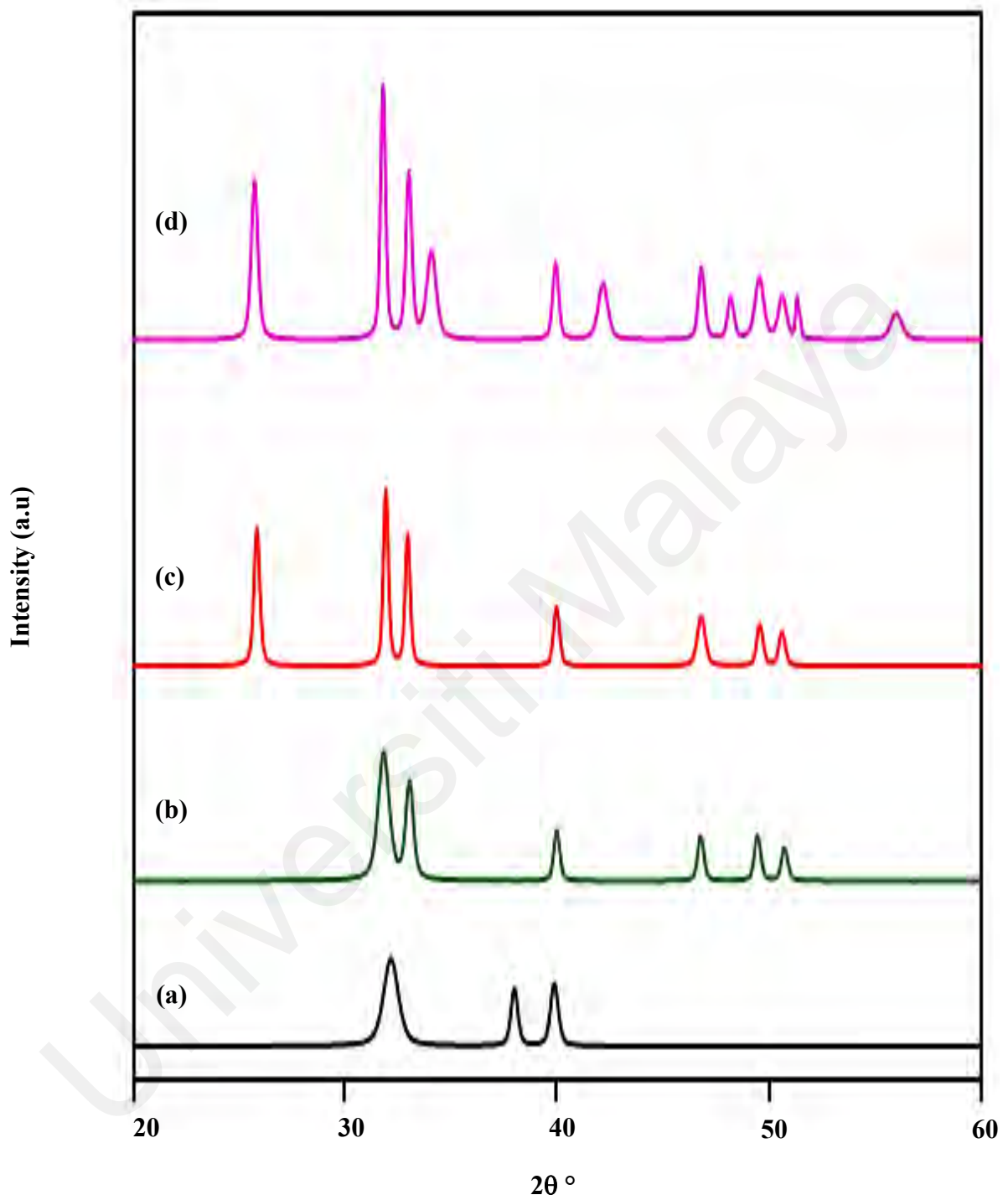


**Figure 4.23: XRD signatures of coated substrates sintered at various temperatures: (a) 900 °C, (b) 950 °C, (c) 1000 °C and (d) 1050 °C. All peaks corresponded to the HA phase.**

### 4.5.3 Microstructural Analysis of Sintered HA Coating

The FESEM microstructure of the HA coating sintered at various temperatures is shown in Figure 4.24. As can be observed that the deposition was successful as there was no visible crack or pinhole in the coating, as typically shown in Figure 4.24 (e) for hydroxyapatite coating sintered at 1050 °C.

In addition, regardless of sintering temperatures, a homogeneous HA structure, comprising of an equiaxed grain morphology having a uniform size across the surface can be noted from Figures 4.24 (a-d), thus demonstrating that the starting HA powder and the deposition conditions employed in the present work were feasible. The results also indicated that a uniform and relatively dense layer of hydroxyapatite, particularly for substrates sintered at 1000 °C and 1050 °C were deposited on titanium. Sintering above 1050 °C was not favourable as delamination of the HA layer was observed. This phenomenon could be associated with the oxidization of the titanium as substrate at high temperatures and could result in the degradation of HA phase (Wei et al., 2001; Ruys et al., 1995; Wei et al., 2005).

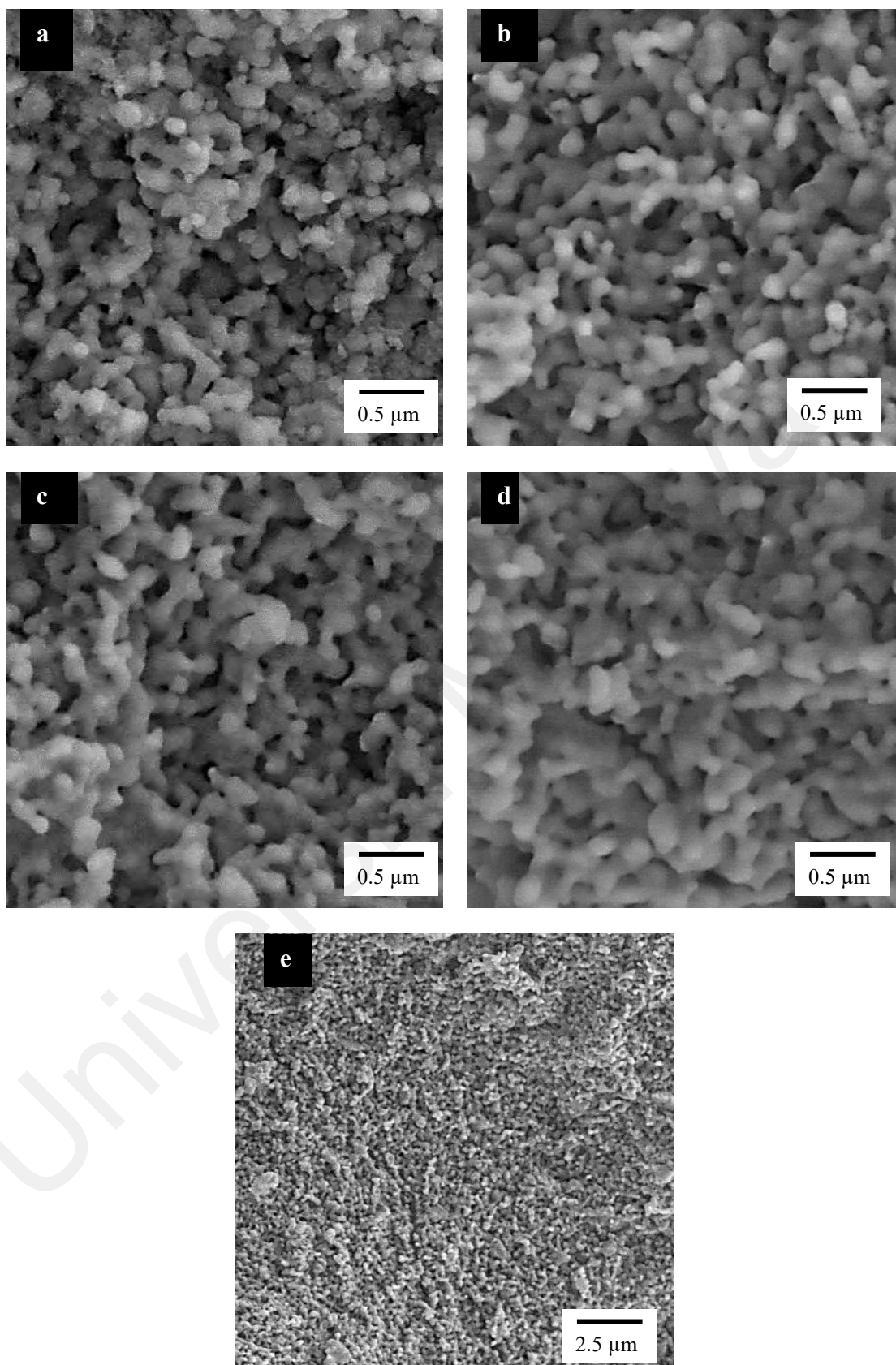


**Figure 4.24: FESEM images of HA coating sintered at (a) 900 °C, (b) 950 °C, (c) 1000 °C and (d & e) 1050 °C.**

#### 4.5.4 EDS Analysis of Sintered HA Coating

The EDX analysis of sintered HA coating at 1050 °C is presented at Figure 4.25. A similar profile was noted for other sintering temperatures. The presence of elements such as Mg, Si and K were expected as it is associated to the eggshell which was used as the starting calcium precursor. The existence of these elements in the HA coating is favourable since such elements are generally found in natural bone composition (Akram et al., 2014; Niakan et al., 2015).

Calcium and phosphate were the major peaks detected by EDS analysis, and according to the data, the Ca/P ratio of the HA coating was calculated to be about 1.67. This value differs from the values of 1.5 to 1.65 as reported by several authors and can be attributed to the different processing method employed and precursors used to synthesis the HA powder (Manso, et al., 2000; Raynaud et al., 2002).

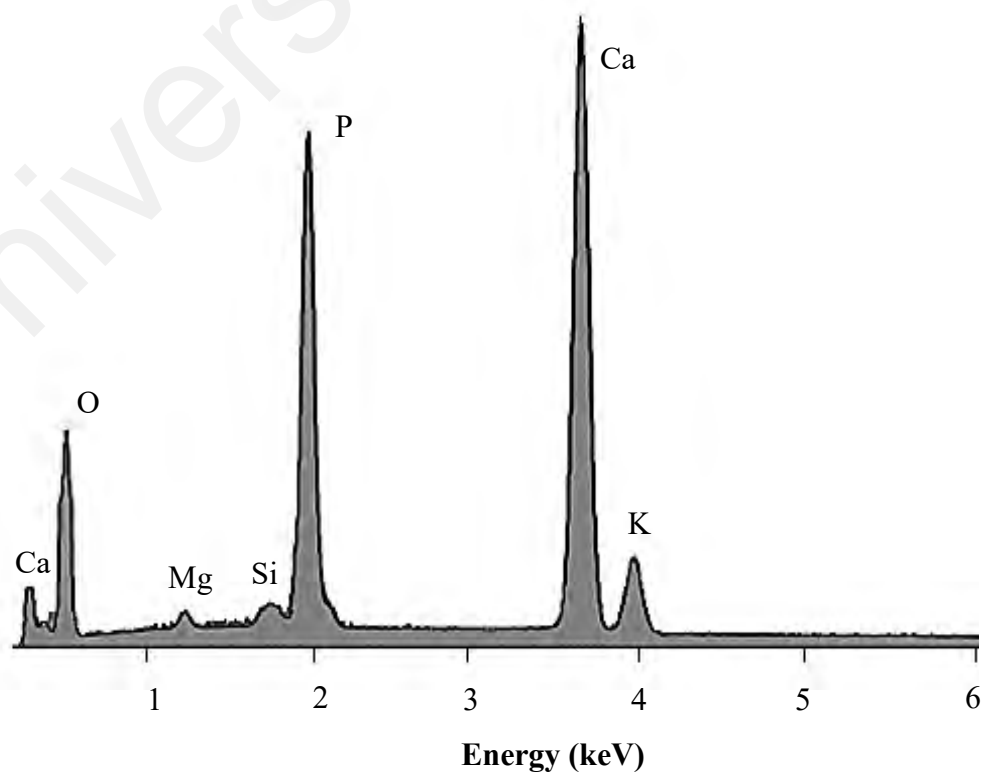


Figure 4.25: Typical EDX analysis of sintered HA coating at 1050 °C.

#### 4.5.5 Topography Analysis of Sintered HA Coating

The roughness and topography analysis of the coated layer was evaluated using the atomic force microscopy at scan angle of  $0^\circ$ , scan size of 5 nm and scan rate of 1 Hz.

Atomic force microscopy image of HA coated surface at the scale of  $5 \text{ nm}^2$  is given in Figure 4.26. The 3D image of deposited specimen showed the formation of a uniform and compact layer of HA. The topography view of the surface revealed the full coverage of HA particles on substrate was achieved through the coating process.

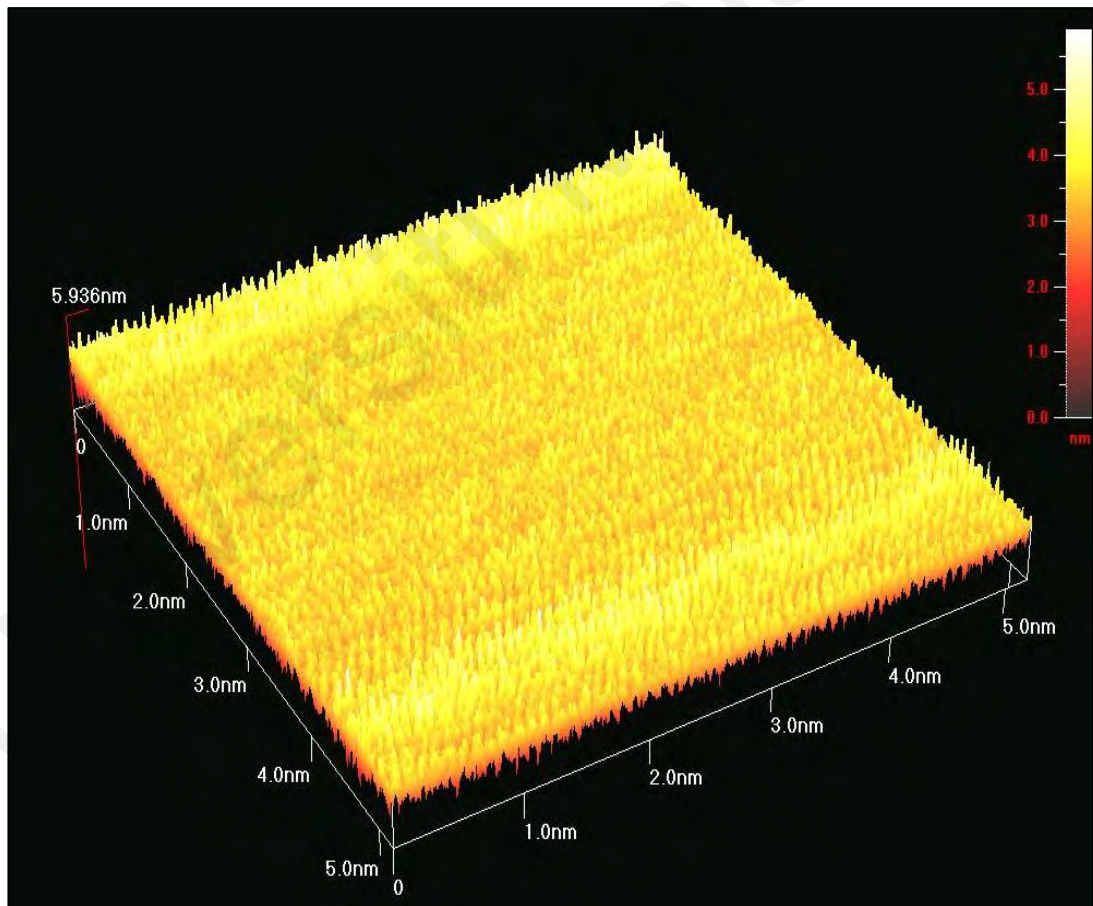
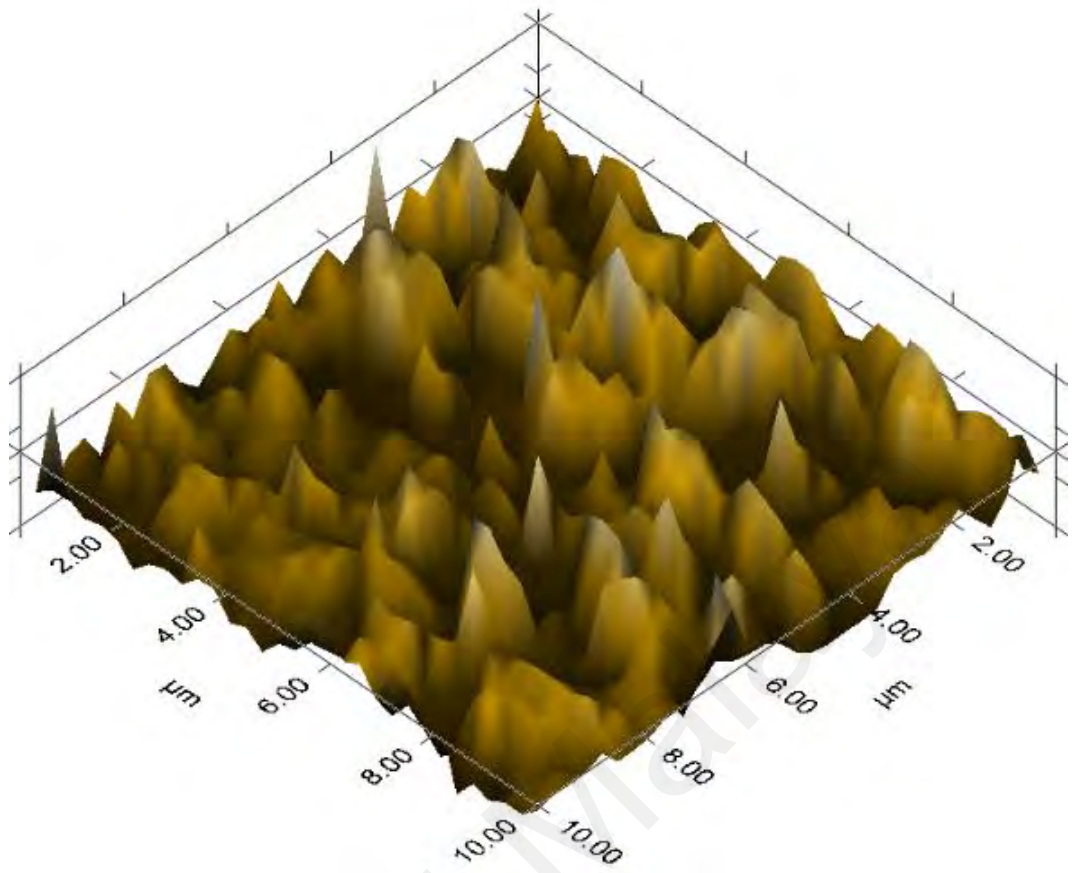


Figure 4.26: 3D images of sintered coating surface at a scale of  $5 \text{ nm}^2$ .



Topography analysis of sintered sample at a scan size of 10  $\mu\text{m}$  is shown in Figure 4.27 and Figure 4.28 shows the roughness schematic of the deposited HA. Surface texture analysis of sample shows the formation of rough surface after sintering. The average roughness of 345 nm was recorded by topographic analysis of sintered specimen. Higher roughness means higher surface area which could provide better condition for biological molecules and bone forming cells, and improve cell attachment to the implant surface and better adhesion with surrounding tissue in biomedical application. Furthermore, It has been confirmed that a suitable roughness can improved the cell adhesion and proliferation, moreover, roughened implant surface showed increased in the amount of translocated bone particles and thereby led to beneficial osteogenic responses similar to autografts improving peri-implant osteogenesis (Mendonca et al., 2009; Rosa et al., 2003; Cai et al., 2006; Lou et al., 2015). There are review articles have reported that higher roughness can be obtained by deposition of thicker layer. Although there is positive correlation between surface roughness and osseointegration, but thick layer ( $> 300 \mu\text{m}$ ) is not favourable because of weak bonding and variance characteristic on the free surface of coating and interface layer with substrate. So, it is more desirable to obtain a thin layer (1  $\mu\text{m}$  -100  $\mu\text{m}$ ) together with high roughness, which was attained in this study, hence it can assumed that it could be usable in biomedical applications (Eliaz et al., 2009; Jung et al., 2012).



**Figure 4.27: 3D images of sintered coating surface sample according to scale of  $10 \mu\text{m}^2$ .**

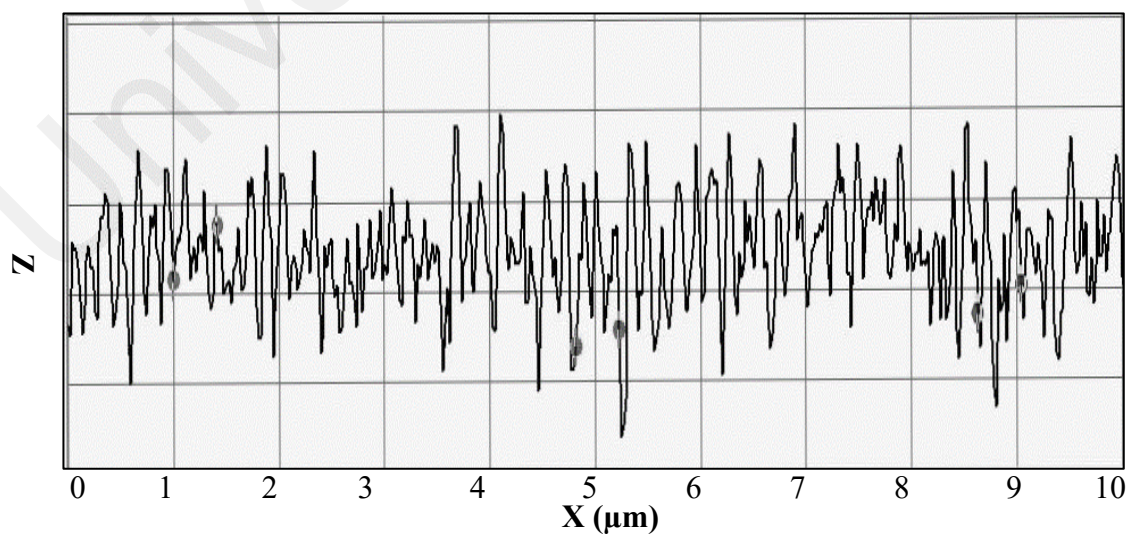


**Figure 4.28: The schematic view of surface roughness profile.**

#### 4.5.6 Cross Sectional Analysis of Sintered HA Coating

A typical cross-sectional view of the coated substrate sintered at 1050 °C is presented in Figure 4.29. A relatively uniform layer with an average thickness of about 20 µm was formed by deposition process. As can be seen in the FESEM picture, the coating and substrate exhibited excellent bonding with each other. This result indicated that the good adhesion between the HA layer and the substrate obtained by electrophoretic deposition could be related to the nano-sized particles of the HA powder, believed to have played a role in reducing the thermal expansion mismatch between the HA and substrate during sintering (Gleiter et al., 1992; Jung et al., 2012; Rad et al., 2014; Thair et al., 2011).

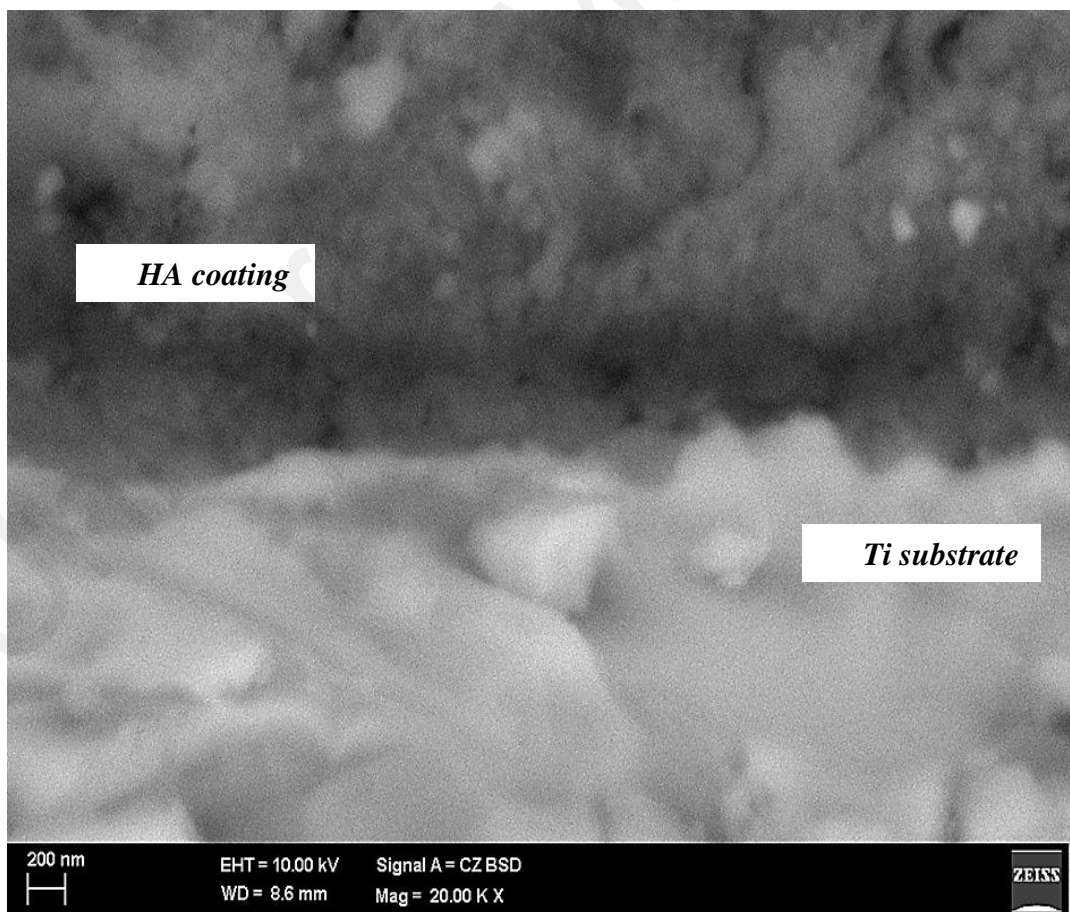


**Figure 4.29: FESEM images of the cross-sectional area of HA coated substrate sintered at 1050 °C.**

The cross sectional view and the compositional profile of the coated substrate sintered at 1050 °C is shown in Figure 4.30. It can be observed that a good bonding exist at the interface of the substrate and HA layer. The compositional signatures of Ca, P and Ti as measured along the  $x$ - $y$ - $z$  line and superimposed on the FESEM micrograph in Figure 4.30 indicated that there was no reaction between the Ti and HA. A smooth transition in the compositional profile can be observe at the bonding interface “point  $y$ ” as shown in Figure 4.30. This results show that the electrophoretic deposition employed in the present work was successful in depositing HA onto Ti substrate without inducing any secondary phase formation. A study by Lou et al. (2015) discussed about the importance of bonding capability of coating in clinical application. From the cross sectional view of the deposited film, it’s assumed that a dense and compact structure without visible micro cracks had a favourable bonding capability (Lou et al., 2015).

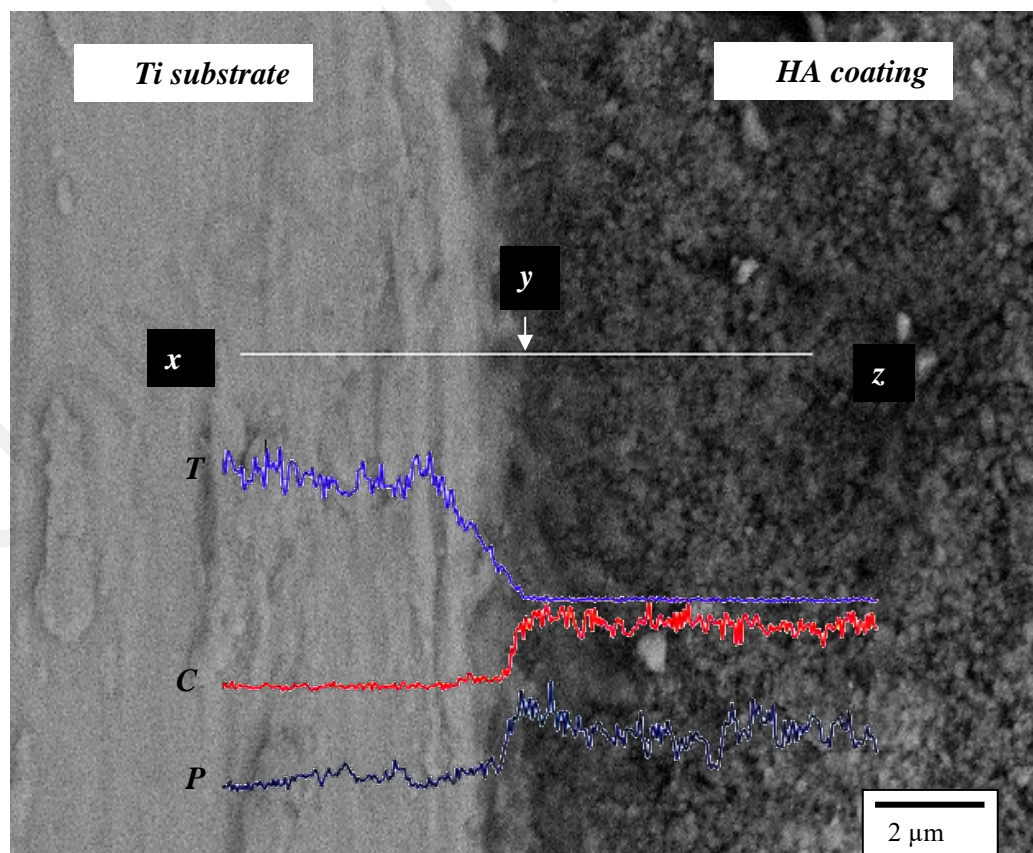


**Figure 4.30: FESEM micrograph of HA coated substrate sintered at 1050 °C showing the nature of the bonding at the interface between the HA coating/Ti substrate and compositional analysis across the interface.**

#### 4.5.7 Indentation Analysis of Sintered HA Coating

Nanoindentation test was performed on coated sample in depth control mode in order to investigate the resistance of produced HA against surface deformation that caused by an external load. Figure 4.31 demonstrated the effect of indenter on HA. Assessment of the image show there is no sign of deformation such as pile-ups and sink-ins and also, there were no any radial cracks around the indentation. The average hardness value of HA deposited on titanium in this study was about  $1.12 \pm 0.2$  GPa which was comparable with hardness of bulk HA and almost higher than the normal range as reported by researchers using the same technique (Karimzadeh et al., 2014; Gross et al., 2010). It is believed that the difference between reported values could be related to the physiochemical properties of green material such as particle size and phase stability which were a function of preparation process and starting material. It have been reported that the degradation of mechanical properties of HA at higher sintering temperature was due to decomposition of this material and phase transition to other phases such as TCP and TTCP. Hoepfner et al. (2003) reviewed the relationship between porosity and hardness of hydroxyapatite. They have highlighted that hardness is a strong function of the porosity. They found that the hardness of HA sample was significantly enhanced after cold isostatically pressing due to more compactness and reduction in the porosity. Using natural calcium source and synthesizing high quality HA powder which is stable at high sintering temperature (Figure 4.11), and also cold isostatically pressing of the coated specimen resulted in a better mechanical properties have led to a higher value of hardness in this study (Ayatollahi & Karimzadeh, 2013; Saber-Samanadari & Gross, 2010; Drevet et al., 2016).

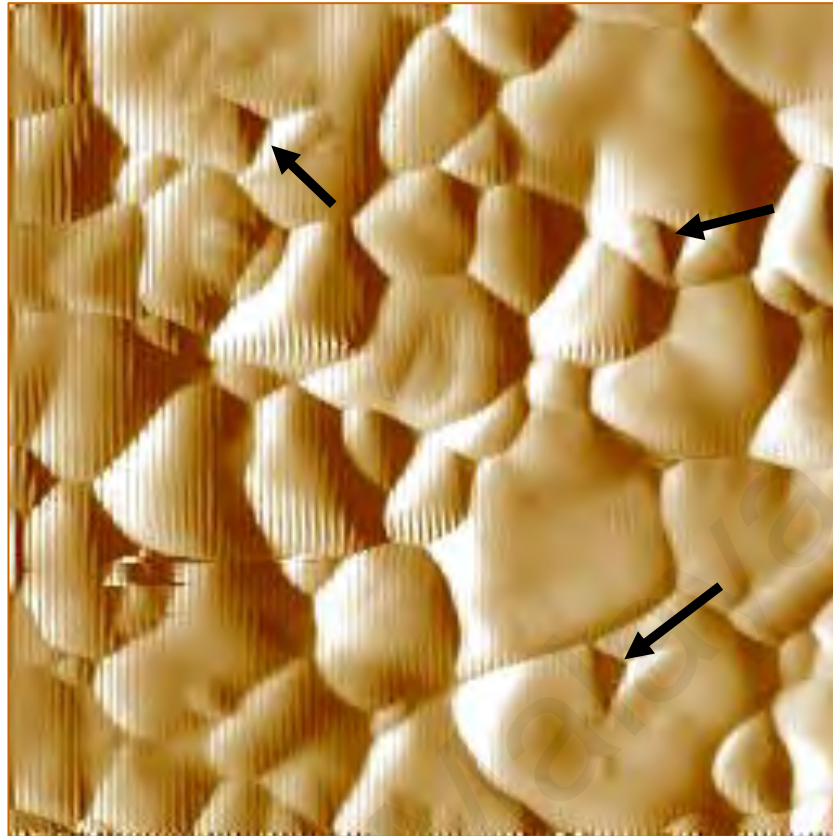


**Figure 4.31: Micrograph image of nano-indentation on HA grains (as shown by the arrows) in the field view of  $5\ \mu\text{m}\times 5\ \mu\text{m}$ .**

#### **4.5.8 Wettability Analysis of Sintered HA Coating**

Figure 4.32 revealed the wettability of coated surface (a) and uncoated surface (b). Higher water contact angle of  $\approx 102^\circ$  was obtained for uncoated surface in comparison to coated surface which presented an aqueous contact angle of  $\sim 72^\circ$ . This result indicated that the sample surface became more hydrophilic and had higher surface wettability after deposition of hydroxyapatite on it. Hydrophilicity of the surface is one of the main factor in coating process. High hydrophilicity as a result of low contact angle is more favourable for biomedical application in order to obtain a high surface coverage. Hydrophilicity or hydrophobicity of the coated surface are related to the surface chemistry and surface charge of the deposited layer. It has been reported that the water contact angle increases monotonically with the incident charge dose (Aronov et al., 2008; Eliaz et al., 2009). The

attached water molecules on the surface enable the interaction of specific molecules such as proteins involvement in the cell substrate interactions. On the other hand calcium ions in hydroxyapatite can aid the adsorption of main proteins such as vitronectin and fibronectin thus leading to better cell attachment. These results indicated that the coated surface expected to perform well in cell attachment and be a good candidate of bone replacement. (Rad et al., 2014; Eliaz et al., 2009; Webster et al., 2001; Atankov et al., 1996; Feng et al., 2004).

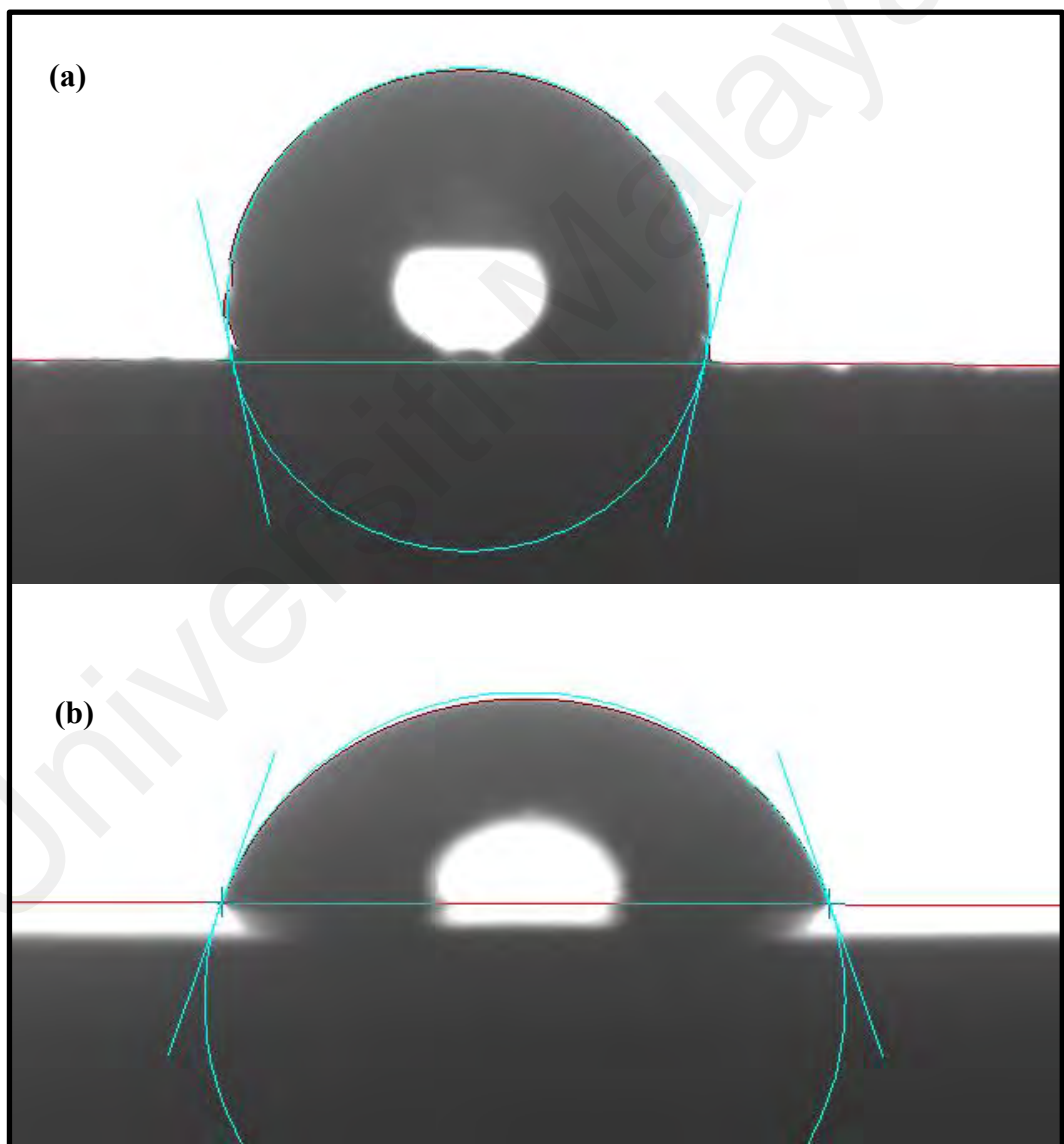


**Figure 4.32: Water drops on non-coated surface (a) and coated surface (b).**

## CHAPTER 5: CONCLUSIONS AND FUTURE WORKS

### 5.1 Conclusion

This research focused on the synthesis of hydroxyapatite from bio waste eggshells, sintering of synthesized hydroxyapatite at different temperatures and coating of the hydroxyapatite on titanium substrate.

The process of converting eggshell to hydroxyapatite through a wet chemical route was presented. Synthesized hydroxyapatite were sintered at the firing temperature range of 900 °C-1400 °C. The sintering behavior and mechanical properties of hydroxyapatite derived from eggshells were investigated in the first part of the study. The conclusions of this study are as listed below:

1. Phase pure and crystalline hydroxyapatite was synthesized successfully via a modified wet chemical precipitation route, using chicken eggshells biowaste as calcium precursor and phosphoric acid as the phosphorus source.
2. Needle like shape nanoparticles of hydroxyapatite with average size of 50 nm was produced. Homogenous structure of hydroxyapatite with an average gran size of 2.5  $\mu\text{m}$  was attained when sintered at 1300 °C.
3. The presence of elements such as Mg, Si and K in the EDS analysis was detected in the HA, believed to be associated with the eggshell which was used as the starting calcium precursor
4. The hydroxyapatite thermal stability was not disrupted even after sintering at high temperature of 1300 °C, however, dissociation of hydroxyapatite to the secondary phases of TCP and TTCP was started at 1350 °C.



5. The bulk density of HA was found to increase with increasing sintering temperature up to 1300 °C. Sintering at 1250-1300 °C was beneficial in producing a solid dense HA body having relative density of 98.5%.
6. The evaluation of HA mechanical properties revealed high Vickers hardness of 5.9 GPa and high fracture toughness of 1.09 MPam<sup>1/2</sup> despite developing large grain size of 2.5 µm.
7. The synthesized eggshell HA exhibited a stoichiometric Ca/P ratio of 1.67 without compromising on the phase stability.
8. Based on the results obtained, the optimum firing temperature for the synthesized HA powder was 1300 °C.

This research has demonstrated the viability of producing highly crystalline, phase pure hydroxyapatite from bio-waste eggshells. Thermal stability and sintering behaviour of synthesized hydroxyapatite was evaluated. From the evaluation of the attained results and characterizations, synthesized hydroxyapatite was found to be a potential candidate for biomedical application.

The process of coating eggshell-derived hydroxyapatite synthesized via a wet chemical precipitation on titanium substrate through electrophoretic deposition method and the sintering behaviour of the deposited HA layer was investigated in the second part of the study. The following conclusions were drawn from this study.

1. The results indicated that a crack-free and phase pure crystalline hydroxyapatite was deposited successfully on the titanium substrate.
2. A relatively uniform layer with an average thickness of about 20 µm and average roughness of 345 nm was formed by deposition process
3. The HA phase was not disrupted and was stable up to 1050 °C, however delamination of the coating occurred when sintered at 1100 °C.

4. Based on the FESEM and phase composition analysis, sintering at 1050 °C was found to be the optimum condition to produce a highly crystalline HA coating characterised by having a homogeneous structure, comprising of equiaxed grain morphology.
5. A good bonding exist at the interface of the substrate and hydroxyapatite layer, while there was no reaction between the titanium and hydroxyapatite.
6. The existence of Mg, Si and K elements in the HA coating was favourable since such elements are generally found in natural bone composition.

This study has demonstrated the viability of employing eggshell as the starting calcium precursor to produce needle-like HA particles suitable for use as coating on titanium using electrophoretic deposition method. The electrophoretic deposition employed in the present work was successful in depositing crack free hydroxyapatite film onto titanium substrate without inducing any secondary phase formation.

## **5.2 Suggestions for Future Work**

The suggestions for future works are as follows;

1. To evaluate different coating method and compare the performance with that produced by EPD technique.
2. To study the biocompatibility of the synthesized eggshell HA coating by conducting in vivo and in vitro study

## REFERENCES

- Abdulrahman, I., Tijani, H. I., Mohammed, B. A., Saidu, H., Yusuf, H., Ndejiko Jibrin, M., & Mohammed, S. (2014). From garbage to biomaterials: an overview on egg shell based hydroxyapatite. *Journal of Materials*, 2014.
- Adeleke, S., Ramesh, S., Bushroa, A., Ching, Y., Sopyan, I., Maleque, M., . . . Sutharsini, U. (2018). The properties of hydroxyapatite ceramic coatings produced by plasma electrolytic oxidation. *Ceramics International*, 44(2), 1802-1811.
- Afshar, A., Ghorbani, M., Ehsani, N., Saeri, M., & Sorrell, C. (2003). Some important factors in the wet precipitation process of hydroxyapatite. *Materials & Design*, 24(3), 197-202.
- Ahmad, Z., Khan, A. U., Farooq, R., Saif, T., & Mastoi, N. R. (2016). Mechanism of Corrosion and Erosion Resistance of Plasma-Sprayed Nanostructured Coatings *High Temperature Corrosion: InTech*.
- Akram, M., Ahmed, R., Shakir, I., Ibrahim, W. A. W., & Hussain, R. (2014). Extracting hydroxyapatite and its precursors from natural resources. *Journal of materials science*, 49(4), 1461-1475.
- Al-Qasas, N. S., & Rohani, S. (2005). Synthesis of pure hydroxyapatite and the effect of synthesis conditions on its yield, crystallinity, morphology and mean particle size. *Separation science and technology*, 40(15), 3187-3224.
- Andreiotelli, M., Wenz, H. J., & Kohal, R. J. (2009). Are ceramic implants a viable alternative to titanium implants? A systematic literature review. *Clinical Oral Implants Research*, 20, 32-47.
- Anné, G., Vanmeensel, K., Vleugels, J., & Van der Biest, O. (2005). *Electrophoretic deposition as a novel near net shaping technique for functionally graded biomaterials*. Paper presented at the Materials Science Forum.
- Aoki, H. (1991). Science and medical applications of hydroxyapatite. *JAAS*, 1991, 123-134.
- Aronov, D., Rosen, R., Ron, E., & Rosenman, G. (2008). Electron-induced surface modification of hydroxyapatite-coated implant. *Surface and Coatings Technology*, 202(10), 2093-2102.

- Ayatollahi, M., & Karimzadeh, A. (2013). Nano-Indentation Measurement of Fracture Toughness of Dental Enamel. *International Journal of Fracture*, 183(1), 113-118.
- Azadmanjiri, J., Berndt, C. C., Wang, J., Kapoor, A., & Srivastava, V. K. (2016). Nanolaminated composite materials: structure, interface role and applications. *RSC Advances*, 6(111), 109361-109385.
- Bandyopadhyay, A., Withey, E. A., Moore, J., & Bose, S. (2007). Influence of ZnO doping in calcium phosphate ceramics. *Materials Science and Engineering: C*, 27(1), 14-17.
- Bardhan, R., Mahata, S., & Mondal, B. (2011). Processing of natural resourced hydroxyapatite from eggshell waste by wet precipitation method. *Advances in Applied Ceramics*, 110(2), 80-86.
- Bermejo, R., Baudín, C., Moreno, R., Llanes, L., & Sánchez-Herencia, A. (2007). Processing optimisation and fracture behaviour of layered ceramic composites with highly compressive layers. *Composites science and technology*, 67(9), 1930-1938.
- Bermejo, R., Pascual, J., Lube, T., & Danzer, R. (2008). Optimal strength and toughness of Al<sub>2</sub>O<sub>3</sub>-ZrO<sub>2</sub> laminates designed with external or internal compressive layers. *Journal of the European Ceramic Society*, 28(8), 1575-1583.
- Bernard, L., Freche, M., Lacout, J., & Biscans, B. (1999). Preparation of hydroxyapatite by neutralization at low temperature—influence of purity of the raw material. *Powder Technology*, 103(1), 19-25.
- Berndt, C., Hasan, F., Tietz, U., & Schmitz, K.-P. (2014). A review of hydroxyapatite coatings manufactured by thermal spray *Advances in calcium phosphate biomaterials* (pp. 267-329): Springer.
- Besra, L., & Liu, M. (2007). A review on fundamentals and applications of electrophoretic deposition (EPD). *Progress in materials science*, 52(1), 1-61.
- Blind, O., Klein, L. H., Dailey, B., & Jordan, L. (2005). Characterization of hydroxyapatite films obtained by pulsed-laser deposition on Ti and Ti-6AL-4v substrates. *Dental materials*, 21(11), 1017-1024.
- Bocanegra-Bernal, M. (2004). Hot isostatic pressing (HIP) technology and its applications to metals and ceramics. *Journal of materials science*, 39(21), 6399-6420.

- Bocanegra-Bernal, M., & De La Torre, S. D. (2002). Phase transitions in zirconium dioxide and related materials for high performance engineering ceramics. *Journal of materials science*, 37(23), 4947-4971.
- Bocanegra-Bernal, M., Domínguez-Rios, C., Garcia-Reyes, A., Aguilar-Elguezabal, A., Echeberria, J., & Nevarez-Rascon, A. (2009). Hot isostatic pressing (HIP) of  $\alpha$ -Al<sub>2</sub>O<sub>3</sub> submicron ceramics pressureless sintered at different temperatures: Improvement in mechanical properties for use in total hip arthroplasty (THA). *International Journal of Refractory Metals and Hard Materials*, 27(5), 900-906.
- Boccaccini, A., Keim, S., Ma, R., Li, Y., & Zhitomirsky, I. (2010). Electrophoretic deposition of biomaterials. *Journal of the Royal Society Interface*, 7(Suppl 5), S581-S613.
- Boccaccini, A. R., & Zhitomirsky, I. (2002). Application of electrophoretic and electrolytic deposition techniques in ceramics processing. *Current Opinion in Solid State and Materials Science*, 6(3), 251-260.
- Bousack, H. (1985). Hot Isostatic Pressing (HIP): Techniques, applications and economical use. *NASA STI/Recon Technical Report N*, 85.
- Bueno, S., & Baudin, C. (2009). Design and processing of a ceramic laminate with high toughness and strong interfaces. *Composites Part A: Applied Science and Manufacturing*, 40(2), 137-143.
- Cai, K., Bossert, J., & Jandt, K. D. (2006). Does the nanometre scale topography of titanium influence protein adsorption and cell proliferation? *Colloids and surfaces B: Biointerfaces*, 49(2), 136-144.
- Chan, H. M. (1997). Layered ceramics: processing and mechanical behavior. *Annual review of materials science*, 27(1), 249-282.
- Chaudhuri, B., Mondal, B., Modak, D., Pramanik, K., & Chaudhuri, B. (2013). Preparation and characterization of nanocrystalline hydroxyapatite from egg shell and K<sub>2</sub>HPO<sub>4</sub> solution. *Materials Letters*, 97, 148-150.
- Chen, Z., Zhai, J., Wang, D., & Chen, C. (2018). Bioactivity of hydroxyapatite/wollastonite composite films deposited by pulsed laser. *Ceramics International*, 44(9), 10204-10209.
- Chew, W. K., Niakan, A., Nawawi, N., Bang, L., & Ramesh, S. (2015). Influence of powder morphology and sintering temperature on the properties of

hydroxyapatite. *International Journal of Automotive and Mechanical Engineering*, 12, 3089.

Chlup, Z., & Hadraba, H. (2009). *Alumina and Zirconia Based Layered Composites: Part 2 Fracture Response*. Paper presented at the Key Engineering Materials.

Choi, J.-M., Kim, H.-E., & Lee, I.-S. (2000). Ion-beam-assisted deposition (IBAD) of hydroxyapatite coating layer on Ti-based metal substrate. *Biomaterials*, 21(5), 469-473.

Choudhury, P., & Agrawal, D. (2012). Hydroxyapatite (HA) coatings for biomaterials *Nanomedicine* (pp. 84-127): Elsevier.

Clifford, A., Ata, M., & Zhitomirsky, I. (2017). Synthesis, liquid-Liquid extraction and deposition of hydroxyapatite nanorod composites. *Materials Letters*, 201, 140-143.

Clyne, T. W., & Troughton, S. C. (2018). A review of recent work on discharge characteristics during plasma electrolytic oxidation of various metals. *International Materials Reviews*, 1-36.

Conrad, H. J., Seong, W.-J., & Pesun, I. J. (2007). Current ceramic materials and systems with clinical recommendations: a systematic review. *The Journal of prosthetic dentistry*, 98(5), 389-404.

Corni, I., Ryan, M. P., & Boccaccini, A. R. (2008). Electrophoretic deposition: From traditional ceramics to nanotechnology. *Journal of the European Ceramic Society*, 28(7), 1353-1367.

Cui, F., Luo, Z., & Feng, Q. (1997). Highly adhesive hydroxyapatite coatings on titanium alloy formed by ion beam assisted deposition. *Journal of Materials Science: Materials in Medicine*, 8(7), 403-405.

Dahlan, K., Dewi, S. U., Nurlaila, A., & Soejoko, D. (2012). Synthesis and characterization of calcium phosphate/chitosan composites. *International Journal of Basic & Applied Sciences*, 12(1), 50-57.

Dasgupta, S., Tarafder, S., Bandyopadhyay, A., & Bose, S. (2013). Effect of grain size on mechanical, surface and biological properties of microwave sintered hydroxyapatite. *Materials Science and Engineering: C*, 33(5), 2846-2854.

- Davis, J. B., Kristoffersson, A., Carlström, E., & Clegg, W. J. (2000). Fabrication and crack deflection in ceramic laminates with porous interlayers. *Journal of the American Ceramic Society*, 83(10), 2369-2374.
- de Andrade, A. V. C., Stafin, G., de Lara, E. L., Antunes, L., de Souza, E. C. F., Borges, C. P. F., & Antunes, S. R. M. (2017). Morphology of hydroxyapatite crystals obtained through the hydrothermal method. *ECerS2017*, 9, 538.
- De Angelis, G., Medeghini, L., Conte, A. M., & Mignardi, S. (2017). Recycling of eggshell waste into low-cost adsorbent for Ni removal from wastewater. *Journal of Cleaner Production*, 164, 1497-1506.
- De Groot, K., Geesink, R., Klein, C., & Serekian, P. (1987). Plasma sprayed coatings of hydroxylapatite. *Journal of biomedical materials research*, 21(12), 1375-1381.
- Denry, I., & Kelly, J. R. (2008). State of the art of zirconia for dental applications. *Dental materials*, 24(3), 299-307.
- Dinda, G., Shin, J., & Mazumder, J. (2009). Pulsed laser deposition of hydroxyapatite thin films on Ti-6Al-4V: effect of heat treatment on structure and properties. *Acta biomaterialia*, 5(5), 1821-1830.
- Dorozhkin, S. V. (2010). Bioceramics of calcium orthophosphates. *Biomaterials*, 31(7), 1465-1485.
- Drevet, R., Jaber, N. B., Fauré, J., Tara, A., Larbi, A. B. C., & Benhayoune, H. (2016). Electrophoretic deposition (EPD) of nano-hydroxyapatite coatings with improved mechanical properties on prosthetic Ti6Al4V substrates. *Surface and Coatings Technology*, 301, 94-99.
- Driessens, F., & Verbeeck, R. (1988). Relation between physico-chemical solubility and biodegradability of calcium phosphates. *Implant materials in biofunction, Advances in biomaterials, Amsterdam: Elsevier*, 105-111.
- Durdu, S., Usta, M., & Berkem, A. S. (2016). Bioactive coatings on Ti6Al4V alloy formed by plasma electrolytic oxidation. *Surface and Coatings Technology*, 301, 85-93.
- Dzhurinskiy, D., Gao, Y., Yeung, W.-K., Strumban, E., Leshchinsky, V., Chu, P.-J., . . . Maev, R. G. (2015). Characterization and corrosion evaluation of TiO<sub>2</sub>: n-HA coatings on titanium alloy formed by plasma electrolytic oxidation. *Surface and Coatings Technology*, 269, 258-265.

- Eanes, E. D. (1998). Amorphous calcium phosphate: thermodynamic and kinetic considerations *Calcium phosphates in biological and industrial systems* (pp. 21-39): Springer.
- Ebrahimi-Kahrizsangi, R., Nasiri-Tabrizi, B., & Chami, A. (2010). Synthesis and characterization of fluorapatite–titania (FAP–TiO<sub>2</sub>) nanocomposite via mechanochemical process. *Solid State Sciences*, 12(9), 1645-1651.
- Eliaz, N., Shmueli, S., Shur, I., Benayahu, D., Aronov, D., & Rosenman, G. (2009). The effect of surface treatment on the surface texture and contact angle of electrochemically deposited hydroxyapatite coating and on its interaction with bone-forming cells. *Acta biomaterialia*, 5(8), 3178-3191.
- Elizondo-Villarreal, N., Martínez-De-La-Cruz, A., Guerra, R. O., Gómez-Ortega, J., Torres-Martínez, L., & Castaño, V. (2012). Biomaterials from agricultural waste: eggshell-based hydroxyapatite. *Water, Air, & Soil Pollution*, 223(7), 3643-3646.
- Evis, Z., & Webster, T. (2011). Nanosize hydroxyapatite: doping with various ions. *Advances in Applied Ceramics*, 110(5), 311-321.
- Fang, Y., Agrawal, D. K., & Roy, D. M. (1994). Thermal stability of synthetic hydroxyapatite. *Hydroxyapatite and related materials*, 269-282.
- Feng, B., Weng, J., Yang, B., Qu, S., & Zhang, X. (2004). Characterization of titanium surfaces with calcium and phosphate and osteoblast adhesion. *Biomaterials*, 25(17), 3421-3428.
- Ferkel, H., & Hellmig, R. (1999). Effect of nanopowder deagglomeration on the densities of nanocrystalline ceramic green bodies and their sintering behaviour. *Nanostructured materials*, 11(5), 617-622.
- Ferrari, B., & Moreno, R. (2010). EPD kinetics: a review. *Journal of the European Ceramic Society*, 30(5), 1069-1078.
- Ferrari, B., Sanchez-Herencia, A., & Moreno, R. (1998). Aqueous electrophoretic deposition of Al<sub>2</sub>O<sub>3</sub>/ZrO<sub>2</sub> layered ceramics. *Materials Letters*, 35(5-6), 370-374.
- Ferrari, B., Sanchez-Herencia, A., & Moreno, R. (1998). Electrophoretic forming of Al<sub>2</sub>O<sub>3</sub>/Y-TZP layered ceramics from aqueous suspensions. *Materials research bulletin*, 33(3), 487-499.



- Ferraz, M., Monteiro, F., & Manuel, C. (2004). Hydroxyapatite nanoparticles: a review of preparation methodologies. *Journal of Applied Biomaterials and Biomechanics*, 2(2), 74-80.
- Fleckenstein, C., Mochales, C., Frank, S., Kochbeck, F., Zehbe, R., Fleck, C., & Mueller, W. (2014). Tetragonal and cubic zirconia multilayered ceramics: investigation of electrical parameters during automated EPD processing. *Advances in Applied Ceramics*, 113(1), 35-41.
- Fratzl, P., Gupta, H. S., Fischer, F. D., & Kolednik, O. (2007). Hindered crack propagation in materials with periodically varying Young's modulus—lessons from biological materials. *Advanced Materials*, 19(18), 2657-2661.
- Freeman, R. (2007). Measuring the flow properties of consolidated, conditioned and aerated powders—a comparative study using a powder rheometer and a rotational shear cell. *Powder Technology*, 174(1-2), 25-33.
- Fukuda, Y., & Tanabe, K. (1973). Infrared study of carbon dioxide adsorbed on magnesium and calcium oxides. *Bulletin of the Chemical Society of Japan*, 46(6), 1616-1619.
- Galvan-Ruiz, M., Baños, L., & Rodriguez-Garcia, M. E. (2007). Lime characterization as a food additive. *Sensing and Instrumentation for Food Quality and Safety*, 1(4), 169-175.
- Garvie, R. C., & Nicholson, P. S. (1972). Structure and thermomechanical properties of partially stabilized zirconia in the CaO-ZrO<sub>2</sub> system. *Journal of the American Ceramic Society*, 55(3), 152-157.
- Gergely, G., Wéber, F., Lukács, I., Tóth, A. L., Horváth, Z. E., Mihály, J., & Balázs, C. (2010). Preparation and characterization of hydroxyapatite from eggshell. *Ceramics International*, 36(2), 803-806.
- Gibson, I. R., & Bonfield, W. (2002). Novel synthesis and characterization of an AB-type carbonate-substituted hydroxyapatite. *Journal of Biomedical Materials Research: An Official Journal of The Society for Biomaterials, The Japanese Society for Biomaterials, and The Australian Society for Biomaterials and the Korean Society for Biomaterials*, 59(4), 697-708.
- Gleiter, H. (1992). Materials with ultrafine microstructures: retrospectives and perspectives. *Nanostructured materials*, 1(1), 1-19.

- Gong, J., Miao, H., & Peng, Z. (2004). Analysis of the nanoindentation data measured with a Berkovich indenter for brittle materials: effect of the residual contact stress. *Acta Materialia*, 52(3), 785-793.
- Gross, K., Chai, C., Kannangara, G., Ben-Nissan, B., & Hanley, L. (1998). Thin hydroxyapatite coatings via sol-gel synthesis. *Journal of Materials Science: Materials in Medicine*, 9(12), 839-843.
- Gross, K. A., Saber-Samandari, S., & Heemann, K. S. (2010). Evaluation of commercial implants with nanoindentation defines future development needs for hydroxyapatite coatings. *J. Biomed. Mater. Res. B*, 93(1), 1-8.
- Guazzato, M., Albakry, M., Ringer, S. P., & Swain, M. V. (2004). Strength, fracture toughness and microstructure of a selection of all-ceramic materials. Part II. Zirconia-based dental ceramics. *Dental materials*, 20(5), 449-456.
- Gunasekaran, S., Anbalagan, G., & Pandi, S. (2006). Raman and infrared spectra of carbonates of calcite structure. *Journal of Raman Spectroscopy: An International Journal for Original Work in all Aspects of Raman Spectroscopy, Including Higher Order Processes, and also Brillouin and Rayleigh Scattering*, 37(9), 892-899.
- Hahn, H., & Palich, W. (1970). Preliminary evaluation of porous metal surfaced titanium for orthopedic implants. *Journal of biomedical materials research*, 4(4), 571-577.
- Hamdi, M., Hakamata, S., & Ektessabi, A. (2000). Coating of hydroxyapatite thin film by simultaneous vapor deposition. *Thin Solid Films*, 377, 484-489.
- Hamidi, A., Salimi, M., & Yusoff, A. (2017). *Synthesis and characterization of eggshell-derived hydroxyapatite via mechanochemical method: A comparative study*. Paper presented at the AIP Conference Proceedings.
- Hassan, M. N., Mahmoud, M. M., El-Fattah, A. A., & Kandil, S. (2016). Microwave-assisted preparation of Nano-hydroxyapatite for bone substitutes. *Ceramics International*, 42(3), 3725-3744.
- He, Z., Ma, J., & Wang, C. (2005). Constitutive modeling of the densification and the grain growth of hydroxyapatite ceramics. *Biomaterials*, 26(14), 1613-1621.
- Heidari, F., Razavi, M., Ghaedi, M., Forooghi, M., Tahriri, M., & Tayebi, L. (2017). Investigation of mechanical properties of natural hydroxyapatite samples prepared

by cold isostatic pressing method. *Journal of Alloys and Compounds*, 693, 1150-1156.

Heimann, R. B. (2006). Thermal spraying of biomaterials. *Surface and Coatings Technology*, 201(5), 2012-2019.

Hench, L. L. (1991). Bioceramics: from concept to clinic. *Journal of the American Ceramic Society*, 74(7), 1487-1510.

Herman, H. (1988). Plasma spray deposition processes. *MRS Bulletin*, 13(12), 60-67.

Herø, H., Wie, H., Jørgensen, R. B., & Ruyter, I. E. (1994). Hydroxyapatite coatings on Ti produced by hot isostatic pressing. *Journal of biomedical materials research*, 28(3), 343-348.

Ho, W.-F., Hsu, H.-C., Hsu, S.-K., Hung, C.-W., & Wu, S.-C. (2013). Calcium phosphate bioceramics synthesized from eggshell powders through a solid state reaction. *Ceramics International*, 39(6), 6467-6473.

Hoepfner, T. P., & Case, E. (2003). The influence of the microstructure on the hardness of sintered hydroxyapatite. *Ceramics International*, 29(6), 699-706.

Höland, W., Schweiger, M., Rheinberger, V., & Kappert, H. (2009). Bioceramics and their application for dental restoration. *Advances in Applied Ceramics*, 108(6), 373-380.

Hsiung, J., Tzeng, J., Kung, K., & Chen, H. (2013). A study of thermal spray coating on artificial knee joints. *Life Science Journal*, 10(2), 236-241.

Hui, P., Meena, S., Singh, G., Agarawal, R., & Prakash, S. (2010). Synthesis of hydroxyapatite bio-ceramic powder by hydrothermal method. *Journal of Minerals and Materials Characterization and Engineering*, 9(08), 683.

Hung, K.-Y., Lai, H.-C., Yang, Y.-C., & Feng, H.-P. (2017). Characterization of hydroxyapatite (HA) sputtering targets by APS methods. *Coatings*, 7(11), 197.

Hwang, I.-J., & Choe, H.-C. (2018). Hydroxyapatite coatings containing Zn and Si on Ti-6Al-4V alloy by plasma electrolytic oxidation. *Applied surface science*, 432, 337-346.

- Inthong, S., Tunkasiri, T., Eitssayeam, S., Pengpat, K., & Rujijanagul, G. (2013). Physical properties and bioactivity of nanocrystalline hydroxyapatite synthesized by a co-precipitation route. *Ceramics International*, 39, S533-S536.
- Ishikawa, K., Matsuya, S., Miyamoto, Y., & Kawate, K. (2015). 9.05 e bioceramics. Reference module in materials science and materials engineering. *Compr. Struct. Integr*, 9.
- Ivanova, A. A., Surmeneva, M. A., Tyurin, A., Pirozhkova, T., Shuvarin, I., Prymak, O., . . . Surmenev, R. A. (2016). Fabrication and physico-mechanical properties of thin magnetron sputter deposited silver-containing hydroxyapatite films. *Applied surface science*, 360, 929-935.
- Janković, A., Eraković, S., Mitrić, M., Matić, I. Z., Juranić, Z. D., Tsui, G. C., . . . Park, S. J. (2015). Bioactive hydroxyapatite/graphene composite coating and its corrosion stability in simulated body fluid. *Journal of Alloys and Compounds*, 624, 148-157.
- Jayakumar, R., Menon, D., Manzoor, K., Nair, S., & Tamura, H. (2010). Biomedical applications of chitin and chitosan based nanomaterials—A short review. *Carbohydrate Polymers*, 82(2), 227-232.
- Juang, H. Y., & Hon, M. H. (1996). Effect of calcination on sintering of hydroxyapatite. *Biomaterials*, 17(21), 2059-2064.
- Jung, U.-W., Hwang, J.-W., Choi, D.-Y., Hu, K.-S., Kwon, M.-K., Choi, S.-H., & Kim, H.-J. (2012). Surface characteristics of a novel hydroxyapatite-coated dental implant. *Journal of periodontal & implant science*, 42(2), 59-63.
- Kamalanathan, P., Ramesh, S., Bang, L., Niakan, A., Tan, C., Purbolaksono, J., . . . Teng, W. (2014). Synthesis and sintering of hydroxyapatite derived from eggshells as a calcium precursor. *Ceramics International*, 40(10), 16349-16359.
- Kappert, H. F., & Eichner, K. (2005). *Zahnärztliche Werkstoffe und ihre Verarbeitung. 1. Grundlagen und Verarbeitung* (Vol. 1): Georg Thieme Verlag.
- Karimi, E., Khalil-Allafi, J., & Khalili, V. (2016). Electrophoretic deposition of double-layer HA/Al composite coating on NiTi. *Materials Science and Engineering: C*, 58, 882-890.
- Karimzadeh, A., Ayatollahi, M. R., Bushroa, A., & Herliansyah, M. (2014). Effect of sintering temperature on mechanical and tribological properties of hydroxyapatite

measured by nanoindentation and nanoscratch experiments. *Ceramics International*, 40(7), 9159-9164.

Kazemi, A., Abdellahi, M., Khajeh-Sharafabadi, A., Khandan, A., & Ozada, N. (2017). Study of in vitro bioactivity and mechanical properties of diopside nanobioceramic synthesized by a facile method using eggshell as raw material. *Materials Science and Engineering: C*, 71, 604-610.

Kehoe, S. (2008). *Optimisation of hydroxyapatite (HAp) for orthopaedic application via the chemical precipitation technique*. Dublin City University.

Khalid, M., Mujahid, M., Amin, S., Rawat, R., Nusair, A., & Deen, G. (2013). Effect of surfactant and heat treatment on morphology, surface area and crystallinity in hydroxyapatite nanocrystals. *Ceramics International*, 39(1), 39-50.

Khanaki, A., Abdizadeh, H., & Golobostanfard, M. R. (2015). Electrophoretic Deposition of  $\text{CuIn}_{1-x}\text{Ga}_x\text{Se}_2$  Thin Films Using Solvothermal Synthesized Nanoparticles for Solar Cell Application. *The Journal of Physical Chemistry C*, 119(40), 23250-23258.

Koch, C., Johnson, S., Kumar, D., Jelinek, M., Chrisey, D., Doraiswamy, A., . . . Mihailescu, I. (2007). Pulsed laser deposition of hydroxyapatite thin films. *Materials Science and Engineering: C*, 27(3), 484-494.

Kong, L., Ma, J., & Boey, F. (2002). Nanosized hydroxyapatite powders derived from coprecipitation process. *Journal of materials science*, 37(6), 1131-1134.

Kothapalli, C., Wei, M., Vasiliev, A., & Shaw, M. (2004). Influence of temperature and concentration on the sintering behavior and mechanical properties of hydroxyapatite. *Acta Materialia*, 52(19), 5655-5663.

Krishna, D. S. R., Siddharthan, A., Seshadri, S., & Kumar, T. S. (2007). A novel route for synthesis of nanocrystalline hydroxyapatite from eggshell waste. *Journal of Materials Science: Materials in Medicine*, 18(9), 1735-1743.

Krueger, H., Knote, A., Schindler, U., Kern, H., & Boccaccini, A. (2004). Composite ceramic-metal coatings by means of combined electrophoretic deposition and galvanic methods. *Journal of materials science*, 39(3), 839-844.

Kumar, G. S., Thamizhavel, A., & Girija, E. (2012). Microwave conversion of eggshells into flower-like hydroxyapatite nanostructure for biomedical applications. *Materials Letters*, 76, 198-200.

- Kunst, S. R., Cardoso, H. R. P., Beltrami, L. V. R., Oliveira, C. T., Menezes, T. L., Ferreira, J. Z., & Malfatti, C. d. F. (2015). New sol-gel formulations to increase the barrier effect of a protective coating against the corrosion and wear of galvanized steel. *Materials Research*, 18(1), 138-150.
- Kuppuswamy, H., & Ganesan, A. (2016). Structural, mechanical and in vitro studies on pulsed laser deposition of hydroxyapatite on additive manufactured polyamide substrate. *International Journal of Bioprinting*, 2(2), 194-203.
- Kutty, M. G., Bhaduri, S. B., Zhou, H., & Yaghoubi, A. (2015). In situ measurement of shrinkage and temperature profile in microwave-and conventionally-sintered hydroxyapatite bioceramic. *Materials Letters*, 161, 375-378.
- Kweh, S., Khor, K., & Cheang, P. (1999). The production and characterization of hydroxyapatite (HA) powders. *Journal of materials processing technology*, 89, 373-377.
- Kwok, C., Wong, P., Cheng, F., & Man, H. (2009). Characterization and corrosion behavior of hydroxyapatite coatings on Ti6Al4V fabricated by electrophoretic deposition. *Applied surface science*, 255(13-14), 6736-6744.
- Lacefield, W. (1991). Sputter deposition of Ca-P coatings onto metallic implant. *Ceramics in substitute and reconstructive surgery*, 167-176.
- Landor, I., Vavrik, P., Sosna, A., Jahoda, D., Hahn, H., & Daniel, M. (2007). Hydroxyapatite porous coating and the osteointegration of the total hip replacement. *Archives of orthopaedic and trauma surgery*, 127(2), 81-89.
- Landi, E., Logroscino, G., Proietti, L., Tampieri, A., Sandri, M., & Sprio, S. (2008). Biomimetic Mg-substituted hydroxyapatite: from synthesis to in vivo behaviour. *Journal of Materials Science: Materials in Medicine*, 19(1), 239-247.
- Larker, H., & Larker, H. I. (1991). Engineered Materials Handbook Vol. 4. *Ceramics and Glasses*, 194-201.
- Layrolle, P., Ito, A., & Tateishi, T. (1998). Sol-gel synthesis of amorphous calcium phosphate and sintering into microporous hydroxyapatite bioceramics. *Journal of the American Ceramic Society*, 81(6), 1421-1428.
- Leenakul, W., Tunkasiri, T., Tongsir, N., Pengpat, K., & Ruangsuriya, J. (2016). Effect of sintering temperature variations on fabrication of 45S5 bioactive glass-

ceramics using rice husk as a source for silica. *Materials Science and Engineering: C*, 61, 695-704.

Lemons, J. (1988). Hydroxyapatite coatings. *Clinical orthopaedics and related research* (235), 220-223.

Levingstone, T. J. (2008). *Ceramics for medical applications*: Dublin City University.

Li, T., Lee, J., Kobayashi, T., & Aoki, H. (1996). Hydroxyapatite coating by dipping method, and bone bonding strength. *Journal of Materials Science: Materials in Medicine*, 7(6), 355-357.

Liang, H., Shi, B., Fairchild, A., & Cale, T. (2004). Applications of plasma coatings in artificial joints: an overview. *Vacuum*, 73(3-4), 317-326.

Liang, Z., & Blackburn, S. (2002). Analysis of crack development during processing of laminated ceramic tubes. *Journal of materials science*, 37(19), 4227-4233.

Lin, K., Chen, L., & Chang, J. (2012). Fabrication of dense hydroxyapatite nanobioceramics with enhanced mechanical properties via two-step sintering process. *International Journal of Applied Ceramic Technology*, 9(3), 479-485.

Liu, H., Peng, H., Wu, Y., Zhang, C., Cai, Y., Xu, G., . . . Zhang, Y. (2013). The promotion of bone regeneration by nanofibrous hydroxyapatite/chitosan scaffolds by effects on integrin-BMP/Smad signaling pathway in BMSCs. *Biomaterials*, 34(18), 4404-4417.

Lou, W., Dong, Y., Zhang, H., Jin, Y., Hu, X., Ma, J., . . . Wu, G. (2015). Preparation and characterization of lanthanum-incorporated hydroxyapatite coatings on titanium substrates. *International journal of molecular sciences*, 16(9), 21070-21086.

Lugovskoy, A., & Lugovskoy, S. (2014). Production of hydroxyapatite layers on the plasma electrolytically oxidized surface of titanium alloys. *Materials Science and Engineering: C*, 43, 527-532.

Ma, J., Wang, H., Weng, L., & Tan, G. (2004). Effect of porous interlayers on crack deflection in ceramic laminates. *Journal of the European Ceramic Society*, 24(5), 825-831.

Madhumathi, K., Binulal, N., Nagahama, H., Tamura, H., Shalumon, K., Selvamurugan, N., . . . Jayakumar, R. (2009). Preparation and characterization of novel  $\beta$ -chitin-

hydroxyapatite composite membranes for tissue engineering applications. *International journal of biological macromolecules*, 44(1), 1-5.

- Maleki-Ghaleh, H., Khalili, V., Khalil-Allafi, J., & Javidi, M. (2012). Hydroxyapatite coating on NiTi shape memory alloy by electrophoretic deposition process. *Surface and Coatings Technology*, 208, 57-63.
- Manicone, P. F., Iommetti, P. R., & Raffaelli, L. (2007). An overview of zirconia ceramics: basic properties and clinical applications. *Journal of dentistry*, 35(11), 819-826.
- Manso, M., Jimenez, C., Morant, C., Herrero, P., & Martinez-Duart, J. (2000). Electrodeposition of hydroxyapatite coatings in basic conditions. *Biomaterials*, 21(17), 1755-1761.
- Martínez-Castañón, G., Loyola-Rodríguez, J., Zavala-Alonso, N., Hernández-Martínez, S., Niño-Martínez, N., Ortega-Zarzosa, G., & Ruiz, F. (2012). Preparation and characterization of nanostructured powders of hydroxyapatite. *Superficies y vacío*, 25(2), 101-105.
- Mavis, B., & Taş, A. C. (2000). Dip coating of calcium hydroxyapatite on Ti-6Al-4V substrates. *Journal of the American Ceramic Society*, 83(4), 989-991.
- Mazaheri, M., Haghightazdeh, M., Zahedi, A., & Sadrnezhad, S. (2009). Effect of a novel sintering process on mechanical properties of hydroxyapatite ceramics. *Journal of Alloys and Compounds*, 471(1-2), 180-184.
- Meejoo, S., Maneprakorn, W., & Winotai, P. (2006). Phase and thermal stability of nanocrystalline hydroxyapatite prepared via microwave heating. *Thermochimica acta*, 447(1), 115-120.
- Mendonça, G., Mendonça, D. B., Simões, L. G., Araújo, A. L., Leite, E. R., Duarte, W. R., . . . Cooper, L. F. (2009). The effects of implant surface nanoscale features on osteoblast-specific gene expression. *Biomaterials*, 30(25), 4053-4062.
- Mobasherpour, I., Heshajin, M. S., Kazemzadeh, A., & Zakeri, M. (2007). Synthesis of nanocrystalline hydroxyapatite by using precipitation method. *Journal of Alloys and Compounds*, 430(1-2), 330-333.
- Mohseni, E., Zalnezhad, E., & Bushroa, A. R. (2014). Comparative investigation on the adhesion of hydroxyapatite coating on Ti-6Al-4V implant: A review paper. *International Journal of Adhesion and Adhesives*, 48, 238-257.



- Mondal, S., Mondal, B., Dey, A., & Mukhopadhyay, S. S. (2012). Studies on processing and characterization of hydroxyapatite biomaterials from different bio wastes. *Journal of Minerals and Materials Characterization and Engineering*, 11(01), 55.
- Moritz, K., & Moritz, T. (2010). ZrO<sub>2</sub> ceramics with aligned pore structure by EPD and their characterisation by X-ray computed tomography. *Journal of the European Ceramic Society*, 30(5), 1203-1209.
- Moritz, T., Eiselt, W., & Moritz, K. (2006). Electrophoretic deposition applied to ceramic dental crowns and bridges. *Journal of materials science*, 41(24), 8123-8129.
- Mróz, W., Budner, B., Syroka, R., Niedzielski, K., Golański, G., Słószarczyk, A., ... & Douglas, T. E. (2015). In vivo implantation of porous titanium alloy implants coated with magnesium-doped octacalcium phosphate and hydroxyapatite thin films using pulsed laser deposition. *Journal of Biomedical Materials Research Part B: Applied Biomaterials*, 103(1), 151-158.
- Munz, D., & Fett, T. (2013). Mechanisches Verhalten keramischer Werkstoffe: Versagensablauf, *Werkstoffauswahl, Dimensionierung* (Vol. 8): Springer-Verlag.
- Muralithran, G., & Ramesh, S. (2000). The effects of sintering temperature on the properties of hydroxyapatite. *Ceramics International*, 26(2), 221-230.
- Náhlík, L., Šestáková, L., Hutař, P., & Bermejo, R. (2010). Prediction of crack propagation in layered ceramics with strong interfaces. *Engineering Fracture Mechanics*, 77(11), 2192-2199.
- Nath, S., Basu, B., & Sinha, A. (2006). A comparative study of conventional sintering with microwave sintering of hydroxyapatite synthesized by chemical route. *Trends in Biomaterials & Artificial Organs*, 19(2), 93-98.
- Nelea, V., Pelletier, H., Müller, D., Broll, N., Mille, P., Ristoscu, C., & Mihailescu, I. (2002). Mechanical properties improvement of pulsed laser-deposited hydroxyapatite thin films by high energy ion-beam implantation. *Applied surface science*, 186(1-4), 483-489.
- Niakan, A., Ramesh, S., Ganesan, P., Tan, C., Purbolaksono, J., Chandran, H., & Teng, W. (2015). Sintering behaviour of natural porous hydroxyapatite derived from bovine bone. *Ceramics International*, 41(2), 3024-3029.

- Niakan, A., Ramesh, S., Hamdi, M., Jahanshahi, A., Tan, C., Ching, Y., & Tolouei, R. (2014). Thermal treatment and properties of bovine hydroxyapatite. *Materials Research Innovations*, 18(sup6), S6-117-S116-120.
- Niakan, A., Ramesh, S., Naveen, S. V., Mohan, S., & Kamarul, T. (2017). Osteogenic priming potential of bovine hydroxyapatite sintered at different temperatures for tissue engineering applications. *Materials Letters*, 197, 83-86.
- Niakan, A., Ramesh, S., Tan, C., Purbolaksono, J., Chandran, H., & Teng, W. (2015). Effect of annealing treatment on the characteristics of bovine bone. *Journal of Ceramic Processing Research*, 16(2), 223-226.
- Niakan, A., Singh, R., Tan, C., Shukor, A., Hamdi, M., & Teng, W. (2013). *Characteristics of Sintered Bovine Hydroxyapatite*. Paper presented at the Applied Mechanics and Materials.
- Niihara, K., Morena, R., & Hasselman, D. (1982). Evaluation of  $K_{Ic}$  of brittle solids by the indentation method with low crack-to-indent ratios. *Journal of materials science letters*, 1(1), 13-16.
- Nishikawa, H., & Umatani, S. (2017). Effect of ablation laser pulse repetition rate on the surface protrusion density of hydroxyapatite thin films deposited using pulsed laser deposition. *Materials Letters*, 209, 330-333.
- Oetzel, C., & Clasen, R. (2006). Preparation of zirconia dental crowns via electrophoretic deposition. *Journal of materials science*, 41(24), 8130-8137.
- Olding, T., Sayer, M., & Barrow, D. (2001). Ceramic sol-gel composite coatings for electrical insulation. *Thin Solid Films*, 398, 581-586.
- Oliver, W. C., & Pharr, G. M. (1992). An improved technique for determining hardness and elastic modulus using load and displacement sensing indentation experiments. *Journal of materials research*, 7(6), 1564-1583.
- Orlovskii, V., Komlev, V., & Barinov, S. (2002). Hydroxyapatite and hydroxyapatite-based ceramics. *Inorganic Materials*, 38(10), 973-984.
- Ozeki, K., Yuhta, T., Aoki, H., Nishimura, I., & Fukui, Y. (2000). Crystal chemistry of hydroxyapatite deposited on titanium by sputtering technique. *Bio-medical materials and engineering*, 10(3, 4), 221-227.

- Pal, A., Paul, S., Choudhury, A. R., Balla, V. K., Das, M., & Sinha, A. (2017). Synthesis of hydroxyapatite from Lates calcarifer fish bone for biomedical applications. *Materials Letters*, 203, 89-92.
- Palacio, C., Jaramillo, D., Correa, S., & Arroyave, M. (2017). *Study of the suitability of a commercial hydroxyapatite powder to obtain sintered compacts for medical applications*. Paper presented at the Journal of Physics: Conference Series.
- Pandharipande, S. L., & Sondawale, S. S. (2016). Review on Synthesis of Hydroxyapatite and its Bio-composites.
- Panyata, S., Eitssayeam, S., Rujjanagul, G., Tunkasiri, T., & Pengpat, K. (2012). *Property development of hydroxyapatite ceramics by two-step sintering*. Paper presented at the Advanced Materials Research.
- Park, Y.-S., Yi, K.-Y., Lee, I.-S., Han, C.-H., & Jung, Y.-C. (2005). The effects of ion beam-assisted deposition of hydroxyapatite on the grit-blasted surface of endosseous implants in rabbit tibiae. *International Journal of Oral & Maxillofacial Implants*, 20(1).
- Pon-On, W., Suntornsaratoon, P., Charoenphandhu, N., Thongbunchoo, J., Krishnamra, N., & Tang, I. M. (2016). Hydroxyapatite from fish scale for potential use as bone scaffold or regenerative material. *Materials Science and Engineering: C*, 62, 183-189.
- Prabakaran, K., & Rajeswari, S. (2009). Spectroscopic investigations on the synthesis of nano-hydroxyapatite from calcined eggshell by hydrothermal method using cationic surfactant as template. *Spectrochimica Acta Part A: Molecular and Biomolecular Spectroscopy*, 74(5), 1127-1134.
- Pramanik, S., Agarwal, A. K., Rai, K., & Garg, A. (2007). Development of high strength hydroxyapatite by solid-state-sintering process. *Ceramics International*, 33(3), 419-426.
- Prescott, J. K., & Barnum, R. A. (2000). On powder flowability. *Pharmaceutical technology*, 24(10), 60-85.
- Prokopiev, O., & Sevostianov, I. (2006). Dependence of the mechanical properties of sintered hydroxyapatite on the sintering temperature. *Materials Science and Engineering: A*, 431(1-2), 218-227.

- Qiu, X., Lim, P. N., Tong, S. Y., & Thian, E. S. (2018). Deposition of substituted apatite coatings at different coating patterns via drop-on-demand micro-dispensing technique. *Materials Technology*, 33(6), 406-413.
- Rad, A. T., Solati-Hashjin, M., Osman, N. A. A., & Faghihi, S. (2014). Improved bio-physical performance of hydroxyapatite coatings obtained by electrophoretic deposition at dynamic voltage. *Ceramics International*, 40(8), 12681-12691.
- Rakchat, W., Suzuki, A., Otsuka, Y., Miyashita, Y., & Mutoh, Y. (2017). *Effect of bonding on fretting fatigue behavior of plasma-sprayed hydroxyapatite coating with a polymer pad*. Paper presented at the The Proceedings of Mechanical Engineering Congress, Japan 2017.
- Ramesh, S. (2001). Grain Size– Properties Correlation in Polycrystalline Hydroxyapatite Bioceramic. *Malays. J. Chem*, 3, 35-40.
- Ramesh, S., Aw, K., Tolouei, R., Amiriyani, M., Tan, C., Hamdi, M., . . . Teng, W. (2013). Sintering properties of hydroxyapatite powders prepared using different methods. *Ceramics International*, 39(1), 111-119.
- Ramesh, S., Loo, Z., Tan, C., Chew, W. K., Ching, Y., Tarlochan, F., . . . Sarhan, A. A. (2018). Characterization of biogenic hydroxyapatite derived from animal bones for biomedical applications. *Ceramics International*, 44(9), 10525-10530.
- Ramesh, S., Natasha, A., Tan, C., Bang, L., Niakan, A., Purbolaksono, J., . . . Teng, W. (2015). Characteristics and properties of hydroxyapatite derived by sol–gel and wet chemical precipitation methods. *Ceramics International*, 41(9), 10434-10441.
- Ramesh, S., Natasha, A., Tan, C., Bang, L. T., Ching, C., & Chandran, H. (2016). Direct conversion of eggshell to hydroxyapatite ceramic by a sintering method. *Ceramics International*, 42(6), 7824-7829.
- Ramesh, S., Tan, C., Bhaduri, S., Teng, W., & Sopyan, I. (2008). Densification behaviour of nanocrystalline hydroxyapatite bioceramics. *Journal of materials processing technology*, 206(1-3), 221-230.
- Ramesh, S., Tan, C., Sopyan, I., Hamdi, M., & Teng, W. (2007). Consolidation of nanocrystalline hydroxyapatite powder. *Science and Technology of Advanced Materials*, 8(1-2), 124-130.

- Ramesh, S., Tan, C., Tolouei, R., Amiriyani, M., Purbolaksono, J., Sopyan, I., & Teng, W. (2012). Sintering behavior of hydroxyapatite prepared from different routes. *Materials & Design*, *34*, 148-154.
- Ramesha, S., Adzilaa, S., Jeffreya, C., Tana, C., Purbolaksonoa, J., Noora, A., . . . Teng, W. (2013). Properties of hydroxyapatite synthesized by wet chemical method. *Journal of Ceramic Processing Research*, *14*(4), 448-452.
- Rapacz-Kmita, A., Paluszkiwicz, C., Ślósarczyk, A., & Paszkiewicz, Z. (2005). FTIR and XRD investigations on the thermal stability of hydroxyapatite during hot pressing and pressureless sintering processes. *Journal of Molecular Structure*, *744*, 653-656.
- Raynaud, S., Champion, E., Bernache-Assollant, D., & Laval, J. P. (2001). Determination of calcium/phosphorus atomic ratio of calcium phosphate apatites using X-ray diffractometry. *Journal of the American Ceramic Society*, *84*(2), 359-366.
- Raynaud, S., Champion, E., Bernache-Assollant, D., & Thomas, P. (2002). Calcium phosphate apatites with variable Ca/P atomic ratio I. Synthesis, characterisation and thermal stability of powders. *Biomaterials*, *23*(4), 1065-1072.
- Rhee, S.-H. (2002). Synthesis of hydroxyapatite via mechanochemical treatment. *Biomaterials*, *23*(4), 1147-1152.
- Rho, J.-Y., Kuhn-Spearing, L., & Zioupos, P. (1998). Mechanical properties and the hierarchical structure of bone. *Medical engineering & physics*, *20*(2), 92-102.
- Rivera, E. M., Araiza, M., Brostow, W., Castano, V. M., Diaz-Estrada, J., Hernández, R., & Rodriguez, J. R. (1999). Synthesis of hydroxyapatite from eggshells. *Materials Letters*, *41*(3), 128-134.
- Rosa, A. L., & Beloti, M. M. (2003). Rat bone marrow cell response to titanium and titanium alloy with different surface roughness. *Clinical Oral Implants Research*, *14*(1), 43-48.
- Ryabenkova, Y., Jadav, N., Conte, M., Hippler, M. F., Reeves-McLaren, N., Coates, P. D., ... & Paradkar, A. (2017). Mechanism of hydrogen-bonded complex formation between ibuprofen and nanocrystalline hydroxyapatite. *Langmuir*, *33*(12), 2965-2976.
- Saber-Samandari, S., & Gross, K. A. (2009). Micromechanical properties of single crystal hydroxyapatite by nanoindentation. *Acta biomaterialia*, *5*(6), 2206-2212.

- Sadat-Shojai, M., Khorasani, M.-T., Dinpanah-Khoshdargi, E., & Jamshidi, A. (2013). Synthesis methods for nanosized hydroxyapatite with diverse structures. *Acta biomaterialia*, 9(8), 7591-7621.
- Sadat-Shojai, M., Khorasani, M.-T., & Jamshidi, A. (2012). Hydrothermal processing of hydroxyapatite nanoparticles—A Taguchi experimental design approach. *Journal of Crystal Growth*, 361, 73-84.
- Sahiner, N., Silan, C., Sagbas, S., Ilgin, P., Butun, S., Erdugan, H., & Ayyala, R. S. (2012). Porous and modified HA particles as potential drug delivery systems. *Microporous and Mesoporous Materials*, 155, 124-130.
- Sanosh, K., Chu, M.-C., Balakrishnan, A., Kim, T., & Cho, S.-J. (2009). Utilization of biowaste eggshells to synthesize nanocrystalline hydroxyapatite powders. *Materials Letters*, 63(24-25), 2100-2102.
- Sarkar, P., Huang, X., & Nicholson, P. S. (1993). Zirconia/alumina functionally graded composites by electrophoretic deposition techniques. *Journal of the American Ceramic Society*, 76(4), 1055-1056.
- Shunyan, T., Heng, J., & Chuanxian, D. (2000). Effect of vapor-flame treatment on plasma sprayed hydroxyapatite coatings. *Journal of Biomedical Materials Research: An Official Journal of The Society for Biomaterials, The Japanese Society for Biomaterials, and The Australian Society for Biomaterials and the Korean Society for Biomaterials*, 52(3), 572-575.
- Siddharthan, A., Kumar, T. S., & Seshadri, S. (2009). Synthesis and characterization of nanocrystalline apatites from eggshells at different Ca/P ratios. *Biomedical Materials*, 4(4), 045010.
- Siegel, R., & Eastman, J. (1988). Synthesis, characterization, and properties of nanophase ceramics. *MRS Online Proceedings Library Archive*, 132.
- Singh, R., Tolouei, R., Tan, C. Y., Aw, K., Yeo, W. H., Sopyan, I., & Teng, W. D. (2011). *Sintering of hydroxyapatite ceramic produced by wet chemical method*. Paper presented at the Advanced Materials Research.
- Søballe, K., Hansen, E. S., B.-Rasmussen, H., Jørgensen, P. H., & Bünger, C. (1992). Tissue ingrowth into titanium and hydroxyapatite-coated implants during stable and unstable mechanical conditions. *Journal of Orthopaedic Research*, 10(2), 285-299.

- Sopyan, I., Mel, M., Ramesh, S., & Khalid, K. (2007). Porous hydroxyapatite for artificial bone applications. *Science and Technology of Advanced Materials*, 8(1-2), 116-123.
- Stoch, A., Brożek, A., Kmita, G., Stoch, J., Jastrzebski, W., & Rakowska, A. (2001). Electrophoretic coating of hydroxyapatite on titanium implants. *Journal of Molecular Structure*, 596(1-3), 191-200.
- Suchanek, W., & Yoshimura, M. (1998). Processing and properties of hydroxyapatite-based biomaterials for use as hard tissue replacement implants. *Journal of materials research*, 13(1), 94-117.
- Sun, F., Zhou, H., & Lee, J. (2011). Various preparation methods of highly porous hydroxyapatite/polymer nanoscale biocomposites for bone regeneration. *Acta biomaterialia*, 7(11), 3813-3828.
- Sun, L., Berndt, C. C., Gross, K. A., & Kucuk, A. (2001). Material fundamentals and clinical performance of plasma-sprayed hydroxyapatite coatings: A review. *Journal of Biomedical Materials Research: An Official Journal of The Society for Biomaterials, The Japanese Society for Biomaterials, and The Australian Society for Biomaterials and the Korean Society for Biomaterials*, 58(5), 570-592.
- Tan, C. Y., Singh, R., Teh, Y. C., Tan, Y. M., & Yap, B. K. (2015). The effects of calcium-to-phosphorus ratio on the densification and mechanical properties of hydroxyapatite ceramic. *International Journal of Applied Ceramic Technology*, 12(1), 223-227.
- Tarafdar, J., & ADHIKARI, T. (2015). Nanotechnology in Soil Science. *Rattan, RK, Katyal, JC, Dwivedi, BS, Sarkar, AK, Bhattacharyya, T., et al*, 775-807.
- Testing, A. S. f., & Materials. (2004). *ASTM E112-96 (2004) e2: Standard Test Methods for Determining Average Grain Size*.
- Thair, L., Ismaeel, T., Ahmed, B., & Swadi, A. (2011). Development of apatite coatings on Ti-6Al-7Nb dental implants by biomimetic process and EPD: in vivo studies. *Surface Engineering*, 27(1), 11-18.
- Troczynski, T., & Yang, Q. (2001). Process for making chemically bonded sol-gel ceramics: Google Patents.

- Vahabzadeh, S., Roy, M., Bandyopadhyay, A., & Bose, S. (2015). Phase stability and biological property evaluation of plasma sprayed hydroxyapatite coatings for orthopedic and dental applications. *Acta biomaterialia*, *17*, 47-55.
- Van Dijk, K., Schaeken, H., Wolke, J., Maree, C., Habraken, F., Verhoeven, J., & Jansen, J. (1995). Influence of discharge power level on the properties of hydroxyapatite films deposited on Ti6Al4V with RF magnetron sputtering. *Journal of biomedical materials research*, *29*(2), 269-276.
- Wang, C., Chen, Z., Guan, L., Liu, Z., Wang, P., Zheng, S., & Liao, X. (2000). Structural characterization of ion beam sputter deposited calcium phosphate coatings. *Surface and Coatings Technology*, *130*(1), 39-45.
- Wang, C., Lin, J. C., Ju, C., Ong, H., & Chang, R. (1997). Structural characterization of pulsed laser-deposited hydroxyapatite film on titanium substrate. *Biomaterials*, *18*(20), 1331-1338.
- Wang, J., & Shaw, L. L. (2009). Nanocrystalline hydroxyapatite with simultaneous enhancements in hardness and toughness. *Biomaterials*, *30*(34), 6565-6572.
- Wang, P., Li, C., Gong, H., Jiang, X., Wang, H., & Li, K. (2010). Effects of synthesis conditions on the morphology of hydroxyapatite nanoparticles produced by wet chemical process. *Powder Technology*, *203*(2), 315-321.
- Webster, T. J., Schadler, L. S., Siegel, R. W., & Bizios, R. (2001). Mechanisms of enhanced osteoblast adhesion on nanophase alumina involve vitronectin. *Tissue engineering*, *7*(3), 291-301.
- Wei, M., Ruys, A., Swain, M., Kim, S., Milthorpe, B., & Sorrell, C. (1999). Interfacial bond strength of electrophoretically deposited hydroxyapatite coatings on metals. *Journal of Materials Science: Materials in Medicine*, *10*(7), 401-409.
- White, A. A., Best, S. M., & Kinloch, I. A. (2007). Hydroxyapatite-carbon nanotube composites for biomedical applications: a review. *International Journal of Applied Ceramic Technology*, *4*(1), 1-13.
- Wu, S.-C., Hsu, H.-C., Hsu, S.-K., Chang, Y.-C., & Ho, W.-F. (2015). Effects of heat treatment on the synthesis of hydroxyapatite from eggshell powders. *Ceramics International*, *41*(9), 10718-10724.



- Wu, S.-C., Tsou, H.-K., Hsu, H.-C., Hsu, S.-K., Liou, S.-P., & Ho, W.-F. (2013). A hydrothermal synthesis of eggshell and fruit waste extract to produce nanosized hydroxyapatite. *Ceramics International*, 39(7), 8183-8188.
- Yamashita, K., Yonehara, E., Ding, X., Nagai, M., Umegaki, T., & Matsuda, M. (1998). Electrophoretic coating of multilayered apatite composite on alumina ceramics. *Journal of biomedical materials research*, 43(1), 46-53.
- Yang, Y., Kim, K.-H., & Ong, J. L. (2005). A review on calcium phosphate coatings produced using a sputtering process—an alternative to plasma spraying. *Biomaterials*, 26(3), 327-337.
- Yang, Z., Jiang, Y., Wang, Y., Ma, L., & Li, F. (2004). Preparation and thermal stability analysis of hydroxyapatite derived from the precipitation process and microwave irradiation method. *Materials Letters*, 58(27-28), 3586-3590.
- Zanotto, A., Saladino, M., Chillura Martino, D., & Caponetti, E. (2012). Influence of temperature on calcium hydroxyapatite nanopowders. *Advances in Nanoparticles*, 1, 21-28.
- Zhang, S. (2013). *Hydroxyapatite coatings for biomedical applications*: CRC press.
- Zhang, Z., Huang, Y., & Jiang, Z. (1994). Electrophoretic deposition forming of SiC-TZP composites in a nonaqueous sol media. *Journal of the American Ceramic Society*, 77(7), 1946-1949.
- Zhitomirsky, I., & Gal-Or, L. (1997). Electrophoretic deposition of hydroxyapatite. *Journal of Materials Science: Materials in Medicine*, 8(4), 213-219.

## LIST OF PUBLICATIONS AND PAPERS PRESENTED

1. Roudan, M. A., Ramesh, S., Niakan, A., Wong, Y. H., Zavareh, M. A., Chandran, H., ... & Sutharsini, U. (2017). Thermal phase stability and properties of hydroxyapatite derived from bio-waste eggshells. *Journal of Ceramic Processing Research*, 18(1), 69-72.
2. Roudan, M. A., Ramesh, S., Wong, Y. H., Chandran, H., Krishnasamy, S., Teng, W. D., & Bang, L. T. (2017). Sintering behavior and characteristic of bio-based hydroxyapatite coating deposited on titanium. *Journal of Ceramic Processing Research*, 18(9), 640-645.

Universiti Malaysia